THE DEVELOPMENT AND APPLICATION OF

TIME-RESOLVED ION MOMENTUM SPECTROMETRY

By

John Timothy Stults

A DISSERTATION

Submitted to
Michigan State University
in partial fulfillment of the requirements
for the degree of

DOCTOR OF PHILOSOPHY

Department of Chemistry

1985

ABSTRACT

THE DEVELOPMENT AND APPLICATION OF
TIME-RESOLVED ION MOMENTUM SPECTROMETRY

By

John Timothy Stults

Time-resolved ion momentum spectrometry (TRIMS) has been developed
as a promising new mass spectrometry/mass spectrometry (MS/MS)
technique. Compared to more conventional MS/MS techniques, TRIMS offers
several advantages, including adaptability to many older mass
spectrometers, simpler operation, lower cost, energy-independent
assignment of daughter and stable ion masses, and the potential for
more rapid data acquisition.

In TRIMS, mass analysis is produced by simultaneous momentum and
velocity determinations: measurement of ion flight times through a
magnetic sector instrument. An ion's mass is determined by the product
of the magnetic field strength (proportional to momentum), and the
flight time (inversely proportional to velocity) at which the ion is
observed. Daughter ions formed in the field-free region between the
source and the magnet maintain the velocity of their parents. The
flight time measurement for a daughter thus serves to identify its
parent mass. Appropriate combinations of the magnetic field and/or
flight time allow all conventional MS/MS scans to be obtained.

An LKB-9000 single-focusing magnetic sector mass spectrometer has
been modified for TRIMS experiments. Ion source pulsing, time-resolved

detection, an extended flight path, and a collision cell have been added. To optimize the performance of the instrument for TRIMS, a data acquisition/instrument control system has been designed and implemented.

The technique has the capability for providing good resolution of daughter and stable ions, although parent ion identification is limited by the flight time resolution and the kinetic energy release from the parent dissociation process. Initial spatial and kinetic energy distributions of ions in the ion source contribute to degraded resolution. Optimization of instrument parameters can reduce this problem. Experiments have shown that sensitivity is one of the limitations of the TRIMS technique. Ion storage by space charge trapping in the ion source has reduced this limitation.

Time-resolved ion momentum spectrometry has been applied to the measurement of kinetic energy release in metastable decompositions. This measurement is an area in which TRIMS could find considerable use since it provides adequate daughter ion mass resolution in addition to the energy measurement.

ACKNOWLEDGMENTS

When so much time and effort is invested in a single endeavor such as this, many individuals deserve words of thanks. My advisors, Chris Enke and Jack Watson, deserve special acknowledgement for their guidance, counsel, and passion for excellence. I am equally grateful to Jack Holland who, among other things, taught me to defend my ideas against vigorous criticism. These and the other members of the "umbrella group," John Allison and David Pinkston, provided the creative atmosphere which nurtured much of this work. The assistance of Carl Myerholtz, Bruce Newcome, Adam Schubert, and Brian Eckenrode in completing much of the data system is also greatly appreciated.

Many others deserve notice for their support, but I especially want to thank Vicki McPharlin, Brian Musselman, Mike Davenport, Marty Rabb, Russ Geyer, and the members of the Watson and Enke groups for their help and friendship. I also want to express my gratitude to Dr. T.R. Williams, whose concern and advice over the years guided me into the field of analytical chemistry. Not least of all, my wife, Cheryl, deserves much credit for her love and endurance during this period.

TABLE OF CONTENTS

LIST OF TABLES

LIST OF FIGURES

CHAPTER I

HISTORICAL OVERVIEW

Introduction

The field of mass spectrometry has undergone tremendous growth in the past decade. From its early days as a tool for measuring atomic masses and characterizing simple organic molecules, the technique has matured into a valuable tool that can probe even the complex structures of trace biological compounds. This progress is both a tribute to the ingenuity of many researchers and a natural outgrowth of recent advances in technology.

Improvements in instrumentation have, without a doubt, played a major role in making mass spectrometry one of the most important analytical techniques available today. The computer has made instrument control, data acquisition, and data analysis much simpler. New ionization techniques such as laser desorption (1), plasma desorption (2), and fast atom bombardment (3-5) permit ionization of large, nonvolatile molecules. To date, time-of-flight measurements (6) and high-field magnets (7) provide for mass analysis of these large ions.

The development of mass spectrometry/mass spectrometry (MS/MS) has been another advancement in instrumentation (8,9). As the name implies, MS/MS involves two mass measurements to determine an ion's

mass before and after a fragmentation event. Since the fragmentation pathway can be quite specific to the structure of the ion, this technique has become important for many applications involving structure determination and mixture analysis.

The development of a new MS/MS technique, time-resolved ion momentum spectrometry (TRIMS) (10-12) is the topic of this dissertation. This new technique will be shown to possess certain advantages over more conventional MS/MS techniques. In TRIMS, mass determinations are based on the simultaneous measurement of ion velocity and momentum. The simultaneous nature of the measurement, in contrast to the sequential or serial nature of most MS/MS instruments, provides the opportunity for more rapid scanning of the entire data field. With the advent of very high speed electronics, it should be possible to obtain all the MS/MS information for a sample within the time frame of chromatographic peak elution. The combined momentum and velocity measurements also produce mass values for ions that are independent of ion energy, leading to improvements in resolution over some MS/MS techniques. In the following pages of this dissertation, the principles, the instrumental implementation, the performance, and the application of this technique will be described.

This chapter provides a brief introduction to MS/MS: the nomenclature, instrumentation, and applications. Conventional instruments are described, both to give a foundation for the description of time-resolved ion momentum spectrometry, and to provide

a background for comparison of the techniques. The use of time-of-flight measurements combined with sector instruments will be reviewed so as to put TRIMS in an historic perspective. A brief description of mass measurement by TRIMS is then followed with a discussion of the potential for this exciting new technique.

Mass Spectrometry/Mass Spectrometry

As the problems facing analytical chemists become more and more complex, there is a demand for techniques that can provide increased sensitivity and/or selectivity with shorter analysis times. Mass spectrometry/mass spectrometry, by its multidimensional nature, has from its inception proven to be a key instrumental technique in many modern analytical problems, especially those involving mixture analysis or structure elucidation.

In a typical MS/MS experiment: (a) ions are formed and extracted from the ion source, (b) the precursor (parent) mass is selected, (c) the ions undergo subsequent fragmentation (either spontaneous or induced), (d) the product (daughter) mass is selected, and (e) a detector measures the ion beam intensity. This sequence is shown in Figure 1.1. Alternatively, the ion fragmentation may precede both mass analysis steps, provided the mass analyzers can determine both the parent and daughter ion masses solely from the daughter ion characteristics.
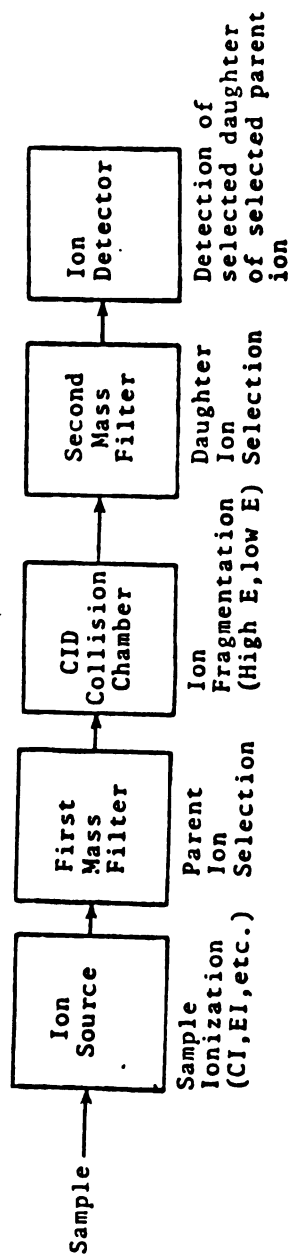
Figure 1.1. Operational sequence in an MS/MS experiment.

Another term, tandem mass spectrometry, often is used as a synonym for mass spectrometry/mass spectrometry. "Tandem," however, implies two analyzers, one following the other. Mass spectrometry/mass spectrometry is a more general term since it does not imply any specific configuration.

Mass spectrometry/mass spectrometry adds a dimension of information to conventional mass spectrometry: the parent ion-daughter ion relationship. The manner in which these multidimensional data are obtained and utilized depends on the ion fragmentation processes and the mass analyzers employed. The fragmentation processes and mass analyzers currently used are described below.

Fragmentation Processes

Of the several mechanisms of daughter ion formation in MS/MS, metastable decomposition is the simplest (13,14). Ions formed in the ion source have a range of internal energies that govern their fragmentation behavior. Ions that acquire a sufficient amount of energy during ionization may undergo spontaneous unimolecular dissociation in the ion source. On the other hand, if the ion internal energy is low, the probability that the ion will remain intact until it reaches the detector is increased. There is an intermediate range of energies for which dissociations with rate constants in the range of $k = 10^{-5} - 10^{-6}$ sec^{-1} produce significant fragmentation during the period of time between ion formation and detection. Under these circumstances, the parent ion is said to be a metastable ion; the

fragmentation process is called metastable decomposition or dissociation. This is a unimolecular process; the ion spontaneously falls apart. The extent of dissociation observed depends upon the internal energy, the rate constant, and the mass spectrometer optics.

Unimolecular dissociations are accompanied by the release of kinetic energy, the extent of which depends on the internal energy and the molecular structure (15-17). The kinetic energy release can be characteristic of specific ion or classes of ions, and its measurement often provides useful analytical information.

Collisionally activated dissociation (CAD) or collision-induced dissociation (CID) occurs when an ion collides with a neutral atom or molecule (18,19). The energy of the collision is partially transferred to internal energy of the ion, resulting in subsequent unimolecular dissociation. The nature of the collision depends on the energy involved. Low energy collisions (<100 eV), such as those that occur in quadrupole instruments, involve vibrational excitation during "head-on" collisions (20-22). High energy collisions (>1000 eV), that typically occur in magnetic sector instruments, involve electronic excitation from "glancing" collisions (23-25). The fragmentation distribution for high energy collisions appears to be fairly independent of the collision energy. For molecular ion parents, the fragmentation is usually very similar to that produced by 70 eV electron impact ionization, simplifying interpretation (26). In low energy collisions, however, the fragmentation can vary considerably with the collision energy. This variability is structure dependent and has been used as

an added degree of selectivity.

Other reactions such as charge exchange, charge stripping, and addition/substitution reactions can occur during collision (19,27,28). These often provide further analytical selectivity for certain types of compounds. Photodissociation (1) is another method of producing daughter ions, especially when addition of a known amount of energy (through resonance absorption) is desired.

Mass Analyzers

There are four major types of mass analyzers used in conventional mass spectrometry (29): the magnetic sector, the quadrupole filter, the time-of-flight drift tube, and the ion cyclotron resonance cell. These analyzers are combined in various ways to make MS/MS measurements.

In magnetic sector instruments (30), ions are produced continuously, external to the magnetic field, and are accelerated toward the magnet by beam shaping potentials such that all have the same final kinetic energy (2-10 keV). As depicted in Figure 1.2, the magnet disperses ions according to momentum just as a prism disperses the wavelengths of light. Ions of different momenta travel paths of different radii through the magnetic field. Since all ions have the same nominal energy, ions of different mass will have different momenta. Usually a pair of slits form an ion optic system and the magnetic field is changed to allow ions of progressively increasing or decreasing mass to travel through the exit slit to the detector. Often
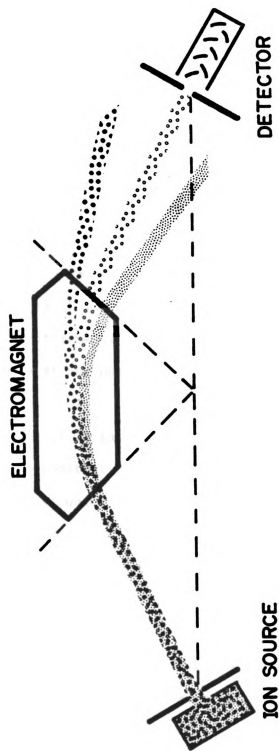
Figure 1.2. Mass separation in a magnetic sector mass analyzer.
(Reprinted with permission from ref. 29. Copyright 1983 American
Chemical Society.)

the magnetic sector is combined with an electric sector to form a double-focusing mass spectrometer, providing higher resolving power. The electric sector separates ions on the basis of energy-to-charge ratio, and it serves to reduce the range of energies of the transmitted ions. The improved precision in energy allows the magnetic momentum analyzer to determine mass with higher resolution.

The quadrupole mass filter (31) consists of four rods through which ions travel after acceleration to constant energy (5-50 eV). RF and DC voltages are applied to the rods which cause oscillation of the ions, shown in Figure 1.3. The voltage and frequency levels are adjusted so that ions of only one mass have a stable trajectory through the quadrupole at any one time.

For time-of-flight (TOF) measurements (32,33), ions are accelerated to constant energy (2-10 keV), but the acceleration voltage is pulsed very quickly to produce packets of ions. As an ion packet leaves the source, it passes into a field-free region where it separates into smaller packets. As shown in Figure 1.4, ions of different mass-to-charge ratio will have different velocities and so require different amounts of time to travel to the detector, which is situated at a fixed distance from the ion source. The flight time of each packet thus identifies the mass of ions in that packet.

The ion cyclotron resonance (ICR) cell is situated completely within a magnetic field (34). As shown in Figure 1.5, after pulsed ion formation, the ions move in circular orbits, the frequency of their
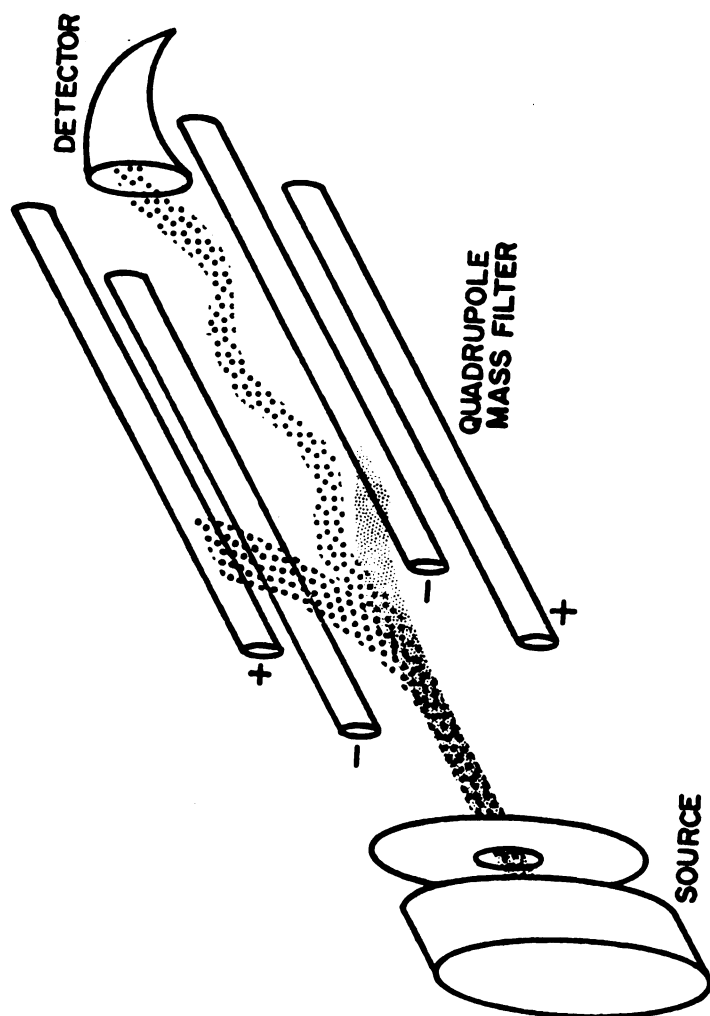
Figure 1.3. Mass separation in a quadrupole mass filter. (Reprinted with permission from ref 29. Copyright 1983 American Chemical Society.)
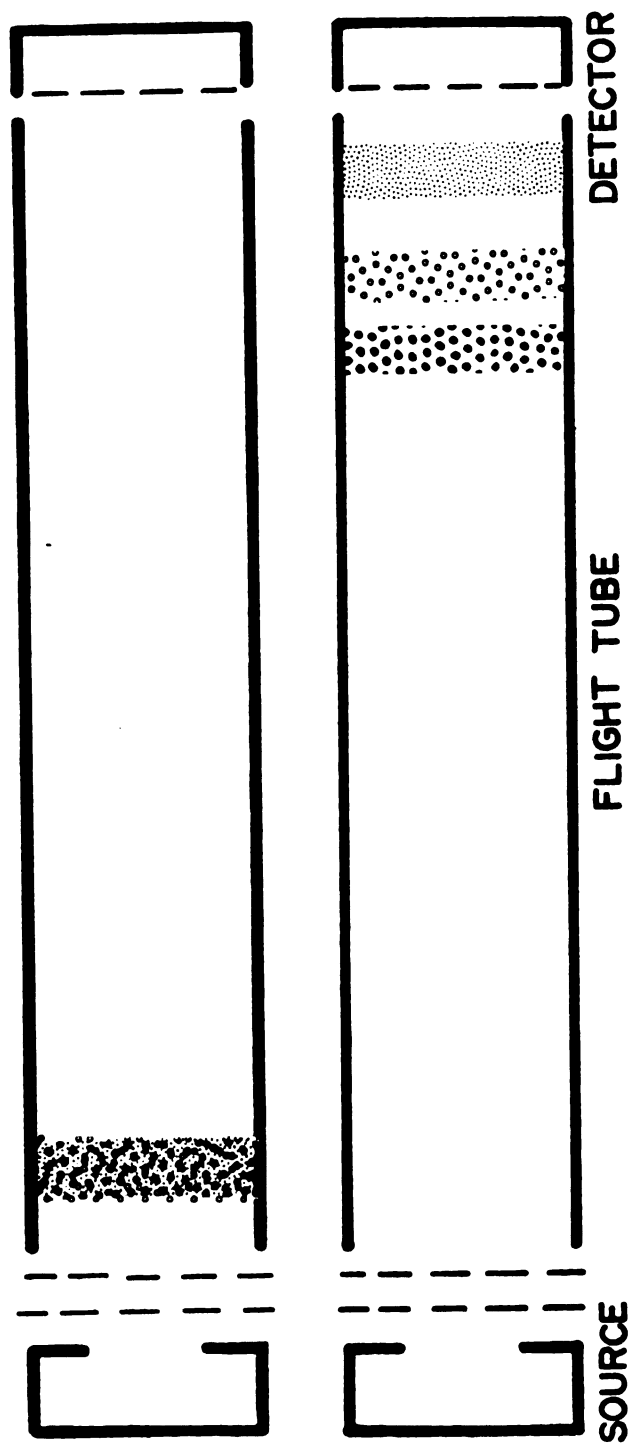
Figure 1.4: Mass separation in a time-of-flight drift tube. (Reprinted with permission from ref. 29. Copyright 1983 American Chemical Society.)
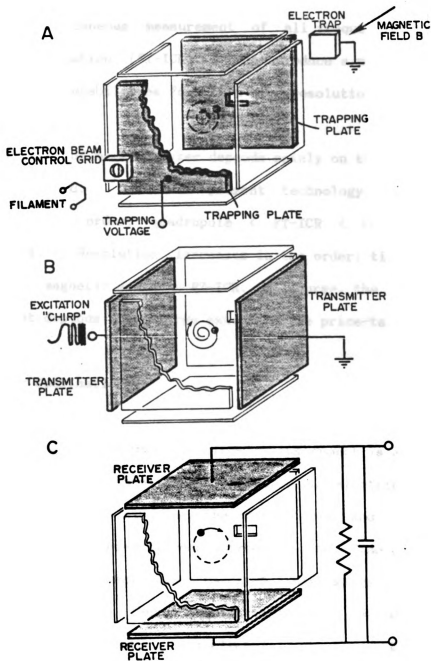
Figure 1.5. Mass separation in an ion cyclotron resonance cell.
(a) ion formation, (b) excitation, (c) detection.
(Reprinted with permission from ref 29. Copyright 1983
American Chemical Society.)

motion being inversely proportional to their mass. Measurement of the intensity of the signal at individual frequencies produces a mass spectrum. Simultaneous measurement of all frequencies followed by Fourier Transformation (FT-ICR) (35) can produce a mass spectrum very quickly with the capabilities for ultra-high resolution.

The choice of mass analyzer depends mainly on the mass range and resolution desired. Based on present technology, the mass range increases in the order: quadrupole < FT-ICR < magnetic sector < time-of-flight. Resolution increases in the order: time-of-flight < quadrupole < magnetic sector < FT-ICR. Of course, the performance of the instrument depends to a large extent on the price-tag.

Mass Analyzer Combinations

A mass spectrometry/mass spectrometry instrument is a combination of two or more mass analyzers. Magnetic and electric sectors and quadrupole mass filters have been the primary ones used. FT-ICR as an MS/MS device has only recently been introduced (36). Time-of-flight has been used only in specialized research instruments. It is common practice to abbreviate these combinations as EB, BE, QQ, QT, etc., where B=magnetic sector, E=electric sector, Q=quadrupole, T=time-of-flight.

The tandem sector MS/MS instruments are conventional double-focusing mass spectrometers in which the electric sector and accelerating voltages have been uncoupled (37-40). In a BE instrument,

as shown in Figure 1.6a, the magnet selects the parent ion,
fragmentation occurs in the second field-free region (between the
sectors), and the electric sector selects the daughter ion. The
daughter ion has less energy than the parent due to loss of the neutral
mass so the electric sector, an energy filter, acts as the daughter ion
mass analyzer. For this reason, the BE instrument is also sometimes
called MIKES (mass analyzed ion kinetic energy spectrometer) (41).

Fragmentations occurring in the first field-free region of a BE
instrument can also be measured. The identities of the parent and
daughter ions are calculated from both the magnetic and electric field
values necessary for the ions to reach the detector. The EB instrument
operates in an identical fashion, but only collisions occurring in the
first field-free region can be used.

The triple quadrupole (QQQ) (42) instrument, shown schematically
in Figure 1.6b, uses the first quadrupole to select the parent ion and
the third quadrupole to select the daughter mass. Collisions occur in
the center quadrupole, operated in a non-mass-selective (rf only) mode.
This quadrupole acts as a focusing unit to reduce the scattering in
low energy CAD (43).

More recently three- (44-46) and four-sector (47,48) instruments
(EBE,BEEB,etc.) and hybrid instruments (BEQQ) (49) have been
introduced. In the hybrid instruments the first quadrupole is a
collsion chamber that can be used in either the high or low energy
mode. These provide for high resolution in either the parent or
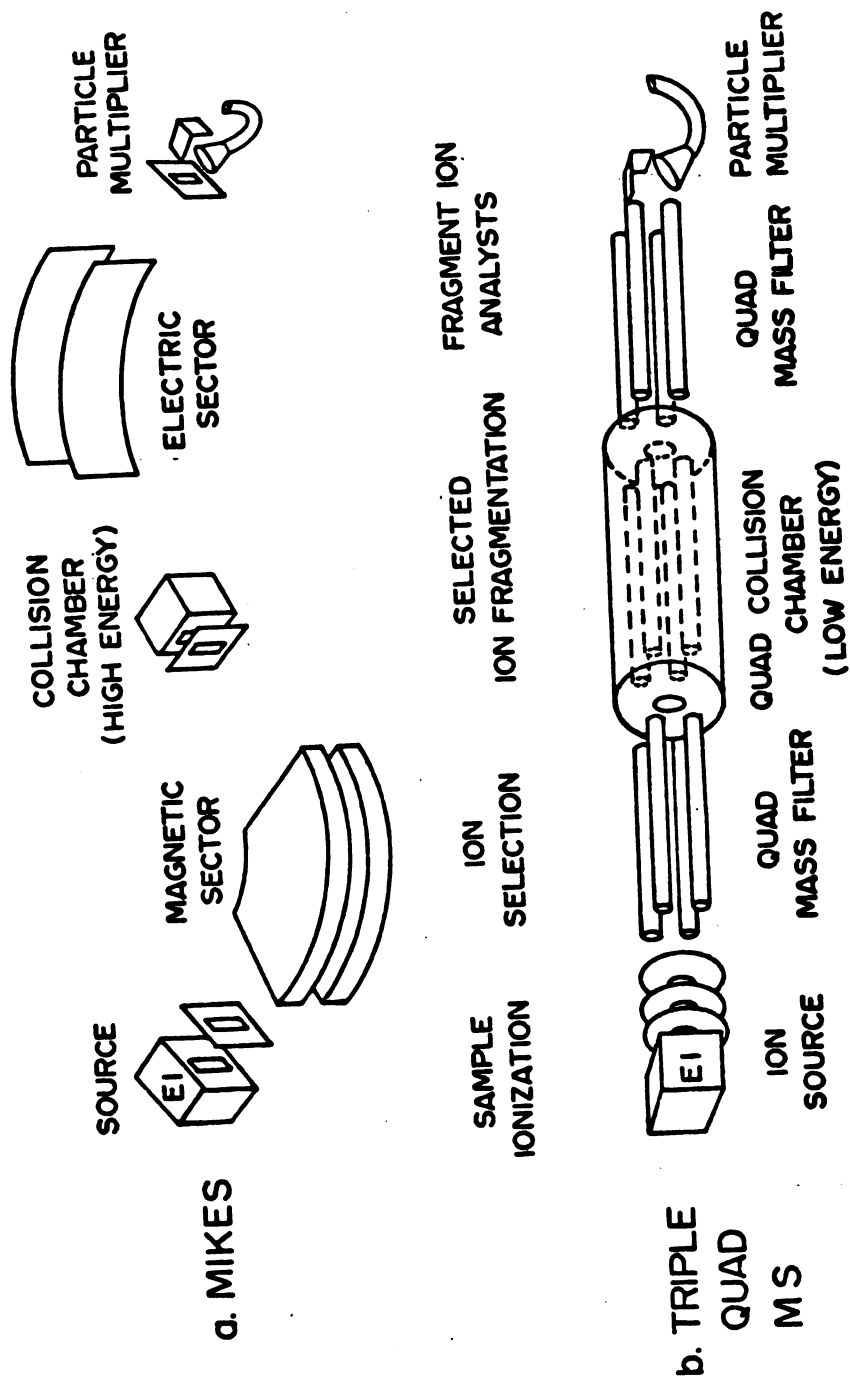
Figure 1.6. Sequential MS/MS instruments: (a) BE, (b) QQQ geometry.

daughter ion selection, or both. The FT-ICR has also recently been shown to provide high resolution daughter spectra (36) as well as the ability to perform multiple stages of MS/MS (50).

The selection of the type of instrument depends mainly, as does the selection of a conventional instrument, on the resolution and mass range requirments, and cost. Other factors such as type of collision (high or low energy), sensitivity, and scanning speed can be important.

Scanning Modes

There are several methods of scanning an MS/MS instrument in order to obtain the information desired (42). A daughter scan is produced by selecting a parent mass with the first mass analyzer and scanning the second mass analyzer. This scan produces a mass spectrum of the parent ion. For a parent scan, the second mass analyzer is set to select daughter ons of a single mass. Then the first mass analyzer is scanned. The resulting parent ion scan shows all the parents which undergo fragmentation to produce the selected product ion. A third type of scan, the neutral loss scan, is produced by scanning both mass analyzers simultaneously such that the difference in mass between the parent and daughters remains constant. This scan is really a parent ion scan for constant neutral loss and shows all parents that fragment to give the same neutral loss.

The method of accomplishing these scans depends on the type of instrument. A simple scan of a single device such as a quadrupole or

electric sector can produce a parent or a daughter scan. Other types of linked scans require much more sophisticated instrument control to scan several devices according to a mathematical relationship.

Applications

Selection of the appropriate scan is dictated by the type of analysis to be performed. MS/MS is used in a variety of applications which can be divided into two major classifications: mixture analysis and structure elucidation.

For mixture analysis (51), the sample being ionized in the source is composed of several components (see Figure 1.7). A "soft ionization" technique is preferentially used, such a chemical ionization (52,53), so that in the ideal case, only molecular ions are formed with little fragmentation. Parent ion selection by the first mass analyzer separates one component from the others. Fragmentation of the parent is effected by CAD. Following fragmentation, a daughter scan produces the equivalent of a mass spectrum of the compound. Thus, the first mass analysis stage serves as a separation step. MS/MS is especially useful in "targeted" mixture analysis where identification and/or quantification of certain known compounds in a complex mixture is desired.

This mixture analysis scheme has been applied to fast atom bombardment ionization in which the background from the glycerol matrix interferes with the mass spectrum (54). Selection of the molecular ion
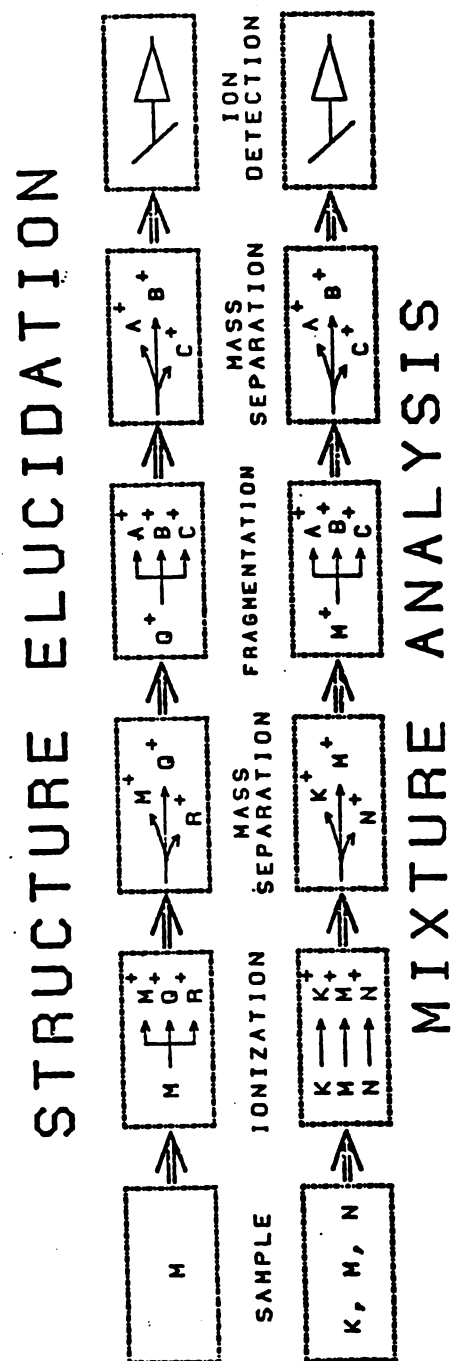
Figure 1.7. Mass analysis schemes for MS/MS applications: structure elucidation and mixture analysis.

(or molecular adduct ion) by the first mass analyzer discriminates against the glycerol ions. The second mass analyzer produces the mass spectrum of the collision-induced daughters of the selected parent.

Neutral loss scans are valuable for screening a mixture for a certain type of compound. For example, negatively-charged molecular ions of organic acids often display a loss of CO_2 (44 daltons) (55,56). Nitrated polycyclic aromatic hydrocarbons usually show loss of OH (17 daltons) (57). Polychlorinated biphenyls show loss of Cl_2 (70 daltons) (58).

Parent scans are also used for screening mixtures. For instance, phthalates in environmental samples have been identified by first screening for mass 149, a characteristic fragment ion for this class of compounds (59,60).

Structure elucidation experiments, in contrast, use a single compound (see Figure 1.7). When a single compound is ionized, the resulting fragment ions, if any, represent certain structural features of the original molecule. However, ions at any given mass can have one of many possible structures. Even if the elemental composition is known by high resolution measurements, there can be a number of isomeric structures. Further fragmentation by CAD can produce daughter fragments that often give more insight into the exact structure (61).

Limitations of Present Instruments

One of the common features of the MS/MS instruments described so far is their tandem nature — parent and daughter mass analyzers are sequential and temporally exclusive. Only one parent-daughter pair can be evaluated at once. This puts a limit on the speed at which many scans can be obtained. If many different ions could be detected simultaneously, the possibilities for much faster scanning could be substantially improved.

Boerboom et al (62) have developed a tandem magnetic sector (BB) instrument in which the second magnet disperses the daughter ions along a multichannel detector. All daughter ions are collected simultaneously. In FT-ICR, all daughter ions are also measured simultaneously after a selected parent ion is subjected to collision (36).

These multiplexed instruments also have drawbacks. The multichannel BB instrument is cumbersome and has a limited range of daughter ions that can be viewed simultaneously. FT-ICR, although it shows considerable promise, requires at least 20 ms for data acquisition per daughter scan and the Fourier Transform takes several seconds per scan.

The new technique developed in this thesis work, time-resolved ion momentum spectrometry, involves measurement of ion velocities as the ions move through a magnetic sector instrument (11). Velocity

measurement by TOF serves as a measure of the parent mass since collision and fragmentation do not substantially alter the velocity. The momentum measurement of the B sector can be combined with the velocity value to yield the daughter ion mass. Time-of-flight measurements can be completed on the microsecond time scale so all velocity measurements for each sector field value could be completed almost instantaneously. In the time necessary to scan the sector once, all parent-daughter combinations could be scanned.

MS/MS Utilizing Time-of-Flight

Renaissance in TOF

Time-of-flight mass spectrometry has been used for several decades. Except for a brief time in the late 1950s, however, the TOF instrument has not enjoyed the popularity that other instruments have. With the recent advances in ionization techniques and in high-speed electronics, TOF is again gaining importance. There are two basic reasons supporting this rise in popularity (29). First, it has a virtually unlimited mass range. One merely waits a long enough period of time for the ion to drift to the detector. Second, it can produce complete spectra at a rapid rate. A signal representing the spectrum of masses 1-1000 daltons can be produced every 100 μs. Transient or rapidly changing samples can be analyzed accurately. In addition, the high transmission of the instrument makes effective use of the ions in each pulse.

The time-of-flight mass spectrometer has seen use with Californium-252 plasma desorption to produce spectra of ions larger than mass 10,000 (6,63). It is also used for transient ionization techniques such as laser desorption (64,65). Its fast scanning capabilities have also attracted attention for use in capillary gas chromatography-mass spectrometry (29,66).

Resolution Improvements

One of the drawbacks of the time-of-flight measurements is the relatively poor resolving power. A conventional instrument yields at most a resolution of 650 (50% valley) at mass 614 (67). A number of techniques have been tried in order to improve on this value. Wiley and McLauren (32) employed multiple focusing grids to correct for ion formation in different regions of the ion source and "time-lag focusing" to correct for different initial thermal velocities. Sanzone et al (68) used time-dependent extraction pulses to improve the resolution. Neither technique has been able to push the resolution up to 1000.

More recently, focusing devices have been used to improve the resolution. Perhaps the most successful of these has been the electrostatic reflection mirror introduced by Mamyrin et al (69). Ions travel into a retarding electric field gradient that eventually turns the ions around and accelerates them toward the detector. Those ions with higher energy will move farther into the mirror before being turned around. Their higher energy is thereby compensated by a longer

flight path, resulting in a resolution of up to 3500.

Other focusing schemes utilize electric or magnetic fields. Both electric (70,71) and magnetic sectors (72,73) have been used as filters to remove ions with extraneous energies. Electric sectors have been used for "time-focusing" (74) -- ions of different energy travel different paths through the sectors so that the path length compensates for the energy or initial position differences (75-85). Magnetic sectors have likewise been suggested as focusing devices (85-87).

Combinations of time-of-flight and magnetic or electric sectors have been used for quite some time in nuclear physics. Particles formed in plasmas and high-energy collisions have widely varying energy, mass, and charge. Measurement of velocity plus momentum or energy can often sort out the wide variety of particles formed (88-96). Likewise, in plasmas produced by lasers, combinations of TOF and electric or magnetic sectors have been used to measure the mass and energy (97-104).

MS/MS by Time-of-flight

Although time-of-flight has not been used commercially for MS/MS, there have been instruments built that utilize the technique. The earliest techniques used decelerating fields in the flight path (105-113). Ions that dissociate in the flight tube have less energy than the stable ions; deceleration will cause them to slow down more than the stable ions. Knowledge of the stable ion masses and the

deceleration field value enables daughter mass assignment to be made.

More conventional MS/MS experiments have been performed with ET
(114-116), BT (117), QT (118), and TT (119,120) combinations. The
latter instrument used precisely timed gate pulses to control the ion
movement. With the exception of the ET instrument, the TOF measurement
in these instruments occurs after the fragmentation step, i.e., TOF is
used solely to determine the daughter ion mass. Analogous to the BT
instrument, a magnetic sector combined with a Wien velocity analyzer
has been used both for MS/MS (121) and nuclear particle studies (122).
Wien analyzers are crossed ExB fields that select ions on the basis of
velocity.

Time-Resolved Ion Momentum Spectrometry

The combinations of magnetic sectors with time-of-flight
measurements described above were mainly concerned with measurement of
ion velocity and ion momentum to yield the correct mass-to-charge
ratio. It is also possible to utilize the velocity and momentum
measurements for MS/MS experiments (10-12). When an ion dissociates
after acceleration from the ion source, the mass, momentum, and kinetic
energy change but the velocity remains the same. Therefore, velocity
measurement can yield the parent mass identity while momentum plus
velocity analysis yields the daughter mass. This process is shown in
Figure 1.8 for two ions, M_a and M_b, formed in the ion source.
Dissociation yields a number of different ions. Simultaneous momentum
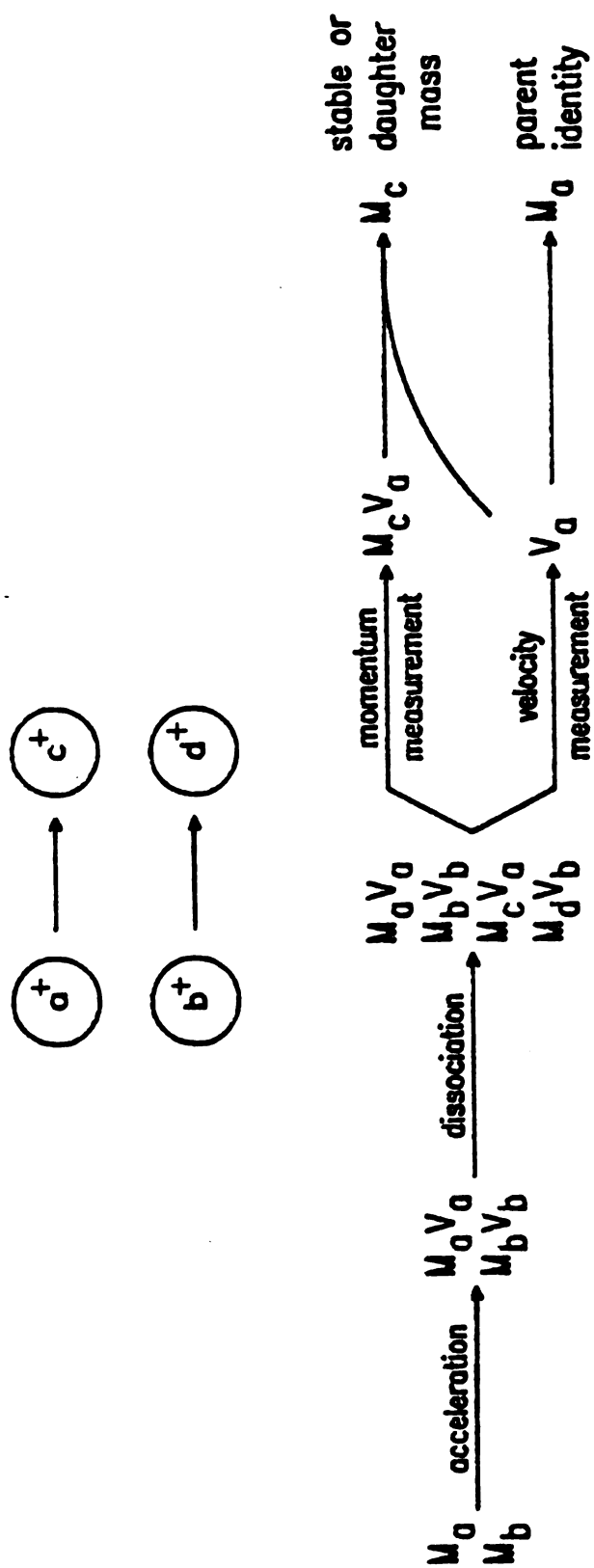
Figure 1.8. Parent and daughter mass analysis in TRIMS by simultaneous momentum and velocity measurements.

and velocity measurements can identify the mass of each daughter ion and its precursor mass.

In time-resolved ion momentum spectrometry, a single magnetic sector mass spectrometer was modified for ion source pulsing and time-resolved detection. The magnetic sector provides analysis of ion momentum while the combination of a pulsed ion source and time-resolved detection system provides analysis of the ion velocity through the instrument. In this configuration there is not a separate time-of-flight section, but rather the flight time is measured through the magnetic sector instrument. Since the ion optics rigidly define the radius of curvature at which ions are detected, the distance traveled by all observed ions will be the same.

Figure 1.9 illustrates the basic components of a single sector mass spectrometer and shows the separation of ions based on velocity and momentum. Approximately monoenergetic ions extracted in a brief pulse from the source may undergo fragmentation in the field-free region preceding the magnet. The magnetic field disperses the ions according to their momenta, daughter ions now having less momentum than their parents. At the same time, ions become separated along the ion path as a result of their different velocities. Unlike the momentum, however, the velocity of a daughter ion remains essentially the same as that of its parent ion, altered only slightly by the dissociation process, so all daughter ions of the same parent will have nearly identical velocities. For a single value of the magnetic field, the ion packet corresponding to stable ions with the selected momentum
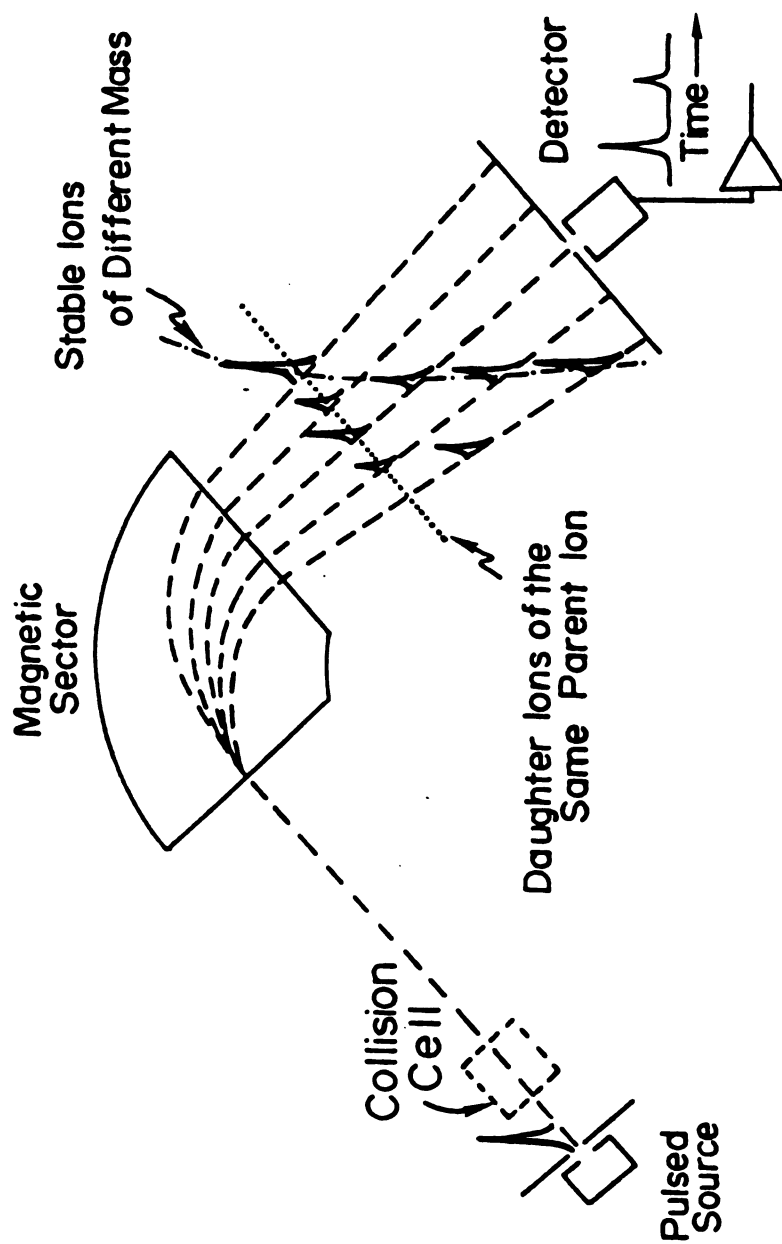
Figure 1.9. Mass analysis in TRIMS by measurement of ion flight times in a magnetic sector instrument. Daughter ions appear at the same flight time as their parents. (Reprinted with permission from ref. 11. Copyright 1983 American Chemical Society.)

will arrive at the detector, followed in time by daughter ions with the same momentum which originated from fragmentation of progressively heavier (and slower) parents. If a current-time curve is taken for each value of magnetic field strength (momentum), the complete set of MS/MS spectra for the sample can be obtained from the resulting data set. As will be shown in the next chapter, the mass assignment for any ion (daughter or stable ion) is based solely on the combination of its arival time and required magnetic field strength, and is completely independent of its energy. Daughter ion, parent ion, and neutral loss spectra can be constructed from the complete data set or can be obtained by various independent and linked scans of the magnetic field strength and ion arrival time.

Time-Resolved Ion Kinetic Energy Spectrometry

Just as momentum and velocity measurements can produce MS/MS data in the TRIMS instrument, so can energy and velocity measurements (11,12,114-116). For collisions that occur before the electric sector, velocity measurement can yield the parent mass identity while energy analysis yields the daughter mass. Utilizing an electric sector to determine the daughter mass is similar to the MIKES (or BE) instrument (41). For this reason the name time-resolved ion kinetic energy spectrometry (TRIKES) has been adapted. Although the problems with daughter ion resolution that plagues MIKES likewise apply to TRIKES, TRIKES does not require a bulky magnet so instrumentation can be much simpler.

It should be noted that "time-resolved mass spectrometry" techniques have been described in several other applications. These techniques do not utilize the time-resolution to obtain mass values, but rather measure the time dependence of ion formation (123-125), ion dissociation (126,127), or ion-molecule reactions (128,129).

The time-resolved spectrometers described offer new and potentially advantageous forms of MS/MS. Electric sectors are inexpensive and simple to operate, and many older single magnetic sector mass spectrometers exist. The addition of ion source pulsing and time-resolved detection to these instruments could extend, at low cost, the capabilities for MS/MS to many laboratories unable to bear the expense of new instruments.

Both TRIMS and TRIKES are potentially powerful techniques. J.D. Pinkston has developed the TRIKES technique and his work is found elsewhere (116). The theory, implementation, and application of TRIMS will be described in detail in subsequent chapters.

REFERENCES

1. Cotter, R. J. Anal. Chem. 1984, 56, 485A-504A.

2. Macfarlane, R. D. Anal. Chem. 1983, 55, 1247A-1264A.

3. Barber, M.; Bordoli, R. S.; Sedgwick, R. D.; Tyler, A. N. Nature 1981, 293, 270-275.

4. Rinehart, K. L., Jr. Science 1982, 218, 454-460.

5. Busch, K. L.; Cooks, R. G. Science 1982, 218, 247-260.

6. Macfarlane, R. D.; Torgerson, D. F. Int. J. Mass Spectrom. Ion Phys. 1976, 21, 81-92.

7. Dell, A.; Taylor, G. W. Mass Spectrom. Rev. 1984, 3, 357-394.

8. McLafferty, F. W., Ed., "Tandem Mass Spectrometry"; Wiley-Interscience: New York, 1983.

9. Yost, R. A.; Fetterolf, D. D. Mass Spectrom. Rev. 1983, 2, 1-45.

10. Enke, C. G.; Stults, J. T.; Holland, J. F.; Pinkston, J. D.; Allison, J.; Watson, J. T. Int. J. Mass Spectrom. Ion Phys. 1983, 46, 229-232.

11. Stults, J. T.; Enke, C. G.; Holland, J. F. Anal. Chem. 1983, 55, 1323-1330.

12. Enke, C. G.; Holland, J. F.; Stults, J. T. U.S. Patent 4 472 631, 1984.

13. Cooks, R. G.; Beynon, J. H.; Caprioli, R. M.; Lester, G. R. "Metastable Ions"; Elsevier: New York, 1973.

14. Holmes, J. L.; Terlouw, J. K. Org. Mass Spectrom. 1980, 15, 383-396.

15. Jones, E. G.; Bauman, L. E.; Cooks, R. G.; Beynon, J. H. Org. Mass Spectrom. 1973, 7, 185.

16. Larka, E. A.; Howe, I.; Beynon, J. H.; Zaretskii, Z. V. I. Org. Mass Spectrom. 1981, 16, 465-466.

17. Voyksner, R. D.; Hass, J. R.; Bursey, M. M. Anal. Chem. 1983, 55, 914-920.

18. Cooks, R. G., Ed., "Collision Spectroscopy"; Plenum: New York, 1978.

19. Levsen, K.; Schwarz, H. Mass Spectrom. Rev. 1983, 2, 77-148.

20. Yost, R. A.; Enke, C. G.; McGilvery, D. C.; Smith, D.; Morrison, J. D. Int. J. Mass Spectrom. Ion Phys. 1979, 30, 127-136.

21. Douglas, D. J. J. Phys. Chem. 1982, 86, 185-191.

22. Dawson, P. H.; Douglas, D. J. In "Tandem Mass Spectrometry"; McLafferty, F. W., Ed.; Wiley-Interscience: New York, 1983; pp. 125-148.

23. Yamoaka, H.; Dong, P.; Durup, J. J. Chem. Phys. 1969, 51, 3465-3476.

24. Kim, M. S.; McLafferty, F. W. J. Am. Chem. Soc. 1978, 100, 3279-3282.

25. Todd, P. J.; McLafferty, F. W. In "Tandem Mass Spectrometry"; McLafferty, F. W., Ed.; Wiley-Interscience: New York, 1983; pp. 149-174.

26. Jennings, K. R. Int. J. Mass Spectrom. Ion Phys. 1968, 1, 227-235.

27. Beynon, J. H.; Cooks, R. G. J. Phys. E, 1974, 7, 10-18.

28. Cooks, R. G.; Beynon, J. H. In "Mass Spectrometry"; Maccoll, Ed.; International Review of Science, Physical Chemistry, Series Two, 1975.

29. Holland, J. F.; Enke, C.G.; Allison, J.; Stults, J. T.; Pinkston, J. D.; Newcome, B.; Watson, J. T. Anal. Chem. 1983, 55, 997A.

30. Wollnik, H. Adv. Electron. Electron. Phys., Suppl. 13B, 1980, 133-172.

31. Dawson, P. H., Ed., "Quadrupole Mass Spectrometry";

32. Wiley, W. C.; McLaren, I. H. Rev. Sci. Instrum. 1955, 26, 1150.

33. Price, D.; Milnes, G. J. Int. J. Mass Spectrom. Ion Phys. 1984, 60, 61-81.

34. Wanczek, K. P. Int. J. Mass Spectrom. Ion Phys. 1984, 60, 11-60.

35. Gross, M. L.; Rempel, D. L. Science 1984, 226, 261-268.

36. Cody, R. B.; Freiser, B. S. Anal. Chem. 1982, 54, 1431-1433.

37. Boyd, R. K.; Beynon, J. H. Org. Mass Spectrom. 1977, 12, 163-165.

38. Boyd, R. K.; Porter, C. J.; Beynon, J. H. Int. J. Mass Spectrom. Ion Phys. 1982, 44, 199-214.

39. Jennings, K. R.; Mason, R. S. In "Tandem Mass Spectrometry"; McLafferty, F. W., Ed.; Wiley-Interscience: New York, 1983; pp. 197-222.

41. Beynon, J. H.; Cooks, R. G.; Amy, J. W.; Baitinger, W. E.; Ridley, T. Y. Anal. Chem. 1973, 45, 1023A-1031A.

42. Yost, R. A.; Enke, C. G. Anal. Chem. 1979, 51, 1251A.

43. Dawson, P. H.; Fulford, J. E. Int. J. Mass Spectrom. Ion Phys. 1982, 42, 195-211.

44. Russel, D. H.; Smith, D. H.; Warmack, R. J.; Bertram, L. K. Int. J. Mass Spectrom. Ion Phys. 1980, 35, 381-391.

45. Gross, M. L.; Chess, E. K.; Lyon, P. A.; Cross, F. W.; Evans, S.; Tudge, H. Int. J. Mass Spectrom. Ion Phys. 1982, 42, 243-254.

46. Rabrenovic, M.; Brenton, A. G.; Beynon, J. H. Int. J. Mass Spectrom. Ion Phys. 1983, 52, 175-182.

47. McLafferty, F. W.; Todd, P. J.; McGilvery, D. C.; Baldwin, M. A. J. Am. Chem. Soc. 1980, 102, 3360-3363.

48. Hass, J. R.; Green, B. N.; Bateman, R. H.; Bott, P. A.; presented at the 32nd Annual Conference on Mass Spectrometry and Allied Topics, San Antonio, TX, May 27-June 1, 1984, bound volume pp. 380-381.

49. Glish, G. L.; McLuckey, S. A.; Ridley, T. Y.; Cooks, R. G. Int. J. Mass Spectrom. Ion Phys. 1982, 41, 157-177.

50. Cody, R. B.; Burnier, R. C.; Freiser, B. S. Anal. Chem. 1982, 54, 2225-2228.

51. Kondrat, R. W.; Cooks, R. G. Anal. Chem. 1978, 50, 81A.

52. Munson, M. S. B.; Field, F. H. J. Am. Chem. Soc. 1966, 88, 1621.

53. Harrison, A. G. "Chemical Ionization Mass Spectrometry"; CRC Press: Boca Raton, FL, 1983.

54. Amster, I. J.; Baldwin, M. A.; Cheng, M. T.; Procter, C. J.; McLafferty, F. W. J. Am. Chem. Soc. 1983, 105, 1654-1655.

55. Zakett, D.; Schoen, A. E.; Kondrat, R. W.; Cooks, R. G. J. Am. Chem. Soc. 1979, 101, 6781-6783.

56. Hunt, D. F.; Giordani, A. B.; Rhodes, G.; Herold, D. A. Clin. Chem. (Winston-Salem, N.C.) 1982, 28, 2387-92.

57. Schuetzle, D.; Riley, T. L.; Prater, T. J.; Harvey, T. M.; Hunt, D. F. Anal. Chem. 1982, 54, 265-271.

58. Shushan, B.; Boyd, R. K.; Anal. Chem. 1981, 53, 421-427.

59. Gallegos, E. J. Anal. Chem. 1976, 48, 1348-1351.

60. Hunt, D. F.; Shabanowitz, J.; Harvey, T. M.; Coates, M. Anal. Chem. 1985, 57, 525-537.

61. Kruger, T. L.; McLaughlin, J. L.; Ranieri, R. L. J. Org. Chem. 1977, 42, 4161.

62. Louter, G. J., Boerboom, A. J. H., Stalmeier, P. F. M.; Tuithoff, H. H.; Kistemaker, J. Int. J. Mass Spectrom. Ion Phys. 1980, 33, 335.

63. Sundqvist, B.; Kamensky, I.; Hakansson, P.; Kjellberg, J.; Salehpour, M.; Widdiyasekera, S.; Fohlman, J.; Peterson, P. A.; Roepstorff, P. Biomed. Mass Spectrom. 1984, 11, 242-257.

64. Cotter, R. J.; Tabet, J. C. Int. J. Mass Spectrom. Ion Phys. 1983, 53, 151-166.

65. Guest, W. H. Int. J. Mass Spectrom. Ion Phys. 1984, 60, 189-199.

66. Gohlke, R. S. Anal. Chem. 1962, 34, 1332-1333.

67. Pinkston, J. D., personal communication, 1985.

68. Browder, J. A.; Miller, R. L.; Thomas, W. A; Sanzone, G. Int. J. Mass Spectrom. Ion Phys. 1981, 37, 99-108.

69. Mamyrin, B. A.; Karatev, V. I.; Shmikk, D. V.; Zagulin, V. A. Sov. Phys.-JETP (Engl. Transl.) 1973, 37, 45-48; Zh. Eksp. Teor. Fiz. 1973, 64, 82-89.

70. Fenner, N. C.; Daly, N. R. Rev. Sci. Instrum. 1966, 37, 1068-1070.

71. Pinkston, J. D.; Allison, J.; Watson, J. T.; presented at the 32nd Annual Conference on Mass Spectrometry and Allied Topics, San Antonio, TX, May 27-June 1, 1984, bound volume pp. 534-535.

72. Bykovskii, Yu. A.; Dymovich, V. I.; Kozyrev, Yu. P.; Nevolin, V. N.; Sil'nov, S. M. Sov. Phys. Tech. Phys. (Engl. Tranl.) 1971, 15, 1877- 1879; Zh. Tekh. Fiz. 1970, 40, 2401-2404.

73. Kovalev, N. D.; Shmikk, D. V.; Feoktistov, I. Yu. Sov. Phys.-Tech. Phys. (Engl. Transl.) 1978, 23, 718-720; Zh. Tekh. Fiz. 1978, 48, 1282-1285.

74. Bakker, J. M. B. Dyn. Mass Spectrom. 1976, 4, 25-37.

75. Bakker, J. M. B. Adv. Mass Spectrom. 1971, 5, 278-282.

76. Bakker, J. M. B. Int. J. Mass Spectrom. Ion Phys. 1971, 6, 291-295.

77. Moorman, C. J.; Parmater, J. Q. U.S. Patent 3 576 992, 1971.

78. Poschenrieder, N. P. U.S. Patent 3 863 068, 1975.

79. Nose, N. Shitsuryo Bunseki, 1983, 31, 165-172.

80. Poschenrieder, W. P. Int. J. Mass Spectrom. Ion Phys. 1972, 9, 357-373.

81. Kilius, L. R.; Hallin, E. L., Chang, K. H.; Litherland, A. E. Nucl. Instrum. Methods Phys. Res. 1981, 191, 27-33.

82. Carrico, J. Phys. E. 1977, 10, 31-36.

83. Nishikawa, O.; Kurihara, K.; Nachi, M.; Konishi; Wada, M. Rev. Sci. Instrum. 1981, 52, 810-818.

84. Bakker, J. M. B.; Freer, D. A.; Todd, J. F. J. Dyn. Mass Spectrom. 1981, 6, 91-110.

85. Poschenrieder, W. P.; Oetjen, G.-H. J. Vac. Sci. and Technol 1972, 9, 212-215.

86. Poschenrieder, W. P. Int. J. Mass Spectrom. Ion Phys. 1971, 6, 413-426.

87. Firk, F. W. K. Nucl. Instrum. Meth. 1979, 162, 539-563.

88. Eubank, H. P.; Wilkerson, T. D. Rev. Sci. Instrum. 1963, 34, 12-18.

89. Wood, R. M.; Edwards, A. K.; Steuer, M. F. Rev. Sci. Instrum. 1976, 47, 1471-1474.

90. Warmack, R. J.; Stockdale, J. A. D.; Compton, R. N. Int. J. Mass Spectrom. Ion Phys. 1978, 27, 239-247.

91. Warmack, R. J.; Stockdale, J. A. D.; Compton, R. N. J. Chem. Phys. 1978, 68, 916-925.

92. Betts, R. R. Nucl. Instrum. Meth. 1979, 162, 531-538.

93. Volkov, V. V. Nucl. Instrum. Meth. 1979, 162, 623-636.

94. Purser, K. H.; Litherland, A. E.; Gove, H. E. Nucl. Instrum. Meth. 1979, 162, 637-656.

95. Artukh, A. G.; Avdeichikov, V. V.; Ero, J.; Gridnev, G. F.; Mikeev, V. L.; Volkov, V. V. Nucl. Instrum. Meth. 1970, 83, 72-76.

96. Su, C. S. Nucl. Instrum. Methods Phys. Res., Sect. A. 1984, 220, 431-432.

97. Eloy, F.; Unsold, E. U.S. Patent 4 322 629, 1982.

98. Bykovskii, Yu. A.; Dorofeev, V. I.; Dymovich, V. I.; Nikolaev, B. I.; Ryzhikh; Sil'nov, S. M. Sov. Phys.-Tech. Phys. (Engl. Transl.) 1969, 13, 986-988; Zh. Tekh. Fiz. 1968, 38, 1194-1196.

99. Bykovskii, Yu. A.; Basova, T. A.; Belousov, V. I.; Gladskoi, V. M.; Gorshkov, V. V.; Degtyarev, V. G.; Laptev, I. D.; Nevolin, V. N. J. Anal. Chem. USSR (Engl. Transl.) 1976, 31, 1528-1530; Zh. Anal. Khim. 1976, 31, 2092-2096.

100. Bykovskii, Yu. A.; Vasil'ev, N. M.; Degtyarenko, N. N.; Nevolin, V. N. Sov. Phys.-Tech. Phys. (Engl. Transl.) 1973, 17, 1397-1399; Zh. Tekh. Fiz. 1972, 42, 1749-1751.

101. Tonon, G.; Rabeau, M. Plasma Phys. 1973, 15, 871-882.

102. Kovalev, I. D.; Maksimov, G. A.; Suchkov, A. I.; Larin, N. V. Int. J. Mass Spectrom. Ion Phys. 1978, 27, 101-137.

103. Goforth, R. R. Rev. Sci. Instrum. 1976, 47, 548-552.

104. Fassett, J. D.; Travis, J. C.; Moore, L. J.; Lytle, F. E. Anal. Chem. 1983, 55, 765-770.

105. Hunt, W. W., Jr.; Huffman, R. E.; McGee, K. E. Rev. Sci. Instrum. 1964, 35, 82-87.

106. Hunt, W. W., Jr.; Huffman, R. E.; Saari, J.; Wassel, Q.; Betts, J. F.; Paufve, E. H.; Wyess, W.; Fluegge, R. A. Rev. Sci. Instrum.

107. Haddon, W. F.; McLafferty, F. W. Anal. Chem. 1969, 41, 31-36.

108. Fromont, M. J.; Johnsen, R. H. Int. J. Mass Spectrom. Ion Phys. 1970, 4, 235-249.

109. Knewstubb, P. F.; Reid, N. W. Int. J. Mass Spectrom. Ion Phys. 1970, 5, 361-380.

110. Ryan, P. W.; Futrell, J. H.; Vestal, M. L. Chem. Phys. Lett. 1973, 18, 329-332.

111. Boesl, U.; Neusser, H. J.; Weinkauf, R.; Schlag, E. W. J. Phys. Chem. 1982, 86, 2857-2863.

112. Dugger, D. L.; Kiser, R. W. J. Chem. Phys. 1967, 47, 5054-5061.

113. Ferguson, R. E; McCulloh, K. E.; Rosenstock, H. M. J. Chem. Phys. 1965, 42, 100-106.

114. Nose, N. Shitsuryo Bunseki 1983, 31, 173-182.

115. Nose, N. Shitsuryo Bunseki 1983, 31, 183-188.

116. Pinkston, J. D. Ph.D. Dissertation, Michigan State University, East Lansing, Michigan, in progress.

117. Gandy, R. M.; Ampulski, R.; Prusaczyk, J.; Johnsen, R. H. Int. J. Mass Spectrom. Ion Phys. 1977, 24, 363-371.

118. Glish, G. L.; Goeringer, D. E. Anal. Chem. 1984, 56, 2291-2295.

119. Paulson, J. F.; Dale, F.; Studniarz, S. A. Int. J. Mass Spectrom. Ion Phys. 1970, 5, 113-126.

120. Knewstubb, P. F.; Field, D. Int. J. Mass Spectrom. Ion Phys. 1971, 6, 45-55.

121. Kunihiro, F.; Naito, M.; Naito, Y.; Kammei, Y.; Itagaki, Y.; presented at the 32nd Annual Conference on Mass Spectrometry and Allied Topics, San Antonio, TX, May 27-June 1, 1984, bound volume pp. 523-524.

122. Enge, H. A.; Betz, H. D.; Buechner, W. W.; Grodzins, L.; Moore, W. H.; Kanter, E. P. Nucl. Instrum. Meth. 1971, 97, 449-457.

123. VanBreemen, R. B.; Snow, M.; Cotter, R. J. Int. J. Mass Spectrom. Ion Phys. 1983, 49, 35-50.

124. Burgess, D. R., Jr.; Hussla, I.; Stair, P. C., Viswanathan, R.; Weitz, E. Rev. Sci. Instrum. 1984, 55, 1771.

125. VanPuymbroek, J.; Gijbels, R.; Viczian, M.; Cornides, I. Int. J. Mass Spectrom. Ion Phys. 1984, 56, 269-280.

126. Lifshitz, C. Mass Spectrom. Rev. 1982, 1, 309-348.

127. Lifshitz, C.; Goldenberg, M.; Malinovich, Y.; Peres, M. Int. J. Mass Spectrom. Ion Phys. 1983, 46, 269-272.

128. Mohan, V. K.; Tong, T. B. J. Chem. Phys. 1983, 79, 4271.

129. Sloane, T. M.; Ratcliffe, J. W. Combust. Sci. Technol. 1983, 33, 65-74.

CHAPTER II

THEORETICAL PRINCIPLES

The theoretical principle of time-resolved ion momentum spectrometry are derived from a combination of the theories describing magnetic sector and time-of-flight mass spectrometry. This chapter presents the mathematical basis for the principles of operation of the instrument: ion separation, mass assignment and achievement of the various types of MS/MS scans.

Mass Assignment

Stable Ions

Time-of-flight instruments. For any mass spectrometer in which the ions are accelerated out of the source, the energy of the ions, E, is determined by Equation 1, where m is the ion mass, v is the ion

$$E = 1/2mv^2 = zeV + E_i = qV + E_i \qquad (1)$$

velocity, z is the number of charges on the ion, e is the electronic charge, q is the charge on an ion (q = ze), V is the potential difference through which the ion is accelerated, and E_i is the initial energy of the ion. The number of charges, z, is assumed to be +1 throughout this work. The magnitude of the initial energy contribution is usually much smaller than qV. Equation 1 does not take into account

37

that fact that ions do not usually start from a single plane, i.e., that V may not be identical for all ions. Equation 1 can be rewritten to show ion velocity as a function of energy, Equation 2.

$$v = \left(\frac{2E}{m}\right)^{1/2} = \left(\frac{2qV+E_i}{m}\right)^{1/2} \tag{2}$$

A pulse or packet of nominally monoenergetic ions can be produced (assuming $z = 1$) either by pulsing the accelerating voltage or deflecting the ion beam in a time-of-flight mass spectrometer. As Equation 2 shows, after acceleration, the velocity of any ion is inversely proportional to the square root of its mass. As the accelerated ions travel through space, they separate according to mass, the lightest ions traveling fastest. The velocity of each ion can be determined by measuring the time, t, necessary for the ion to reach a detector situated at a fixed distance, d, from the pulse origin, as given by Equation 3.

$$t = d/v \tag{3}$$

Substitution of Equation 2 into Equation 3 yields Equation 4 -- an

$$m = \frac{2Et^2}{d^2} \tag{4}$$

expression relating the mass-to-charge ratio of an ion to its flight time. The traditional relationship for mass determination in a time-of-flight mass spectrometer (1), Equation 5, is obtained by

$$\frac{m}{q} = \frac{2Vt^2}{d^2} \tag{5}$$

substituting qV for E, which, from Equation 1 assumes that E_i is negligibly small. In reality, ions do have initial translational energies, and this initial energy term leads to a degradation in resolving power. For some ionization processes such as laser desorption (6), ions can have considerable initial energy that results in severely degraded resolution. This model also does not take into account that fact that ions usually do not start from a single plane, nor do they undergo instantaneous acceleration to their final velocities. These secondary factors are considered in detail in Chapter 5.

Magnetic sector instruments. Ions traveling in a uniform magnetic field experience a centripetal force that disperses them along various arcs according to their momenta. The radius is related to the momentum by Equation 6, where B is the magnetic field strength and r is the

$$mv = Bqr \qquad (6)$$

radius of each ion's circular path. Combining Equations 2 and 6 to eliminate v gives an expression for mass assignment in a magnetic sector instrument, Equation 7 (2). Again, assuming that E_i is

$$m = \frac{B^2 r^2 q^2}{2E} \qquad (7)$$

negligibly small, Equation 7 can be rewritten as Equation 8, the common

$$\frac{m}{q} = \frac{B^2 r^2}{2V} \qquad (8)$$

expression for mass assignment in a magnetic sector instrument.

Unfortunately, as with the time-of-flight measurement, the E_1 contribution is small but finite. One of the main limitations of resolution in conventional magnetic sector mass spectrometers is the minor spread in ion energies.

TRIMS instruments. Simultaneous measurement of the ion momentum with a magnetic sector and measurement of the ion velocity with a time-of-flight measurement is another method of determining ion mass. Combining Equations 3 and 6 gives Equation 9, the mass assignment

$$\frac{m}{q} = Bt\left(\frac{r}{d}\right) \tag{9}$$

function for ions in the TRIMS instrument (3). The combination of a momentum analyzer and a velocity analyzer produces a mass-to-charge ratio that is independent of the ion energy. In effect, the velocity contribution to the mass assignment cancels. Thus, the combination of magnetic sector and time-of-flight mass analyzers produces an instrument with potentially higher resolution than that attainable by either analyzer alone.

Parent and Daughter Ions

An important consequence of the energy-independent mass determination is the ability to accurately assign mass for stable ions as well as ions which change mass in the field-free region between the ion acceleration region and the magnetic sector. This fact can be exploited to perform experiments normally done by mass

spectrometry/mass spectrometry.

Consider Figure 2.1 which shows the metastable decomposition of acetyl salicylic acid (aspirin) to form the salicylic acid daughter ion by loss of a neutral ketene molecule. The mass, kinetic energy, and momentum of the daughter ion are all lower than those of the parent but the velocity remains very nearly the same. The stable ion mass 138 formed in the ion source, on the other hand, has higher kinetic energy, velocity, and momentum than any daughter ion of the same mass. These differences in mass and velocity form the basis for separation of parent and daughter ions in TRIMS.

A daughter ion, m_2^+, can arise from either unimolecular decay or collisionally activated dissociation occurring in the field-free region preceding the magnet, according to Equation 10. It will be transmitted

$$m_1^+ \longrightarrow m_2^+ + m_3^+ \tag{10}$$

to the detector when the field strength corresponds to its momentum. The combination of magnetic field strength and arrival time can be used to make an accurate mass assignment according to Equation 9. Thus, masses of all stable and daughter ions will be determined accurately by the combination of momentum and velocity. The velocity of a daughter ion will be nearly the same as that of its precursor (parent) ion since the release of kinetic energy in the fragmentation process alters the velocity only slightly (4). Hence, the use of the measured flight time of the daughter ion can be used in Equation 5 to identify the mass of

Aspirin
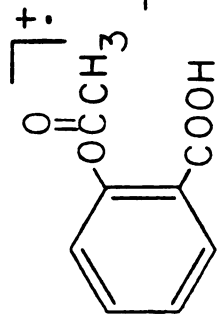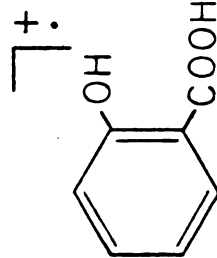
parent ion	daughter ion	neutral loss

parent ion: structure with OCCH$_3$ (O double bond) and COOH, charged +·

daughter ion: structure with OH and COOH, charged +·

neutral loss: $H_2C=C=O$

parent ion
mass=180.0
k.e.=3500eV
vel.=61,240m/s
mom.=1.102x10^7

daughter ion
mass=138.0
k.e.=2683eV
vel.=61,240m/s
mom.=8.450x10^6

neutral loss
mass=42.0
k.e.=817eV
vel.=61,240m/s
mom.=2.572x10^6

stable ion mass = 138.0
k.e.=3500eV
vel.=69,940m/s
mom.=9.652x10^6

Figure 2.1. Changes in the characteristics of the aspirin molecular ion following metastable decomposition.

the parent from which the daughter originated.

For comparison, ions that dissociate in the field-free region of a conventional time-of-flight mass analyzer appear at the same arrival time as the parent ion mass. The daughter mass is not readily identified. In contrast, ions that dissociate in the field-free region (between the acceleration lens and the magnet) of a conventional magnetic sector instrument do not appear at either the parent or daughter mass, but rather at an "apparent mass," m^*, given by Equation 11 (4). This equation can be derived by combination of Equations 2, 6,

$$m^* = m_2^2/m_1 \qquad (11)$$

and 8, considering that the mass in Equation 2 is m_1 when the ion is accelerated out of the source, the mass in Equation 6 is m_2 when the ion is analyzed by the magnetic sector, and the mass in Equation 8 is m^* for the mass normally calculated from B and V. The apparent mass m^* will be used in subsequent chapters when discussing mass calibration along the momentum axis for TRIMS.

Ion Energy Determination

In addition to the mass-to-charge ratio, it is also helpful at times to be able to measure the energy-to-charge ratio. This value would be useful for stable ions with non-constant energy, such as those formed in nuclear experiments (5) or by laser desorption (6). It would also be helpful for measuring the energy spread of daughter ions due to kinetic energy release in ion dissociation processes (4).

The energy of an ion in a TRIMS instrument is given by Equation 12. This equation is derived from Equation 1 by substitution of Equations 3 and 6.

$$\frac{E}{q} = \frac{B}{t} \left(\frac{rd}{2} \right)$$

(12)

The measurement of B and t in a TRIMS instrument, then, provides the mass-to-charge ratio and energy-to-charge ratio for all ions reaching the detector, whether they are stable ions or daughter ions. In addition, for daughter ions, the parent ion mass-to-charge ratio is also determined from the daughter ion arrival time using Equation 5.

Magnetic Field Strength - Arrival Time (B-t) Data Field

Location of Stable and Daughter Ions

In order to understand how MS/MS data can be obtained, it is helpful first to visualize where the ions would be located in the magnetic field-flight time (B-t) data field. Figure 2.2 is a computer generated plot of the B-t data field for an instrument with V=3500 V, d=1.0 m, r=0.2 m. Each location on the plane represents the field and time values at which a specific ion would be found. For instance, all daughter ions of the same parent mass will have identical velocity and time-of-flight according to Equation 5. This is shown by a vertical line for all daughters of parent mass 400. Likewise, all daughter ions of the same mass but derived from different parents will have the same value of B·t, according to Equation 9. The hyperbolic curves represent
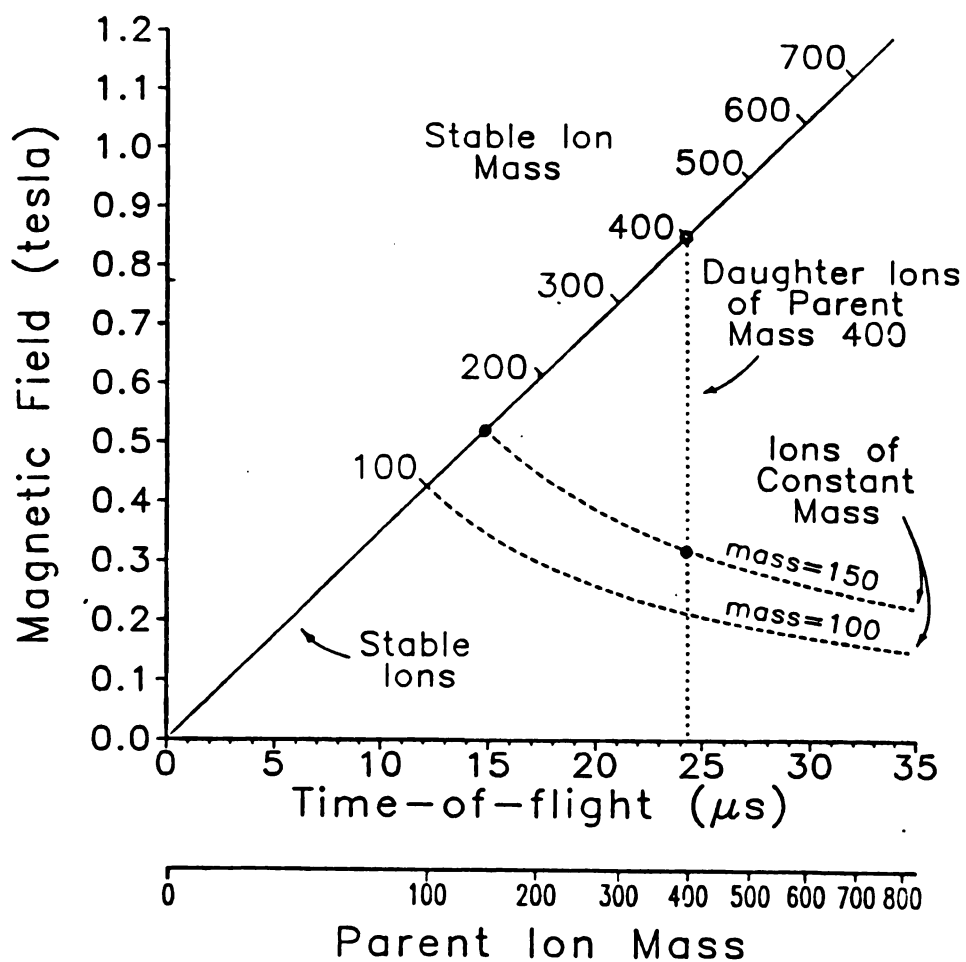
Figure 2.2. The B-t data field for TRIMS showing the expected
  locus of points for different types of ions.
  (Reprinted with permission from ref. 3. Copyright 1983
   American Chemical Society.)

ions of the same B·t product, mass 100 and mass 150 in this case. Stable ions appear at the point where the parent mass is equal to the daughter mass. They also all have the same nominal energy, 3500 eV. Thus, ions of the same energy are represented by a straight diagonal line starting at the origin, the slope determined by the energy according to Equation 12.

Since the correct mass is assigned for daughter and stable ions regardless of their energies, the TRIMS instrument could be used for mass analysis of ions that have widely varying energies. Equations 9 and 12 would provide the mass and energy, respectively, for any detected ion. Figure 2.3 shows the expected locus of points for two masses in the B-t data field (d=1.5 m, r=0.2 m). Several lines of constant energy are plotted to show how the position along a curve of constant B·t (constant mass) varies with energy.

The expected locations of various ions in the B-t data field are shown in more detail in Figure 2.4, this time for ions (accelerated to constant energy) in the molecular ion region of benzene. A conventional mass spectrum would show four ions at m/z 76, 77, 78, 79. These ions are shown for a magnetic sector instrument with no time resolution (y-axis), a time-of-flight instrument with no magnetic dispersion (x-axis), and for TRIMS (entire field). The molecular ion and its ^{13}C isotope show loss of hydrogen by metastable decomposition, $78^+ \longrightarrow 77^+ + H$ and $79^+ \longrightarrow 78^+ + H$. In a scan of a magnetic sector instrument with no time resolution, these metastable decompositions would appear as broadened peaks at apparent mass $m^* = 77^2/78 = 76$ and
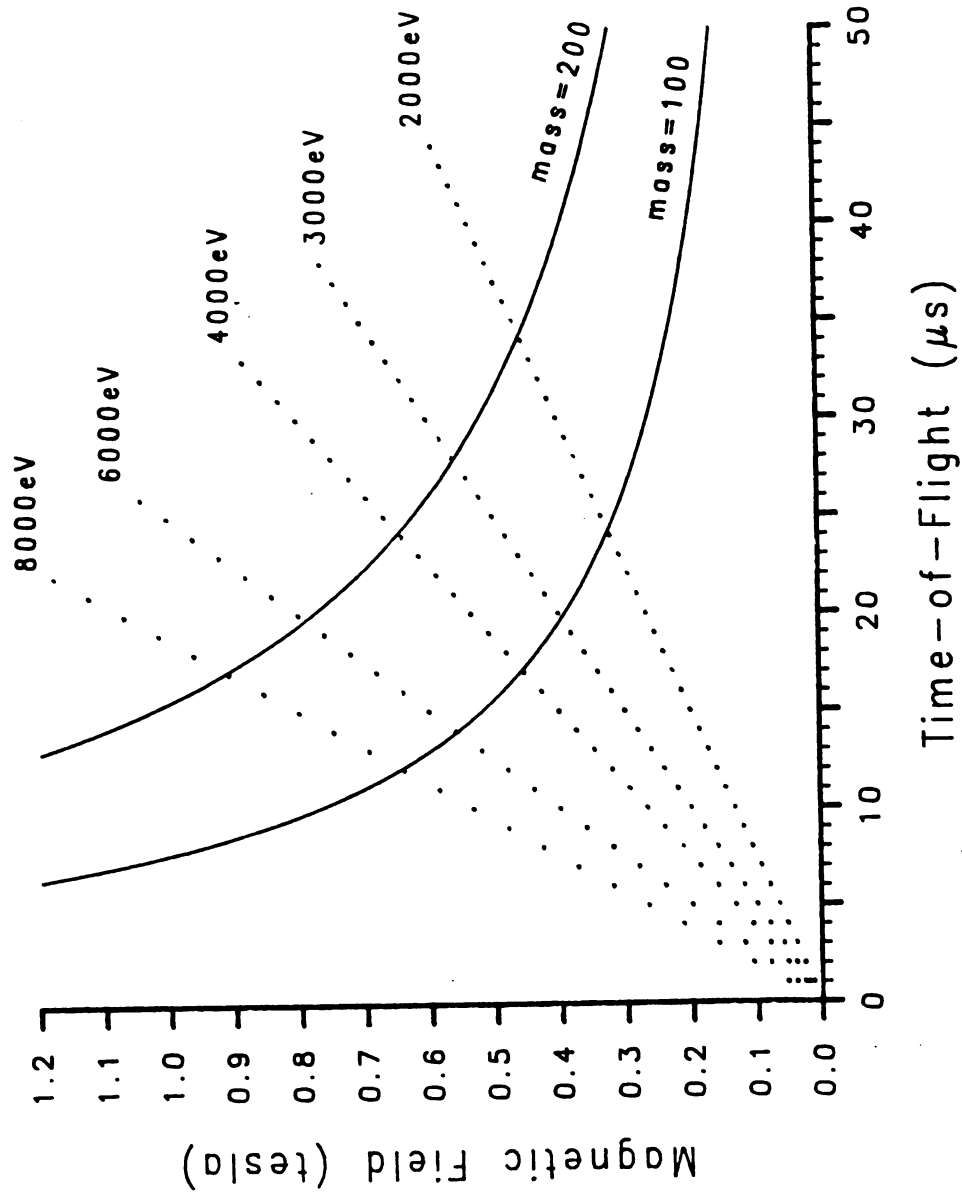
Figure 2.3. The B-t data field showing the expected locus of points for isobaric ions with different energies.
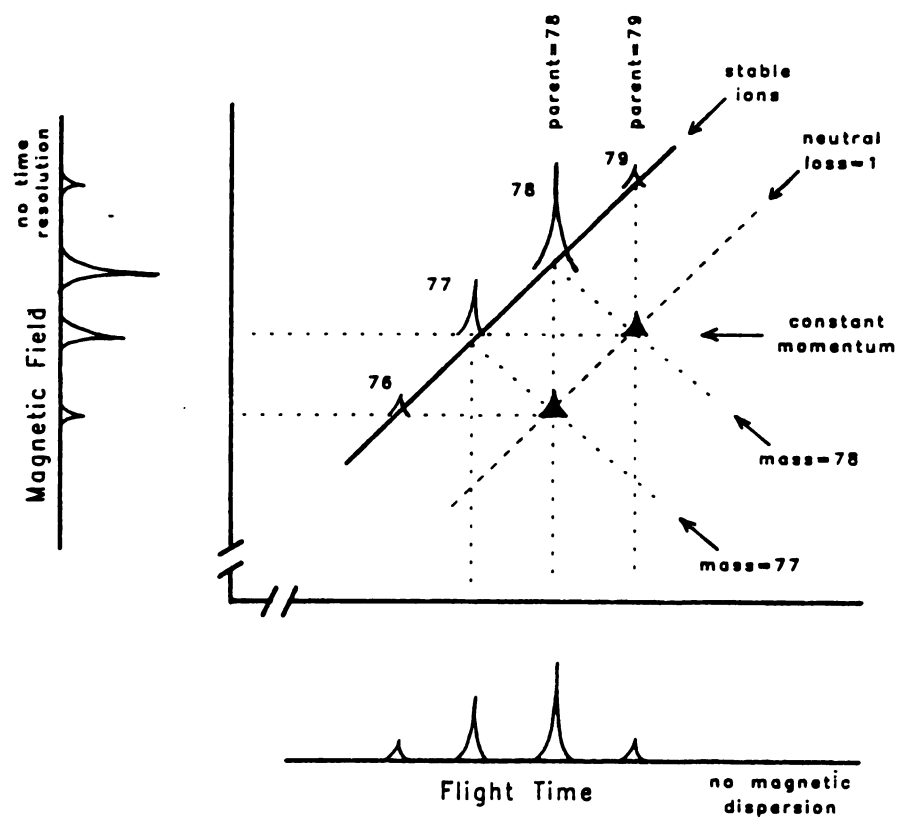
Figure 2.4. Expected location of ions in the B-t data
field for the molecular ion region of benzene.

$m^* = 78^2/79 = 77$, i.e., these metastable peaks would only contribute broadening to the stable ion peaks at m/z 76 and m/z 77. Similarly, in a scan of a time-of-flight instrument with no magnetic dispersion the metastable peaks appear at the same arrival time as the parent peaks, but broadened due to the energetics of dissociation. Thus, there is no clear differentiation of stable and daughter ions. However, the TRIMS instrument can resolve the daughter ions from the stable ions. The daughter ions appear at the same flight time as their parents, as shown in Figure 2.4 by the vertical lines. The daughter ions still appear at the field strength corresponding to their apparent mass as shown by the horizontal lines. They also appear at the same value of B·t as stable ions of the same mass as shown by the hyperbolic curves.

These data can be acquired either by individual MS/MS scans or by acquisition of the full data field with subsequent extraction of the desired data. Individual scans utilize a data acquisition technique called time-slice detection (TSD) (14): for each pulse of the ion source, only those ions detected during a single selected narrow slice of time are recorded. Full data field acquisition can also be accomplished by TSD or by time-array detection (TAD) (14): for each pulse of the ion source, ion current at all arrival times is recorded.

MS/MS Scans

Individual MS/MS scans are usually made: (a) when only a limited amount of information is desired for a sample, (b) when the sample is present for a period of time that is too short for full data field

acquisition, or (c) when the sample quantity is too small to allow full data field acquisiton. Figure 2.5 shows how the various MS/MS scans can be achieved using time-slice detection. A daughter scan (constant parent scan) is made by scanning the magnetic field while the ion arrival time window remains fixed at the arrival time of the selected parent ion, as shown in Figure 2.5a. The daughter mass is determined by the product $B \cdot t$. A parent scan (constant daughter scan) is made by selecting the value of $B \cdot t$ that corresponds to the selected daughter ion mass, then scanning both B and t in a linked fashion so that the product $B \cdot t$ remains constant. This scan is shown in Figure 2.5b. The parent mass is identified at any point by the flight time. The neutral loss scan (parent scan at constant neutral loss) is made by scanning the arrival time for a constant difference $m_3 = m_1 - m_2$. This is also a linked scan that follows Equation 13, derived by taking the difference of Equations 5 and 9. The scan is shown in Figure 2.5c. Again, the flight time identifies the parent mass.

$$m_3 = \frac{2Vet^2}{d^2} - \frac{Bter}{d} \tag{13}$$

A fourth scan, the stable ion scan, will produce a conventional mass spectrum of stable ions with all daughter ions eliminated. This could also be called a constant energy scan. As shown in Figure 2.5d, B and t are scanned in a linked fashion so that the quotient B/t remains constant according to Equation 12. Mass is identified by the product, $B \cdot t$.
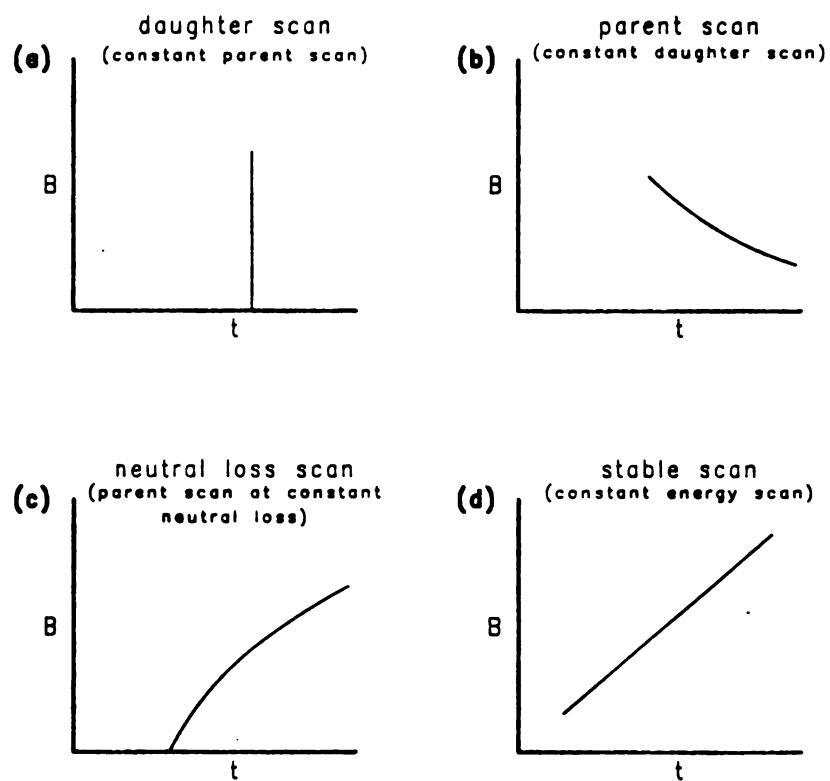
Figure 2.5. Expected location of ions in the B-t data field for different types of MS/MS scans.

Full Data Field Acquisition

Although a great deal of selectivity can be obtained with mass spectrometry/mass spectrometry, single MS/MS scans (e.g., a daughter scan of a particular parent) are sometimes insufficient for identifying a compound. Complex structure elucidation problems often require the maximum amount of spectral information available on a compound. For MS/MS this can mean measurement of all daughter ions of all parents — the entire data field. From this data matrix any mass spectral information could be extracted. Any type of scan could be reconstructed from the matrix of data points — parent, daughter, stable, and neutral loss. Deconvolution techniques could be used to separate poorly resolved peaks. Energy distributions for dissociation reactions could be measured. Overlapping peaks that might give rise to artifacts in a daughter scan could be eliminated. All this information would be available after the experiment; one would not be placed in the position of wishing that just one more measurement had been made.

Full data field acquisition, also called metastable mapping, has been used to a limited extent with multiple sector instruments (7-13). One of the potential advantages of TRIMS over other techniques is the speed with which the full data field could be obtained. In multiple sector instruments, either the magnetic or electric field is scanned rapidly, while the other sector is incremented between each scan. This process can take several minutes.

With TRIMS, a time-of-flight spectrum can be obtained every 100 us
or less. If the time-of-flight spectra could be collected at this
rate, a single scan of the magnetic field would produce the full data
matrix. For parent ions of mass 20-500, the full data matrix could be
obtained in just a few seconds even if several TOF spectra are averaged
at each increment of B. A computer system capable of this high speed
data acquisition is currently under development at MSU (14). With the
acquisition of the full data matrix for a compound in a matter of
seconds, GC/MS/MS and LC/MS/MS experiments would be greatly enhanced.
In addition, for less transient samples, the spectra could also be
further summed for improved sensitivity.

Alternate Modes of Operation

Accelerating Voltage Scans

The preceding discussion on scanning has been based on a constant
accelerating voltage. This is because most modern magnetic sector
instruments are set up for constant accelerating voltage operation. An
alternate method of operation in TRIMS would be to keep either the
magnetic field or the sampled flight time constant and use a variable
accelerating voltage. Mass assignment equations and scan laws are
similar to those derived for constant V. The different scanning
methods are summarized in Table 2.1.

TABLE 2-1. Parent and daughter scan methods
for constant V, B, or t.

	constant $\underline{V}$	constant $\underline{B}$	constant $\underline{t}$
Daughter Scan (constant parent)	scan B constant t	linked scan of V and t constant Vt^2	scan B constant V
Parent Scan (constant daughter)	linked scan of B and t constant $B \cdot t$	scan V constant t	scan V constant B

Scans of the accelerating voltage have been used with multiple sector instruments to achieve daughter scans (15-19). There would be one distinct advantage to scanning the accelerating voltage in TRIMS. Fixed magnets are smaller and require none of the control circuitry that scanning electromagnets need. Thus a much simpler instrument could be constructed, but performance would be compromised. The accelerating voltage can usually be varied over only a limited range and the ion source can become defocused as V is changed, resulting in a loss of resolution and sensitivity (20). In addition, detector response (21), CAD collision cross-sections (22), and the relative contribution of initial thermal energy all change with different ion energies.

Constant Momentum Acceleration

One further variation that is not possible with continuous ion beam instruments is constant momentum acceleration (23). This type of acceleration is achieved by switching the accelerating voltage off before any of the ions traverse the full acceleration field. The advantage of constant momentum acceleration is obtaining an ion flight time that is linear in mass, with a concomitant increase in resolution. However, the thermal energy distribution in the ion source has been shown to degrade resolution more for constant momentum acceleration than for constant energy acceleration in a conventional time-of-flight mass spectrometer (24).

In the TRIMS instrument, any ion energy spread for stable and daughter ions caused by constant momentum acceleration would not be a problem since resolution and mass assignment are independent of the ion energy. Thus linearization of the mass scale could improve the overall resolution of the TRIMS instrument for stable and daughter ions. Unfortunately, a decrease in the flight-time resolution with magnetic dispersion will decrease the ability to precisely assign the parent mass of any daughter ion, already one of the primary limitations of the technique. In addition, achievement of true constant momentum requires a very homogeneous acceleration region (25) which is difficult, if not impossible, to attain when multiple lenses are required in the ion source for proper ion optics in a magnetic sector instrument. Even when this is possible, Poschenrieder (26) has shown that constant momentum acceleration works best with inhomogeneous magnets. For these reasons, we have chosen to limit our initial experiments with TRIMS instrumentation to constant energy acceleration.

Summary

Time-resolved ion momentum spectrometry provides for the separation and measurement of stable ions and daughter ions, irrespective of ion energy, by simultaneous measurement of momentum and velocity. The parent-daughter ion relationship is provided by the daughter ion flight time. Any of the scans obtained with conventional MS/MS instruments can be obtained by TRIMS as well. Daughter ion scans are made by a simple scan of the magnetic field, keeping the sampled

arrival time constant. Other types of scans can be obtained by linked scanning of B and t. Each type of scan could also be reconstructed from an array of intensities if all combinations of B and t were collected. Time-array detection offers the potential for efficiently collecting the complete B-t data field for each sample.

Time-resolved ion momentum spectrometry, as a new technique for performing MS/MS experiments, is an additional tool for the chemist that complements already existing techniques, as will be demonstrated in the chapters that follow.

References

1. Wiley, W.C. Science 1956, 124, 817-820.

2. Barnard, G.P. "Modern Mass Spectrometry"; Institute of Physics: London, 1953, p. 23.

3. Stults, J.T.; Holland, J.F.; Enke, C.G. Anal. Chem. 1983, 55, 1323-1330.

4. Cooks, R.G.; Beynon, J.H.; Caprioli, R.M.; Lester, G.R. "Metastable Ions"; Elsevier: New York, 1973.

5. Purser, K.H.; Litherland, A.E.; Gove, H.E. Nucl. Instrum. Meth. 1979, 162, 637-656.

6. Wood, R.M.; Edwards, A.K.; Steuer, M.F. Rev. Sci. Instrum. 1976, 47, 1471-1474.

7. Warburton, G.A.; Stradling, R.S.; Mason, R.S.; Farncombe, M. Org. Mass Spectrom. 1981, 16, 507-511.

8. Kiser, R.W.; Sullivan, R.E.; Lupin, M.S. Anal. Chem. 1969, 41, 1958-1965.

9. Coutant, J.E.; McLafferty, F.W. Int. J. Mass Spectrom. Ion Phys. 1972, 8, 323-339.

10. Hwang, C.-S.; Kiser, R.W. Int. J. Mass Spectrom. Ion Phys. 1978, 27, 209-226.

11. Fraefel, A.; Seibl, J. Org. Mass Spectrom. 1982, 17, 448-450.

12. Farncombe, M.J.; Mason, R.S.; Jennings, K.R. Int. J. Mass Spectrom. Ion Phys. 1982, 44, 91-107.

13. Shannon, T.W.; Mead, T.E.; Warner, C.G.; McLafferty, F.W. Anal. Chem. 1967, 39, 1748-1754.

14. Holland, J.F.; Enke, C.G.; Allison, J.; Stults, J.T.; Pinkston, J.D.; Newcome, B.; Watson, J.T. Anal. Chem. 1983, 55, 997A.

15. Barber, M.; Elliot, R.M. Presented at the 12th Annual Conference on Mass Spectrometry, Montreal, June 1964.

16. Jennings, K.R. J. Chem. Phys. 1965, 43, 4176-4177.

17. Futrell, J.H.; Ryan, K.R.; Sieck, L.W. J. Chem. Phys. 1965, 43, 1832-1833.

18. Lacey, M.J.; MacDonald, C.G. J. Chem. Soc. Chem. Comm. 1975, 421-422.

19. Weston, A.F.; Jennings, K.R.; Evan, S.; Elliot, R.M. Int. J. Mass Spectrom. Ion Phys. 1976, 20, 317-327.

20. Sweeley, C.C.; Holland, J.F.; Young, N.D.; Blaisen, R.B. Presented at the 22nd Annual Conference on Mass Spectrometry and Allied Topics, Philadelphia, PA, May 19-24, 1974.

21. LaLau, C. In "Advances in Analytical Chemistry and Instrumentation"; Burlingame, A.L., Ed.; Wiley-Interscience: New York, 1970; Vol. 8, pp. 93-120.

22. Yamaoka, H.; Dong, P.; Durup, J. J. Chem. Phys. 1969, 51, 3465-3476.

23. Wolff, M.M.; Stephens, W.E. Rev. Sci. Instrum. 1953, 24, 616-617.

24. Katzenstein, H.S.; Friedland, S.S. Rev. Sci. Instrum. 1955, 26, 324-327.

25. Poschenrieder, W.P. U.S. Patent 3 863 068, 1975.

26. Poschenrieder, W.P. Int. J. Mass Spectrom. Ion Phys. 1971, 6, 413-426.

CHAPTER III

INSTRUMENTATION

Any magnetic sector mass spectrometer should be adaptable to time resolved ion momentum spectrometry by pulsing its ion beam and time-resolving the detected signal. In fact, one of the advantages of TRIMS is the possibility of retrofiting existing magnetic sector instruments to make MS/MS available at a reduced cost. The goal for this first implementation of TRIMS is to achieve optimal resolution and sensitivity by simple and inexpensive modification of a single magnetic sector instrument while maintaining the instrument's ability to function as a conventional mass spectrometer. This chapter describes the instrument, the modifications that have been made to it, and the data system that is used for instrument control and data acquisition.

The Instrument

Time-resolved ion momentum spectrometry has been implemented on an LKB-9000 gas chromatograph-mass spectrometer (GC-MS). A relatively old but functional magnetic sector instrument was chosen, mainly because of its availability, but also because the instrument has a relatively long flight path and the accelerating voltage is fairly high for an older instrument.

Without any modifications, the LKB-9000 GC-MS is a single sector instrument with a 60° magnetic sector, radius = 0.2 m, accelerating

voltage = 3500 V, and flight distance from entrance slit to the exit slit = 1.0 m. The mass range at full accelerating voltage is approximately 800 daltons with a resolution $m/\Delta m$ = 1000 (10% valley definition) (1). The whole instrument is pumped by a single Edwards E04 diffusion pump (Edwards High Vacuum, Buffalo, NY). Inlets to the ion source allow the introduction of samples via direct insertion probe (DIP), heated gas inlet, or gas chromatograph (GC). A dual stage jet separator is used for the GC interface. A Hall effect probe is used to measure the magnetic field strength. The ion detector is a discrete dynode electron multiplier.

Modifications to the instrument have included addition of a new detector, a flight tube extension, an additional diffusion pump, a collision cell, and ion source pulsing circuitry. The modified instrument is shown schematically in Figure 3.1. These modifications are described below.

Ion Beam Pulsing

In order to measure the flight-time of the ions, a very brief packet of ions must be created. A number of different approaches were taken to achieve the best resolution and sensitivity. Regardless of the method, it is essential to maintain the ion optics of the magnetic sector instument so as not to destroy the magnetic field resolution.

Figure 3.2 is a scale drawing of the ion source region. Typical voltages applied to each of the lens are: ionization chamber = 3500 V,
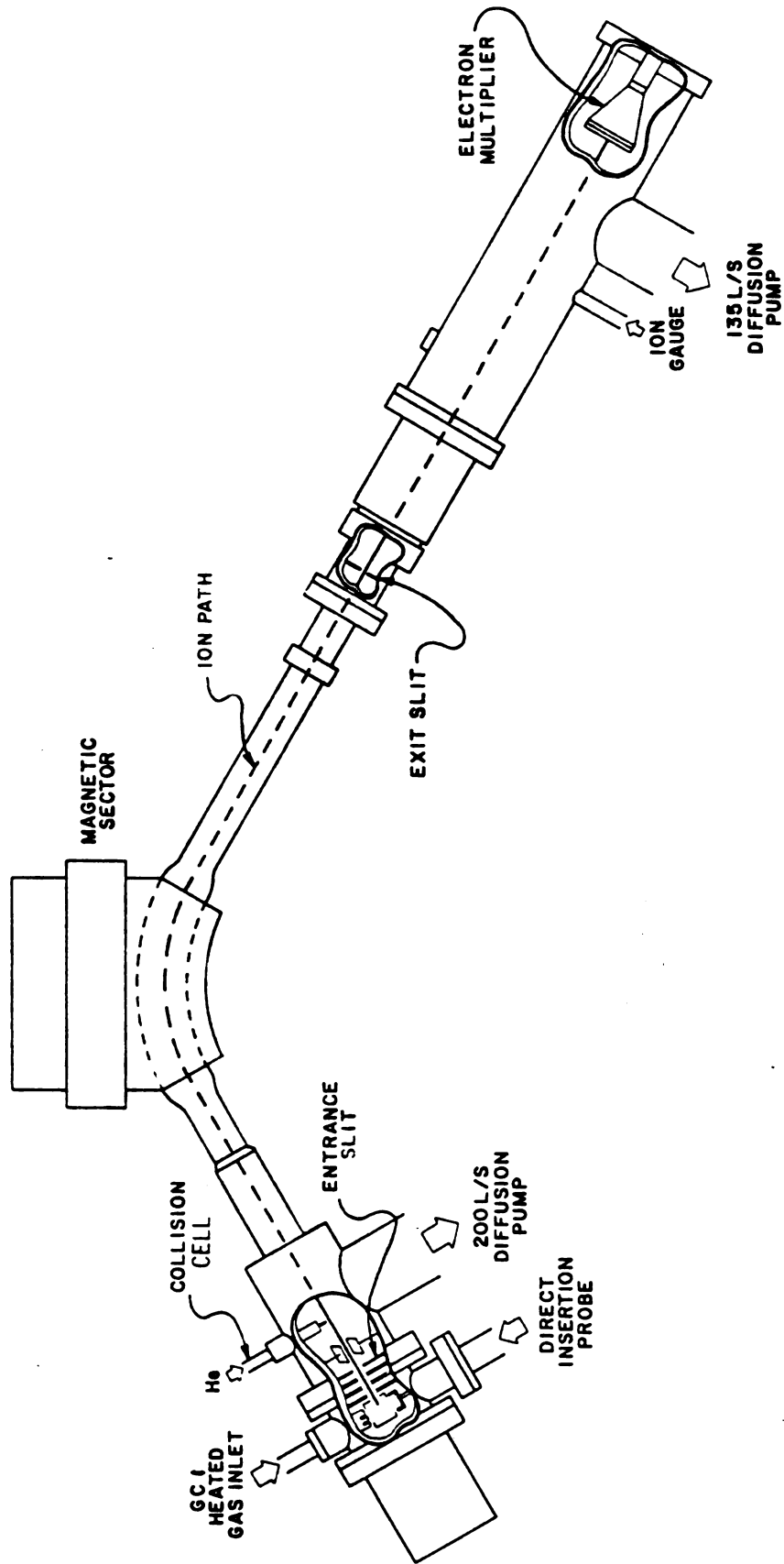
Figure 3.1. LKB-9000 modified for TRIMS by addition of a collision cell, flight tube extension, and CEMA detector.
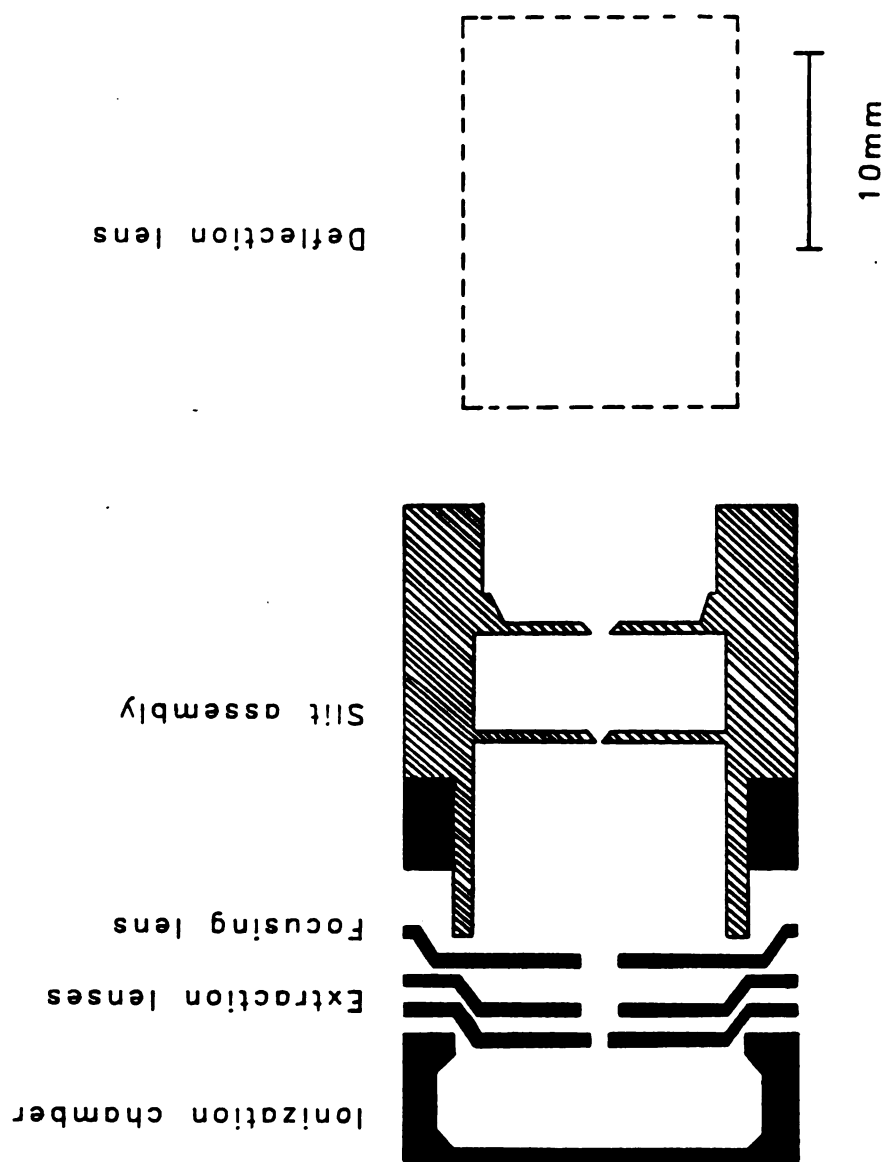
Figure 3.2. LKB-9000 ion source showing lens dimensions (to scale).

extraction lenses = 3485-3500 V, focusing lens = 1700-2900 V, deflection plates = 0-1200V. Not shown are the filament (3430 V), electron lens (3430 V), and the electron trap (3550 V).

The initial attempt at ion pulsing was to deflect the ion beam after full acceleration by following the method of Bakker (2,3). The ion beam deflection plates, located immediately after the entrance slit and normally used for focusing, were used to deflect the ion beam rapidly across the exit slit and thus produce a packet of ions (4). As shown in Figure 3.3, each deflection plate was connected to a separate high voltage dc power supply. After the voltage on each plate was adjusted to give maximum ion beam focus, a 50 V peak-to-peak square wave signal was superimposed on the voltage of one of the plates to deflect the ion beam. The circuit for generating the square wave is shown in Figure 3.4. The beam was deflected away from the exit slit during the HI and LO levels of the square wave so that only during a portion of the rising and falling edges of the square wave was the beam focused on the exit slit. The rising edge of the square wave signal was also used as a start time trigger for the time-resolved readout.

The poor time-of-flight resolution obtained with this approach led to a second method of pulsing, ion beam deflection in the ion source. One of the extraction lenses was biased positive with respect to the other extraction lens by a 9 V battery, thus deflecting the ion beam out of focus. An Avtech model AVI-V-N-A pulse generator (Avtech Electrosystems, Ltd., Ottawa, Ontario, Canada) capable of 0-50 V negative pulses, 5-100 ns variable pulse width, 5 ns rise and fall
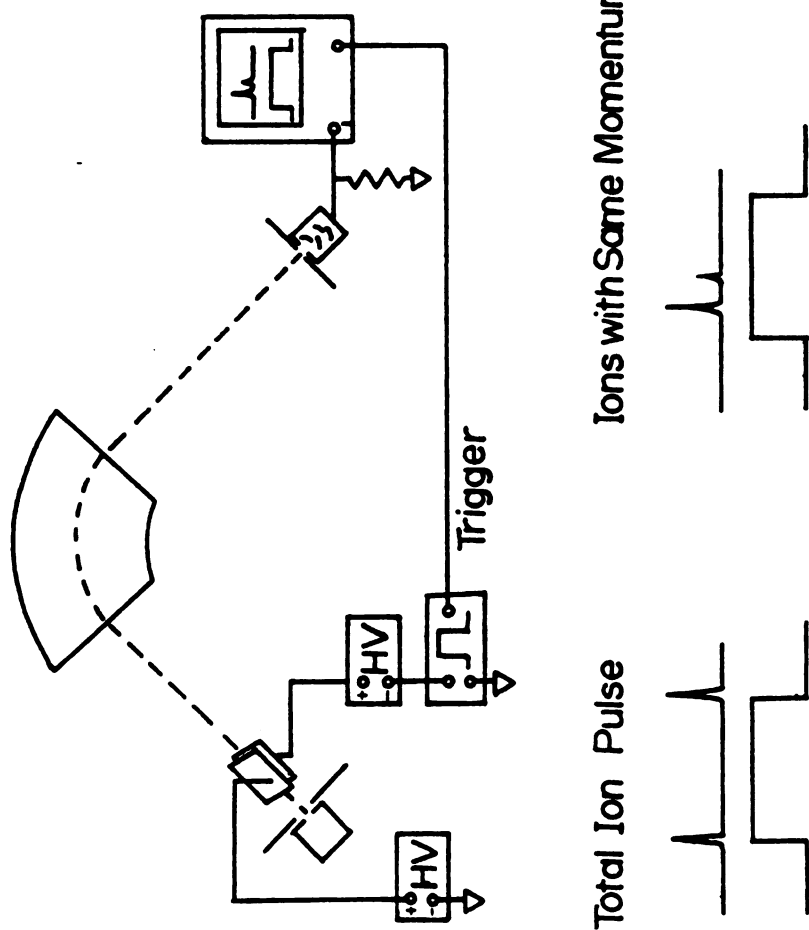
Figure 3.3. Ion pulsing by beam deflection using the deflection plates of the LKB-9000.
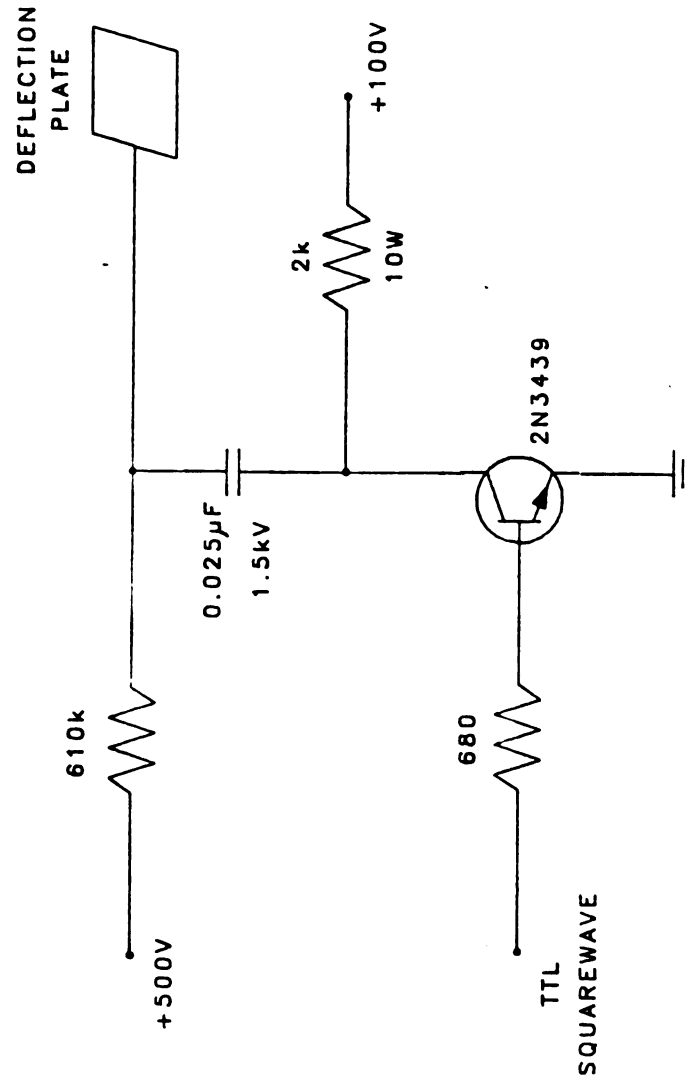
Figure 3.4. Schematic diagram of beam deflection circuit.

times, was electrically floated at the lens potential (see Figure 3.5). By adjusting the voltages so that the ion beam would be in focus when the pulse voltage was at its peak, a rapid pulse would produce a brief packet of ions. Although good resolution was observed with this method, sensitivity was severely limited by the duty cycle. In addition, the short pulse on the extraction lens did not strictly meet the criterion for constant energy acceleration: the field must be on until all the ions have traversed the full field.

A third method of pulsing utilized ion trapping and pulsed extraction (5). The negative space charge of the electron beam was used to trap ions after their formation (6,7). The electron beam was turned on and off by a deflection voltage applied to the electron lens that surrounds the filament. The deflection circuit is shown in Figure 3.6. A -15 V bias applied to the electron lens is sufficient to prevent electrons from entering the ion source. A +15 V pulse supplied by a Chronetics model PG-33 pulse generator (Chronetics, Mt. Vernon, NY) is then used to gate electrons into the ion source. A second pulsing circuit (designed and built by Marty Rabb, MSU Chemistry Department -- see Figure 3.7) puts a negative potential (with respect to the ionization box) on the extraction lenses to draw the positive ions quickly out of the source. The extraction lenses are connected together and biased slightly positive with respect to the ionization box to prevent ions from leaving the souce. The pulse is typically -100 V with a fall time (transition time on the leading edge) of 5 ns and duration of 4 µs. A Wavetek model 802 pulse generator (Wavetek, San Diego, CA) is used to drive this pulsing circuit.
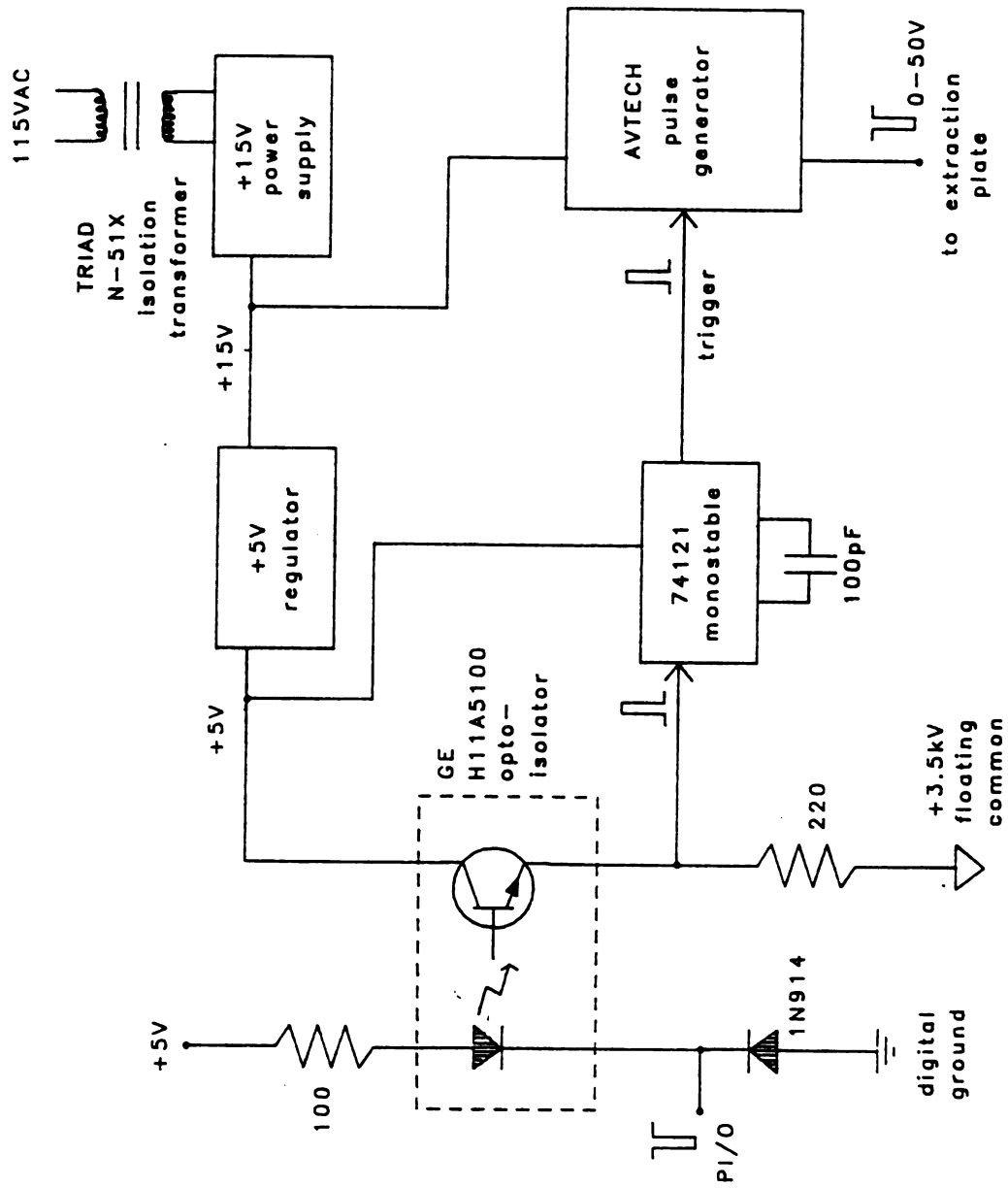
Figure 3.5. Schematic diagram of extraction plate pulsing circuit.
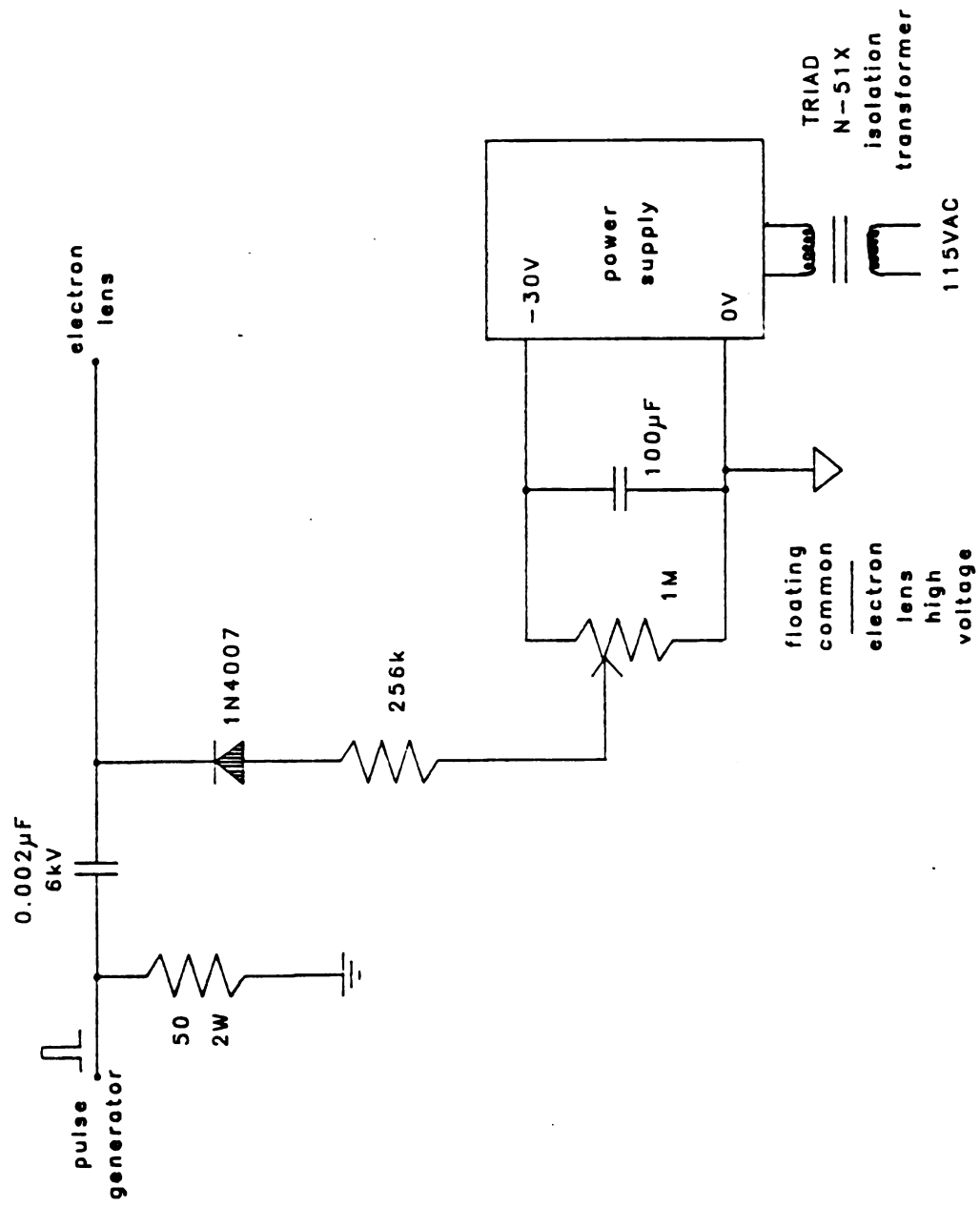
Figure 3.6. Schematic diagram of electron lens pulsing circuit.
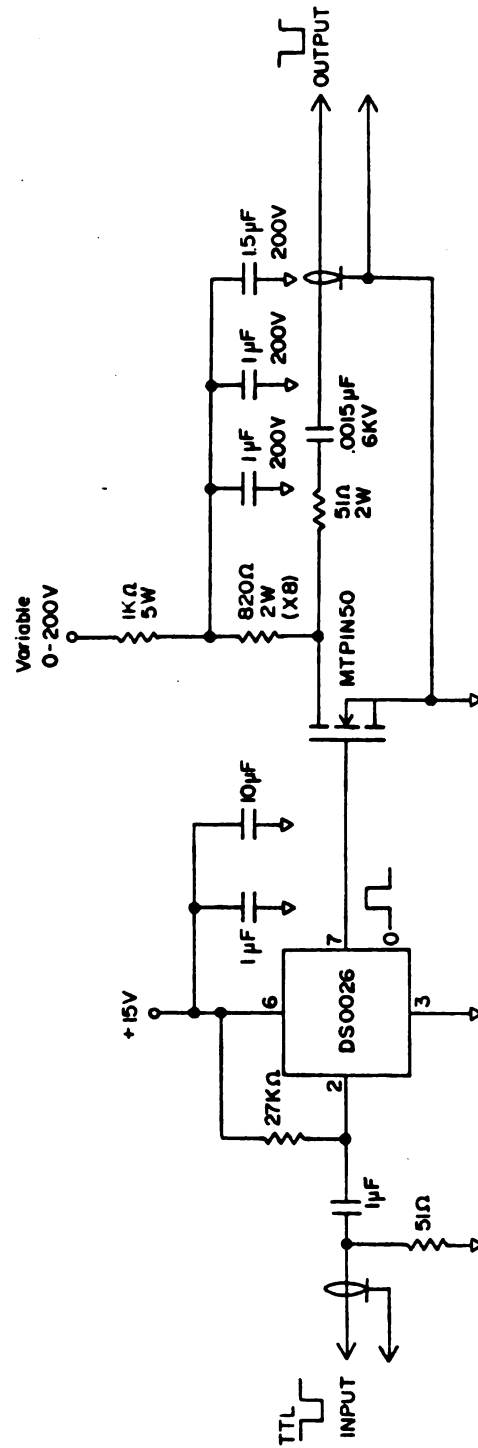
Figure 3.7. Schematic diagram of improved extraction plate pulsing circuit.

The earlier pulsing schemes all suffered from degraded pulse shapes due to improper cabling and the use of the original high-voltage vacuum feedthrus on the LKB-9000. Improved results were obtained by installing MHV feedthrus (Ceramaseal, Inc., New Lebanon Center, NY) very close to the ion source and positioning the pulsing circuits at the feedthru to minimize the cable distances.

The combination of electron lens gating and extraction lens pulsing can be operated in three ways. (a) If the extraction lens is biased to extract ions continuously, a rapid pulse of the electron beam will generate a packet of ions. (b) If the electron beam is left on continuously, the pulse on the extraction lens will accelerate the ions that were produced and stored since the last extraction pulse. In addition, the extraction lens pulse is sufficiently negative to deflect the electron beam and prevent ion formation during the extraction pulse (. The electron pulse can generate and store ions for a specified amount of time and then the extraction pulse can rapidly accelerate those ions out of the ion source. Each of these three ways has advantages in terms of resolution and sensitivity.

Ion Detection

A discrete dynode electron multiplier (RCA Electro-Optics, Princeton, NJ) was used initially for ion detection. It was located in the conventional position directly behind the exit slit. The conversion dynode is a curved surface that might lead to degraded resolution for time-of-flight measurements since different parts of the ion packet

could travel different distances. A channel electron multiplier array (CEMA) (8) was chosen because of its flat front surface. The CEMA used in this instrument is a Galileo FTD 2003 detector (Galileo Electro-optics Corp., Sturbridge, MA). This detector is actually two CEMA plates in a chevron configuration (9), with a special 50 ohm impedance anode and a BNC output jack. The detector is attached to a 6 in Conflat flange (Varian Vacuum Products Division, Lexington, MA) by a BNC-to-N adapter to a 50 ohm 'N'-type vacuum feedthru (Ceramaseal) that carries the signal out of the vacuum. The BNC-to-N adapter provides the necessary mechanical support for the detector. Voltages to the CEMA plates also enter the vacuum through the Conflat flange via four MHV feedthrus (Ceramaseal). The LKB multiplier voltage power supply was used with a simple resistor string voltage divider to produce the proper voltage ratios for the CEMA plates. Since the front CEMA plate is at a high negative voltage, a 70 mesh Nickel grid (Buckbee-Mears, St. Paul, MN) at ground potential was positioned 3 mm in front of the detector to maintain the field-free flight path in the instrument.

The current from the detector is terminated through a 50 ohm resistor to ground. The voltage across this resistor is amplified with a wideband Comlinear E103 non-inverting amplifier (Comlinear Corp., Loveland, CO) to produce a negative voltage that is subsequently measured with the time-resolving electronics. For non-time-resolved measurements, the current is sent into an op-amp current follower with a 10 Mohm feedback resistor.

The CEMA is positioned approximately 0.5 m from the exit slit. This position provides a longer flight path to improve the time-of-flight resolution and to allow the ion beam to spread radially. The exit slit is only a fraction of the size of the CEMA plate (1.5 in diameter). By allowing the beam to spread out, more of the surface of the CEMA is used, reducing the possibility of damaging some of the channels with large beam currents. The extended flight path also provides room for the placement of a diffusion pump in the detector region.

Collision Cell

A collision cell was added to the LKB-9000 to allow collisionally activated dissociation experiments to be performed. The simplest approach was a "collision needle" (10) by which a stream of gas is shot across the ion beam and into the throat of a diffusion pump. A 25 μl syringe was used, mounted through a 3/8 in Cajon Ultra-torr adapter (Cajon Co., Macedonia, OH). The syringe was placed directly above the ion beam, approximately 3 inches from the entrance slit. It is desirable to have the collision region as close as possible to the entrance slit in order to optimize the resolution by taking advantage of the focusing properties of the magnetic sector (11). Unfortunately, inadequate pumping speed plus the lack of differential pumping in the ion source region precluded the proper operation of the collision cell. Addition of a jacket around the collision needle to direct the collision gas toward the diffusion pump did not produce any better results.

The jacket was closed at the bottom to produce a collision cell, as shown in Figure 3.8. Now, rather than a stream of gas, a concentration of gas in the cell produces the collisions. The pumping system is only required to accomodate the "leakage" of gas into the instrument through the slit in the cell. Making the slits narrower (1/32 in) in the cell has further reduced the gas load on the system (12).

Vacuum System

The unmodified LKB-9000 used a single Edwards EO4 diffusion pump to evacuate the instrument. A separate Edwards EO2 diffusion pump and a mechanical pump were used to evacuate the inlet system. The flight tube extension provided room to mount an Edwards Diffstak to pump the detector region more adequately. The second pump is necessary because the exit slit has relatively poor gas conductance as does the magnetic sector region where the flight tube is constricted between the poles of the magnet.

Differential pumping of the ion source and collision regions would be desirable but the geometric constraints of the instrument prevent this from being easily done.

The pressure in the ion source region is measured with a CVC model GPH-100 Penning gauge (CVC, Inc., Rochester, NY) mounted just above the butterfly valve on the EO4 diffusion pump. The pressure in the detector region is measured with a Granville-Phillips model 274
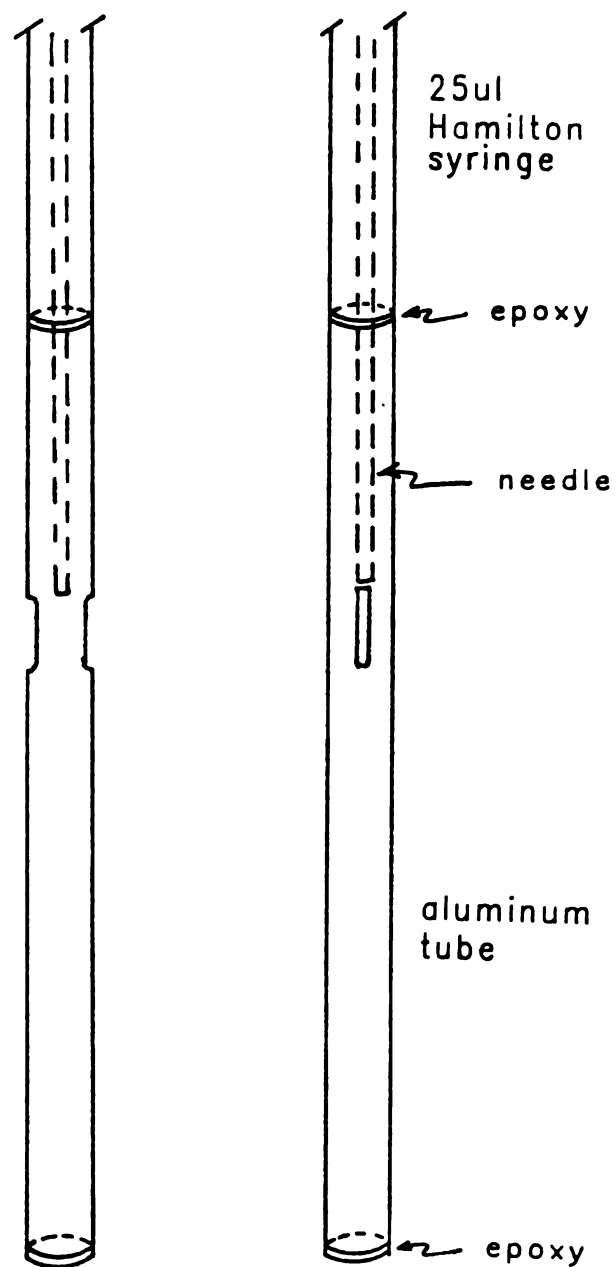
Figure 3.8. Collision cell diagram showing a sheathed "collision needle" (shown actual size).

ionization gauge and model 270 gauge controller (Granville-Phillips Co., Boulder, CO). The ionization gauge is mounted above the Diffstak pump, next to the detector, with a Cajon Ultra-torr adapter. This position is unfortunate because some of the ions formed by the ionization gauge make their way to the detector and cause a constant background at higher electron multiplier voltage settings. Therefore, the ionization gauge is not operated during experiments.

The backing pump pressure for the diffusion pumps is monitored with Granville-Phillips model 270006 thermocouple gauges which are also connected to the model 270 gauge controller. An LKB pirani gauge is used to measure the inlet system pressure.

Typical background vacuum in the instrument is 2×10^{-7} torr as measured by the Penning gauge and 8×10^{-8} torr as measured by the ionization gauge. During operation with no collision gas, the Penning gauge remains below 10^{-6} torr and the ionization gauge remains below 10^{-7} torr. With collision gas, the Penning gauge may reach 5×10^{-5} torr and the ionization gauge 1×10^{-6} torr.

Data/Control System — Hardware

The complexities of modern instrumentation make computers a necessity, not just a convenient option, for control of experiments and acquisition of data. Most mulitidimensional or "hyphenated" techniques such as mass spectrometry/mass spectrometry rely quite heavily on

computer systems in order to optimize their performance. Time-resolved ion momentum spectrometry is no exception. Early experiments with TRIMS utilized either an oscilloscope or a PAR 162/164 boxcar integrator (Princeton Applied Research Corp., Princeton, NJ) for data acquisition. Simple experiments took hours and manual processing of the data required days. These results demonstrated that a data/control system is a necessity for rapid data acquisition and for performing linked scans by TRIMS. This section describes the data/control system that was developed for the TRIMS instrument (13,14).

Microcomputer System

The microcomputer system used for TRIMS was developed at MSU by Bruce Newcome (15) and has been implemented on a number of different instruments. The system is designed for maximum flexibility, ease of construction and modification, and minimal cost. An additional advantage of this system is the large amount of software that is already written for mass spectrometry applications (16-18).

Figure 3.9 is a block diagram showing the general features of the system. The microprocessor controls the ion source pulsing, the magnetic field setting, and the flight time at which ions are sampled. The dashed box in Figure 3.9 encloses the components of the LKB-9000. The delay generator and gated integrator form a digital boxcar integrator for time-resolved detection. The ion signal intensity and the magnetic field strength, as measured by the Hall probe, are
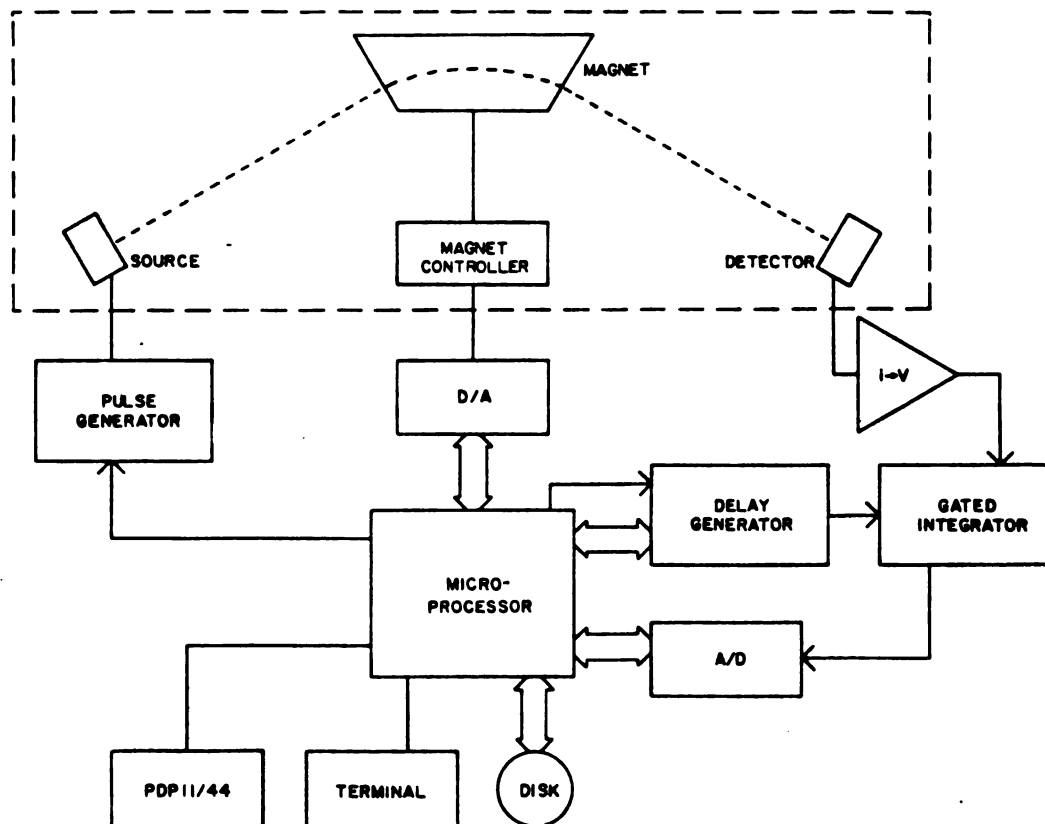
Figure 3.9. Block diagram of TRIMS data system. The LKB-9000 components are enclosed in the dashed box.

digitized by the analog-to-digital converter (ADC). A disk-drive, terminal, and serial communication link to a PDP11/24 minicomputer provide external communication and storage for the microcomputer.

A more detailed schematic of the system is shown in Figure 3.10. The central feature is the "Bruce-bus," located on a "motherboard," that provides access to all data, address, control, and power lines. Individual modules are added to the motherboard, each serving a specific function such as CPU, RAM, ADC, etc. A computer can thus be tailored to fit exactly the needs of a particular system by adding the needed modules. The computer can be further expanded by using several motherboards, interconnected via a backplane. The backplane also furnishes power to the system and connections to external devices. A listing of the modules used in the TRIMS system is given in Table 3.1.

The microprocessor is a 16-bit Intel 8088 (Intel Corp, Santa Clara, CA). An Intel 8087 math co-processor adds 64 bit hardware floating-point capabilities to the system. The operating system resides on 8 kbytes of EPROM. Programs and some data are stored on 40 kbytes of RAM. The peripherals and input/output devices are memory-mapped onto the remaining 16 kbytes of the basic 64 kbytes of memory space. An additional 16 kbytes of RAM are located in extended memory which can be accessed by changing the segment registers of the 8088. The extended memory is used for storing the mass-intensity pairs for each scan. Serial communication lines (RS-232, 9600 baud) are connected to a DEC VT-100 terminal and a PDP11/24 minicomputer. The VT-100 has graphics capabilities (Selenar Corp., Santa Clara, CA) and
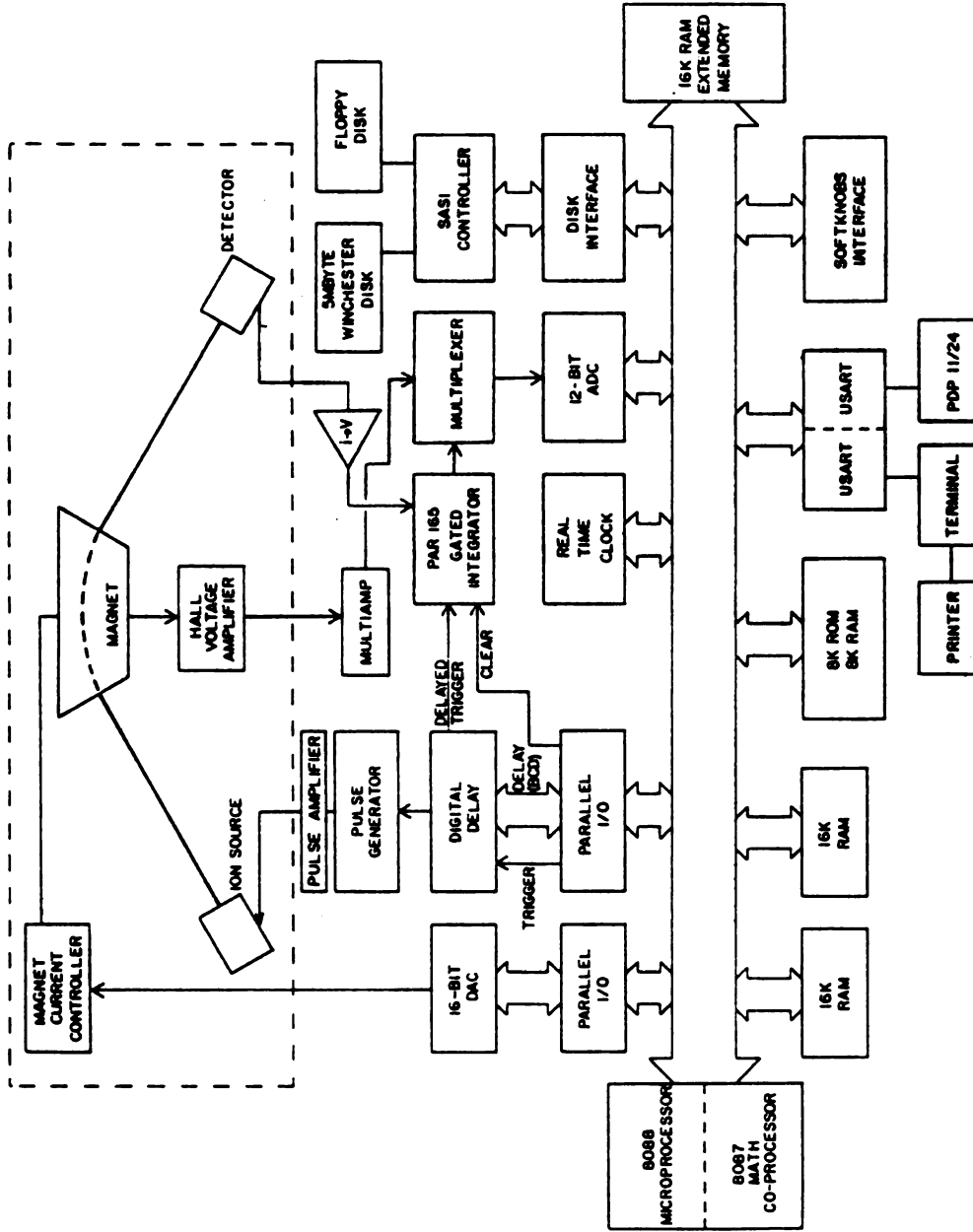
Figure 3.10. Detailed block diagram of the data acquisition/instrument control system for the TRIMS instrument. The LKB-9000 components are enclosed in the dashed box.

TABLE 3.1. Function modules used in the TRIMS data system.

module	IC
8088 CPU	8088, 8259A
8087 adapter	8087, 8288
RAM/ROM	TMM2016
Dual USART	8251A
Address Extender	––
Chip Select	––
SASI Interface	––
Parallel I/O	8255A
Softknobs Interface	––
12-bit ADC	AD574A
Real Time Clock	MM58167A
Active Terminator	––
16-bit DAC*	AD7546KN
Differential Multiplexer	AD7507KN
Multi-amp*	OP07, LM311

74LS TTL logic chips are used throughout

*Modules not mounted on a motherboard

hardcopy of the screen can be made with an Axiom EX-850 video printer (Axiom Corp., San Fernando, CA).

All data and programs are stored on a 5 Mbyte Seagate ST-506 Winchester disk (Seagate Technology, Scotts Valley, CA). Backup is made with a Shugart SA800 8 inch floppy disk drive (Shugart Assoc., Sunnyvale, CA). A DTC-S35 disk controller (Data Technology Corp., Bedford, MA) is interfaced to the computer bus via a SASI (Shugart Assoc. Standard Interface) disk interface module. A real-time clock provides time-intervals for various routines as well as dates and times. Two parallel input-output (PI/O) modules are used, one to drive the remote DAC and the other to set the delay time for the delay generator. An 8-channel differential multiplexer and 12 bit ADC are used to acquire the ion intensity from the gated integrator and to acquire the magnetic field strength from the Hall probe.

More detail of the data acquisition and instrument control subsystems will be given in the following sections.

Ion Source Pulsing

The pulsing circuits shown in Figures 3.6 and 3.7 are driven by the microcomputer and a pair of pulse generators. The circuit connections and a timing diagram are shown in Figure 3.11. A pulse from the microcomputer triggers the Wavetek pulse generator. The pulse generator delivers a sync pulse coincident with the trigger which serves to trigger the Chronetics pulse generator. The amplitude and
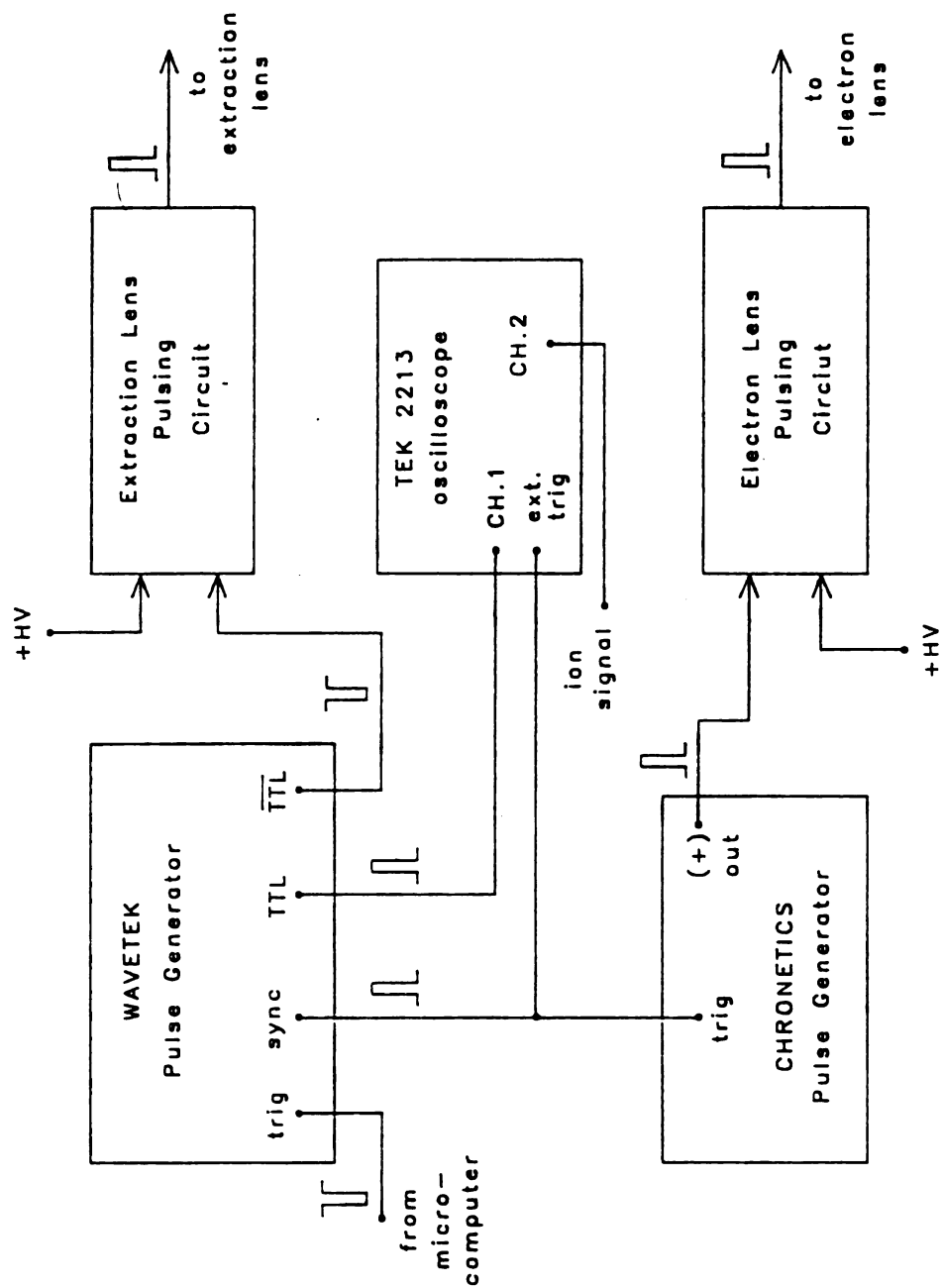
Figure 3.11.   Component connections for pulsing the ion source of the LKB-9000.

width of the pulse to the extraction lens are adjusted manually on the Chronetics pulse generator. The delay between the electron pulse and the extraction pulse is adjusted manually on the Wavetek pulse generator. The timing and pulse widths are adjusted while observing the ion signal on an oscilloscope.

Magnet Control

The magnet can be controlled either manually or by the computer. For digital control, a 16 bit DAC supplies a voltage to the magnet controller. The DAC board, shown schematically in Figure 3.12, is remote from the microcomputer and is optically isolated to provide noise immunity. The digital signal is sent through a PI/O board to the DAC. For convenience in focusing, the digital signal can be manually controlled by a set of "softknobs" (19). These are rotary shaft encoders (Panelcoder model 62, Disc Instruments, Costa Mesa, CA) that, through the softknobs interface, can change the digital value sent to the DAC.

The voltage from a Hall probe is used to measure the magnetic field strength. In order to obtain better resolution of the signal, a multiple amplifier board (19) is used to increase the range of the measurement. The multiamp board provides amplifications of x1, x2, and x4. A comparator on the output of each channel is used to determine which channels, if any, have reached the 10 V upper limit of the 12 bit analog-to-digital converter. The comparator outputs are queried by the microcomputer to determine which amplifier to read. By

85
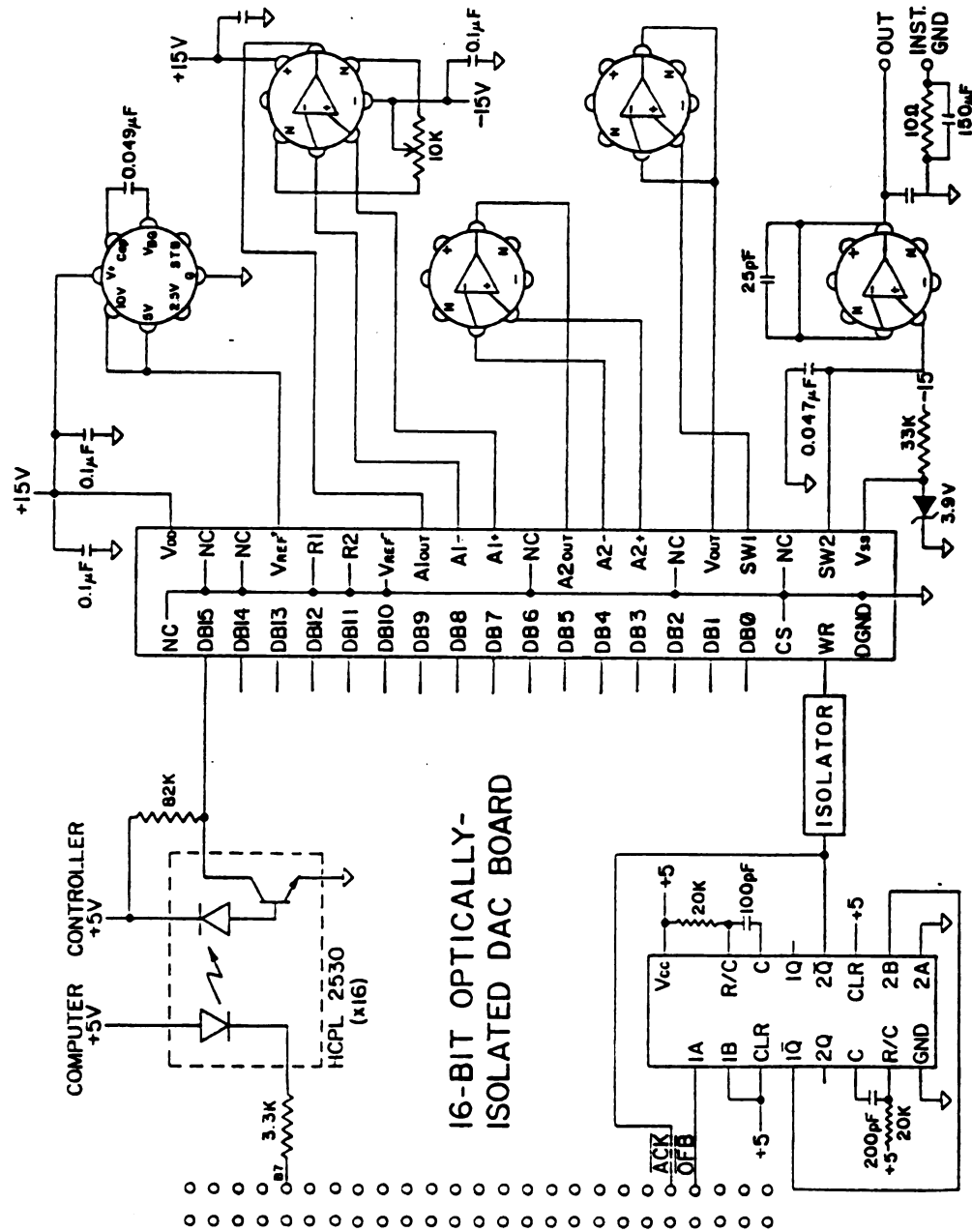
Figure 3.12.   Schematic diagram of 16-bit DAC board for magnet control in the LKB-9000.

this multiplexed technique, a larger dynamic range can be obtained.

The magnet control system can be used in two ways. For a scan, the magnet current can be continually incremented and the Hall voltage read whenever knowledge of the magnetic field strength is required, e.g., when a peak is detected. Alternatively, the Hall voltage can be read continuously as the magnet current is changed until a specified field strength is reached, in essence , a program-controlled feedback mechanism. This latter method could be used, for instance, to set the starting magnetic field value for a scan.

Data Acquisition

Time-resolved detection schemes. Sensitivity in TRIMS is partly dependent on the efficiency of the detection electronics. If every ion that reaches the detector is used for the measurement, there will be greater sensitivity than if only a fraction of those ions is used. Time-resolved detection schemes can be placed in one of two general categories: time interval measurements and timed amplitude measurements (20).

Time interval measurements are pulse counting measurements in which the measured quantity is the time between a start signal (e.g., ionization/acceleration event) and the detection of an ion. The electronics often allow multiple stops for each start signal and utilize one or more time-to-amplitude converters (21) or high-speed

counters (22-25) to measure the time intervals. A multichannel scaler is then used to log and accumulate the number of ions that are detected at each arrival time. After many repetitions, an averages spectrum is produced. This method can only be used for low ion fluxes, e.g., <15 ions per start signal, each separated by >7 ns (24), or hundreds of ions per start signal, but each separated by >900 ns (23). Hundreds or thousands of repetitions must be averaged to obtain reasonable intensity accuracy, but very high timing precision can be achieved.

Timed amplitude measurements, on the other hand, measure the amplitude of the ion signal during a narrow time-window at a specific delay time after the start signal. By monotonically increasing the delay time after successive ionization/acceleration pulses, a spectrum can be acquired. This process is called time-slice detection (TSD) (26). A sampling oscilloscope (27-29) or a boxcar integrator (30) is normally used to make these measurements. Since only one time-slice is sampled after each ionization/acceleration pulse, many thousand pulses are required to obtain a full spectrum (10,000 in the TOF application, or 1 spectrum each second). Signal averaging during each time-slice, if required, further increases the analysis time. An alternative to TSD is time-array detection (TAD) (26). In TAD, the ion signal amplitude is measured during all time slices following each ionization/acceleration pulse. A transient recorder can be used to achieve this function (31-33). However, current commercial transient recorders are limited either by the maximum repetition rate for signal averaging or by the time required to dump the acquired transient before

another one can be acquired. Only 1-100 transients/second can be obtained presently, or less than one transient out of a thousand in the TOF application.

An extension of the transient recorder would not only average full time-scans, but would continue data acquisition while an averaged scan is being dumped to a disk. No information would be lost. A device called an integrating transient recorder (ITR) is currently under development (26) and should, when available, boost sensitivity for full data matrix acquisition by several orders of magnitude over that presently obtainable.

For this implementation of TRIMS, we chose to employ TSD detection. Individual MS/MS scans in TRIMS require only a single time-slice at each magnetic field setting, and TSD provides the necessary repetition rate and signal averaging capabilities.

The digital boxcar integrator. The core of the time-resolved detection electronics is the digital boxcar integrator, consisting of a programmable delay generator (model 4145, Evans Assoc., Berkeley, CA) and a PAR 165 gated integrator. The delay generator provides delay times in 10 ns increments from 100 ns to 1 ms. The gated integrator has selectable aperture durations of 2, 5, 10, and 15 nanoseconds, plus continuously variable durations from 20 ns to 50 ms. The components of this system are shown in Figure 3.13. This figure also shows the extra connections that are necessary for the gated integrator because it is operated without a PAR 164 boxcar mainframe.
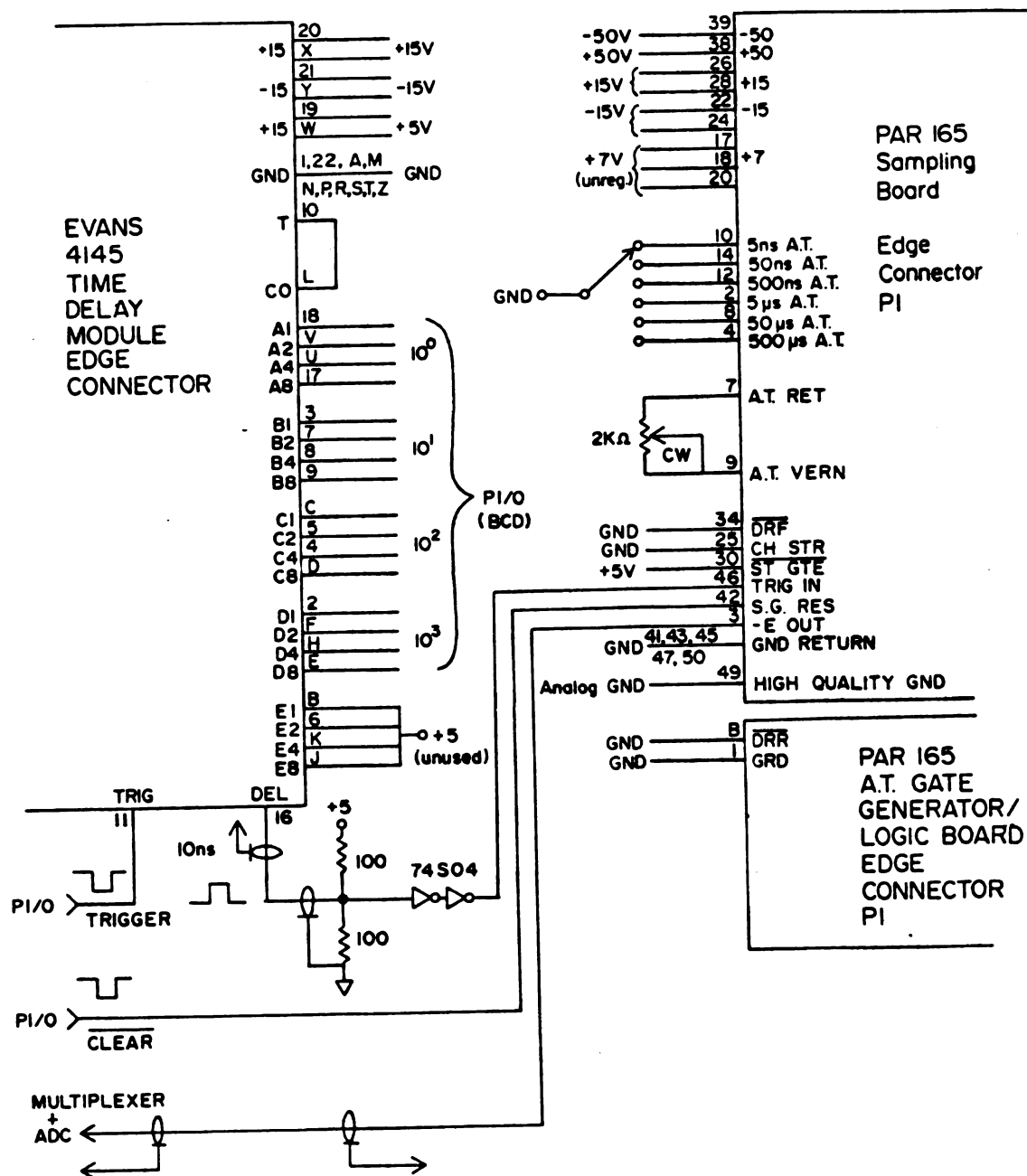
Figure 3.13. Component connections for the digital boxcar integrator.

The boxcar operates in the following manner. The delay time is set on the delay generator by the PI/O. A pulse from the microcomputer, concurrent with the pulse sent to the pulsing circuitry, triggers the delay generator. After the delay time, a trigger is sent to the gated integrator to acquire the ion intensity from the detector. The ion intensity at one delay time from any number of ion source pulses can be integrated to improve the ion statistics before the signal is digitized. This process yields the ion intensity at just one delay time (flight time). Other delay times can be sampled by changing the delay before the next set of pulses.

There are several parameters that require manual adjustment on the PAR 165 gated integrator. The aperture duration (time bin width) can be set for 2, 5, 10, or 15 ns. Longer durations can be set with jumpers on the interface board. Since the delay generator has 10 ns resolution, the same resolution is usually set on the gated integrator. The sensitivity and time-constant switches can be set according to the signal intensity and dynamic range requirements. The sensitivity switch determines the gain of the input · amplifier (50 mV --> gain = 200, 100 mV --> gain = 100, etc.). The time-constant determines the size of the capacitor in the feedback loop of the integrator. A small time constant will give better sensitivity; a large time constant will provide a larger dynamic range.

Data/Control System — Software

The FORTH language (Forth, Inc., Hermosa Beach, CA) was chosen for the TRIMS data system. FORTH is an excellent language for instrument control with a microcomputer (34). It has many of the features of an assembly language such as easy access to memory locations and fast execution speed, yet it has many of the attributes of a high level language such as ease of programming. Each command in FORTH is a "word." The function of a word might be as simple as storing a value at a specific memory location. A word can also be made up of other previously defined words; thus a vocabulary of more and more complicated words can be built. Eventually one can construct a series of high level commands (words) that carry out complicated functions. For instance, the word SSCAN might do all the instrument control and data acquisition functions to acquire a stable ion linked scan and write the data to a disk file.

FORTH is not just an extensible language but also an operating system and an editor. FORTH also allows words to be written in assembly language when execution speed is critical. FORTH code executes faster than higher level languages, it generally takes up much less memory, yet it is easier to write and debug than assembly language code.

Another consideration in choosing FORTH was the large amount of applicable software that had been written in FORTH for the triple

quadrupole mass spectrometer.

FORTH MS/MS Software

A fairly extensive set of software routines has been written for the triple quadrupole mass spectrometer (16-18). A list of the major features of this system is given in Table 3.2. The system is especially suited for controlling the many parameters that are found on the TQMS, such as the lens and quadrupole voltages. Although most of the words are written in FORTH, some of the low-level routines such as the ADC driver and the peak-finding algorithm are written in assembly language to optimize the execution speed.

The data format and file structure utilize the FORTH File Manager (Forth, Inc.) software package. The disk drive is divided into several files, the size of each being determined at the time of system building. Each file is composed of a series of variable length experiments, each of which, in turn, is made up of a series of variable length scans. Each experiment and scan has a header record associated with it that tells the system its size as well as other information. Each scan also has a parameter record that lists all the parameter values for that scan.

Communications with the PDP11 utilizes three routines. TALK (35) allows the microcomputer terminal to act as a dumb terminal on the PDP11. FORTHPIP (36) is a utility for uploading and downloading FORTH programs and data, and for converting files from FORTH format to DEC

TABLE 3.2. Main operating features of the TRIMS
data system software.

Routine	comments
Variable Device Control Table	control parameters each device: range of values, print format, status
Variable Device Parameter Table	values for each device
DEVICE-ADDRESS	address for each device or DAC
DATA-BUFFER	RAM storage of data
DISPLAY routines	graphics
DLIST	data listing
11-COMMUNICATIONS	routines to transfer data to PDP11
SOFTKNOBS	manual control of variable devices
SCAN routines	data collection
Parameter Editor	screen editor for changing variable device values

RSX Files-11 format. UPLOAD (37) provides for transferring whole experiments to the PDP11 with subsequent reformatting for the multidimensional data base in our laboratory.

Software Modifications for TRIMS

Several additions and modifications were made to the TQMS software to adapt it for TRIMS. These modifications involved changing the variable device control table, rewriting the ADC and DAC drivers, and modifying the scanning algorithms to achieve the proper pulse sequences and repetition frequency. In addition, the scanning and calibration routines had to be rewritten to accomodate the magnetic sector and flight time characteristics.

Calibration. Calibration of the TRIMS instrument is achieved by separate calibrations of the magnetic field and time-of-flight. To calibrate the magnetic field, the instrument is first set up for taking mass spectra without time resolution, i.e., conventional mass spectra. The magnet must first be scanned several times in order to set up the flux patterns. Then a scan of the calibration compound is taken with the data system and a list of the Hall values and ion intensities for all the peaks is generated. A calibration table, previously constructed, contains the masses for the calibration compound. From the list of peaks, the operator chooses the Hall values for the two lowest masses in the calibration table. The data system then does a linear extrapolation from those two values and calculates the expected Hall value for the next mass (38). The list of peaks is searched and the Hall value closest to the calculated value, if present within a

specified window, is picked. This observed value is used to calculate the Hall value for the next mass in the calibration table. The process continues for all masses in the calibration table. This method is used because although the relationship between the mass the and square of the Hall value is ideally linear, there are small but reproducible variations in the linearity (produced by slight inhomogeneities in the magnetic field) which require corrections every 40 or 50 daltons.

After the linear extrapolation a table is printed with the old Hall value (from the previous calibration), the calculated Hall value, the observed new Hall value, and the observed peak intensity for each mass in the calibration table. If the values are satisfactory, the operator stores these new values in the calibration file. Subsequent mass assignment for any peak is made by linear interpolation between values in the calibration table.

To calibrate the time-of-flight, the instrument is set up for ion source pulsing and time-resolved detection. For each mass in the calibration table, the instrument slowly increments the magnetic field in the region where those ions are expected to appear. A time scan is taken for each increment of the magnetic field and the flight time of the largest peak, if any, is recorded. After incrementing the magnetic field across the entire peak, the time and magnetic field strength corresponding to the overall maximum intensity found by all the time scans are recorded. The mass-time values for two of the masses are used to calculate a calibration line from which all time-of-flight mass

assignments are made. This type of calibration is possible for the mass-time relationship because it is much more linear than the magnetic field-mass relationship. The Hall values acquired during the pulsed phase of the calibration are placed in a second calibration table from which mass assignments are made by linear interpolation during pulsed experiments. This second mass-Hall value calibration table is necessary because ions appear at slightly lower magnetic field strengths when they are accelerated by pulsed extraction, as described in Chapter 5.

At this point, the mass of any stable ion can be calculated from either the Hall value or the flight time at which it appears. In addition, the flight time of a daughter ion will identify its parent mass. Without any further calibration the daughter ion mass can also be calculated. Equation 11 of Chapter 2 shows that the apparent mass m^* for a daughter ion is related to the parent and daughter ion masses by $m^* = m_2^2/m_1$. The magnetic field calibration provides the apparent mass m^* for the daughter ion and the flight time calibration gives m_1. Thus the product of the two yields m_2, i.e., the mass of any stable or daughter ion is calculated from the square root of the product of the flight time mass and the Hall value apparent mass.

This mass assignment can also be derived from Equation 9 of Chapter 2, the B-t equation for stable and daughter ion masses. The magnetic field strength at which any ion is observed is proportional to the square root of its mass according to Equation 8 of Chapter 2. The

square root of the mass obtained from the magnetic field calibration is really a measure of the magnetic field strength actually experienced by the ion, having been corrected for slight non-linearities in the field that cause the Hall probe to sense a slightly different field. Likewise, the square root of the mass derived from the flight time calibration is a measure of the flight time. The product of these two empirically derived values, then, is proportional to B·t, and hence, to the mass.

Scanning Modes. Table 3.3 lists the types of scans that can be performed with the TRIMS instrument. A SCAN covers a certain mass range and utilizes the peak-finding algorithm to produce mass-intensity pairs. A SWEEP covers a certain range of either the magnetic field or flight time, recording the intensity at every value that is sampled; neither peak-finding nor mass assignment is performed in real time.

In both a SCAN and a SWEEP, each data point is an integrated intensity. The number of pulses that are integrated for each point is determined by the AVG parameter in the variable device parameter table (VDPT). During the integration period, the magnetic field and sampled flight time are not changed.

The DSCAN requires the sampled flight time to be set, depending on the parent mass. The magnet is scanned (incremented) over the range where daughter ions could appear, i.e., up to the parent ion mass. The other types of SCAN's are linked scans; each time the magnetic field is incremented, the computer must read the Hall value and then calculate

TABLE 3.3. Scans available with the TRIMS data system.

scan type	scan name	header no.	comments
magnet scan	BSCAN	0	no time resolution
stable scan	SSCAN	1	
parent scan	PSCAN	2	
daughter scan	DSCAN	3	
neutral loss scan	NSCAN	4	
magnet sweep	MAG SWEEP	5	records magnet DAC values
time sweep	TIM SWEEP	5	records time values
energy sweep	ESWEEP	5	records energy values
time scan acquisition	TSCAN	6	used for data matrix

and set the proper flight time according to the scan law and the calibration tables. With computer control over both the magnetic field and flight time, any scan law can be implemented. The floating point numeric co-processor (Intel 8087) makes the software simple to write and provides rapid execution.

Full data field acquisition with scan reconstruction. An alternate method of data acquisition, when the maximum amount of data is desired, is to acquire the entire three-dimensional data matrix (ion intensity at all values of B and t). From this matrix, the data points for any scan can subsequently be extracted and the scan reconstructed. This matrix is easily acquired by performing multiple time scans, incrementing the magnetic field between each. The SEC DEV (secondary device) parameter keeps track of the Hall value for each scan. A series of routines can go into this matrix of data and extract from it a set of points corresponding to any desired scan.

Several different techniques can therefore be used to acquire MS/MS spectra: individual scans or sweeps, or full data matrix acquisition. These options give the operator maximum flexibility for carrying out an experiment. The format of the data is the same as that for the TQMS, so all the data processing, plotting, archiving, and spectral searching routines written for the TQMS on the PDP11 system (39-41) can be used. In addition, the software on both the TRIMS and TQMS instruments is very similar, so anyone familiar with one system can readily learn to operate the other.

References

1. LKB-9000 Gas Chromatograph-Mass Spectrometer, Operators Manual, LKB Produkter AB, Bromma, Sweden, p. 83.

2. Bakker, J. M. B. J. Phys. E. 1973, 6, 785-789.

3. Bakker, J. M. B. J. Phys. E. 1974, 7, 364-368.

4. Stults, J. T.; Enke, C. G.; Holland, J. F. Anal. Chem. 1983, 55, 1323-1330.

5. Studier, M. H. Rev. Sci. Instrum. 1963, 34, 1367-1370.

6. Baker, F. A.; Hasted, J. B. Phil. Trans. Roy. Soc. London, A 1966, 261, 33-65.

7. Herod, A. A.; Harrison, A. G. Int. J. Mass Spectrom. Ion Phys. 1970, 4, 415-431.

8. Wiza, J. L. Nucl. Instrum. Meth. 1979, 162, 587-601.

9. Colson, W. B.; McPherson, J.; King, F. T. Rev. Sci. Instrum. 1973, 44, 1694-1696.

10. Glish, G. L.; Todd, P. J. Anal. Chem. 1982, 54, 842-843.

11. Wachs, T.; VandeSande, C. C.; Bente, P. F., III; Dymarski, P. P.; McLafferty, F. W. Int. J. Mass Spectrom. Ion Phys. 1977, 23, 21-27.

12. Eckenrode, B., Michigan State University, Chemistry Dept., unpublished work.

13. Stults, J. T.; Newcome, B. H.; Myerholtz, C. A.; Enke, C. G.; Holland, J. F.; presented at the 31st Annual Conference on Mass Spectrometry and Allied Topics; Boston, May 8-11, 1983; bound volume p. 162.

14. Stults, J. T.; Myerholtz, C. A.; Newcome, B. H.; Enke, C. G.; Holland, J. F. Rev. Sci. Instrum., submitted for publication.

15. Newcome, B. H.; Enke, C. G. Rev. Sci. Instrum. 1984, 55, 2017-2022.

16. Myerholtz, C. A. Ph.D. Dissertation, Michigan State University, East Lansing, MI, 1984.

17. Myerholtz, C. A.; Newcome, B. H.; Enke, C. G.; presented at the 31st Annual Conference on Mass Spectrometry and Allied Topics; Boston, May 8-11, 1983; bound volume p. 171.

18. Myerholtz, C. A.; Enke, C. G.; presented at the 30th Annual Conference on Mass Spectrometry and Allied Topics; Honolulu, June 6-11, 1982; bound volume p. 845.

19. Newcome, B. H. Ph.D. Dissertation, Michigan State University, East Lansing, MI, 1984.

20. Hahn, B. K.; Enke, C. G. Anal. Chem. 1973, 45, 651A.

21. Hudor, A. M. Rev. Sci. Instrum. 1981, 52, 819.

22. Macfarlane, R. D. Anal. Chem. 1983, 55, 1247A.

23. Turko, B. T.; Macfarlane, R. D.; McNeal, C. J. Int. J. Mass Spectrom. Ion Phys. 1983, 53, 353.

24. Bonner, R. F.; Bowen, D. V.; Chait, B. T.; Lipton, A. B.; Field, F. H. Sippach, W. F. Anal. Chem. 1980, 52, 1923.

25. Armente, M.; Santoro, V.; Spinelli, N.; Vandi, F. Int. J. Mass Spectrom. Ion Phys. 1979, 30, 57.

26. Holland, J. F.; Enke, C. G.; Allison, J.; Stults, J. T.; Pinkston, J. D.; Newcome, B.; Watson, J. T. Anal. Chem. 1983, 55, 997A.

27. Plumb, I. C.; Cooper, G. H.; Heap, D. G. J. Phys. E 1977, 10, 744.

28. Taylor, D. G.; Turley, T. J.; rodgers, M. L.; Peterson, S. H.; Demas, J. N. Rev. Sci. Instrum. 1980, 51, 855.

29. Pearson, T. D. L.; Demas, J. N.; Davis, S. Anal. Chem. 1982, 54, 1899.

30. Ramaley, L.; Ling, K.; Burkholder, D.; Ieki, M.; Jones, W. E. Chem. Biomed. Environ. Instrum. 1979, 9, 335.

31. Denoyer, E.; VanGrieken, R.; Adams, F.; Natusch, D. F. S. Anal. Chem. 1982, 54, 26A.

32. Dunbar, R. C.; Armentrout, P. Int. J. Mass Spectrom. Ion Phys. 1977, 24, 465.

33. Lincoln, K. A. Dyn. Mass Spectrom. 1981, 6, 111.

34. Dessey, R. E. Anal. Chem. 1983, 55, 650A.

35. written by Ralph Thiim, MSU Chemistry Dept., East Lansing, MI.

36. Hoffman, P. A.; Enke, C. G. Computers & Chemistry 1983, 7, 47–50.

37. written by Phil Hoffman, MSU Chemistry Dept., East Lansing, MI.

38. Martin, F. E.; Holland, J. F.; Sweeley, C. C. In "Biomedical Applications of Mass Spectrometry, First Supplementary Volume"; Waller, G. R.; Dermer, O. C., Eds.; Wiley-Interscience:New York, 1980; p. 51.

39. Hoffman, P. A.; Enke, C. G.; presented at the 31st Annual
    Conference on Mass Spectrometry and Allied Topics; Boston, May
    8-11, 1983; bound volume p. 556.

40. Giordani, A. B.; Gregg, H. R.; Hoffman, P. A.; Cross, K. P.;
    Beckner, C. F.; Enke, C. G.; presented at the 32nd Annual
    Conference on Mass Spectrometry and Allied Topics; San Antonio, May
    27-June 1, 1984; bound volume p. 648.

41. Crawford, R. W.; Brand, H. R.; Wong, C. M.; Gregg, H. R.; Hoffman,
    P. A.; Enke, C. G. Anal. Chem. 1984, 56, 1121-27.

CHAPTER IV

EVALUATION OF INSTRUMENT PERFORMANCE

Introduction

The instrumentation described in the previous chapter has been used to confirm the theory that was developed for TRIMS. This chapter describes the mass separation and mass assignment capabilities of TRIMS. Examples of all types of MS/MS scans are shown in order to prove the viability of the technique for MS/MS experiments. Peak contours in the B-t data field are evaluated to show that they arise from ions with initial spatial and energy distributions in the ion source. Evaluation of the resolution and sensitivity is then made to demonstrate the performance of the present implementation and to predict the potential usefulness and limitations of the technique.

Comparison of Results and Theory

A single compound, n-decane, was chosen to test the theory of TRIMS. With over 100 metastable decompositions (1,2), n-decane provides many daughter ions with which to demonstrate the principles of this technique. The data in this first experiment, obtained before construction of the microcomputer system, were taken with a PAR 162/164 analog boxcar integrator (Princeton Applied Research Corp., Princeton, NJ) and recorded on strip chart paper. Pulsing was produced by beam deflection (3).

103

The most intense stable ions were used for calibration in this experiment. The measured flight time and magnetic field strength values for these peaks are given in Table 4.1. The magnetic field strength was measured with the Hall probe and digitized using a PDP8/e computer (4). These digitized values are proportional to the magnetic field strength and are listed as fsu (field strength units). The ion masses and measured flight time values were fit by linear least squares regression to the conventional time-of-flight equation (Chapter 2, Equation 4) and a timing offset was calculated to correct for delays in the electronic measurement and pulsing. A large electric field existed in the region between the exit slit and the conversion dynode of the electron multiplier. The increase in ion energy produced a larger increase in velocity for daughter ions than for the parent ions. As a result, daughter ions apeared at slightly shorter arrival times than their parent ions. Therefore, a second correction to the flight time was necessary to account for ion acceleration near the electron multiplier (3).

The ion masses and magnetic field values were likewise fit to the conventional magnetic sector equation (Chapter 2, Equation 4) and an offset was calculated for the Hall values. The flight time and magnetic field values, corrected for offsets, are also listed in Table 4.1. Using the corrected values for B and t, the data in Table 4.1 were fit to Equation 9 of Chapter 2 (the B·t mass assignment equation) to obtain a value of $er/d = 0.2423 \pm 0.0003$ Da us^{-1} fsu^{-1}. This value was used for subsequent mass assignment based on B and t.

Table 4.1.   Stable ion flight time and magnetic field measurements
for n-decane.

actual mass	t_{meas}	t_{corr}	B_{meas}	B_{corr}
39.0	9.08 μs	7.58 μs	21.19 fsu	21.33 fsu
41.0	9.28	7.78	21.70	21.84
42.0	9.34	7.84	21.95	22.09
43.0	9.44	7.94	22.23	22.37
56.1	10.59	9.07	25.36	25.50
57.1	10.67	9.15	25.57	25.71
70.1	11.66	10.13	28.37	28.51
71.1	11.74	10.21	28.57	28.71
84.1	12.66	11.12	31.06	31.20
85.1	12.72	11.18	31.26	31.40
99.1	13.64	12.09	33.75	33.89
113.1	14.46	12.90	36.08	36.22
142.2	16.01	14.43	40.48	40.62

*fsu = field strength units (see text)

A search was made for the most intense of the n-decane daughter ions produced by metastable decomposition. A list of the peaks observed is given in Table 4.2 along with the measured and corrected values for the flight time and magnetic field strength. The value of er/d calculated from the stable ion calibration was used to calculate the daughter ion masses, based on Equation 9 of Chapter 2. Likewise, the corrected flight time was used to calculate the parent ion mass. The correspondence between the actual and calculated masses is very good, considering the poor resolution observed with the first implementation and the slight non-linearities in the mass-field strength calibration.

The stable and daughter ions from Tables 4.1 and 4.2 are plotted in Figure 4.1 as diamonds in the B-t data field. The dotted lines were calculated from the calibration for constant daughter and constant parent masses.

The accuracy of the parent and daughter ion mass assignments demonstrate that knowledge of the flight time and magnetic field strength at which an ion is observed does provide the necessary information for both parent and daughter mass assignment. The product B·t can be related to the mass of a given ion, the particular values of B and t being determined solely by the ion energy. The close correspondence between the B-t plot of Figure 4.1 and the theoretical B-t plot (Chapter 2, Figure 2) further supports the developed theory and shows that TRIMS successfully separates daughter ions from stable ions in a magnetic sector instrument.

Table 4.2. Daughter ion flight time and magnetic field measurements for n-decane.

| --actual mass-- | | tmeas | tcorr | Bmeas | Bcorr | --calcd mass-- | | % rel int |
m1	m2					m1	m2	
41.0	39.0	9.26 μs	7.76 μs	20.62 fsu	20.76 fsu	41.0	39.0	0.2
43.0	41.0	9.40	7.90	21.21	21.35	42.5	40.9	0.3
57.1	41.0	10.64	9.13	18.44	18.58	56.8	41.1	0.6
70.1	55.0	11.66	10.14	22.29	22.43	70.0	55.1	0.2
71.1	43.0	11.70	10.18	17.32	17.46	70.6	43.1	0.8
84.1	69.1	12.62	11.09	25.51	25.65	83.8	68.9	0.2
85.1	43.0	12.66	11.14	15.84	15.98	84.5	43.1	0.4
85.1	57.1	12.70	11.17	20.95	21.09	85.0	57.1	0.5
99.1	57.1	13.54	12.06	19.44	19.58	99.0	57.2	1.2
113.1	57.1	14.40	12.86	18.22	18.36	112.6	57.2	0.3
113.1	71.1	14.42	12.88	22.67	22.81	113.0	71.2	0.6
142.2	85.1	15.98	14.42	24.17	24.31	141.6	84.9	0.1
142.2	99.1	15.96	14.40	28.14	28.28	141.3	98.7	0.3
142.2	113.1	16.02	14.46	32.19	32.33	142.4	113.3	0.4

*fsu = field strength units (see text)
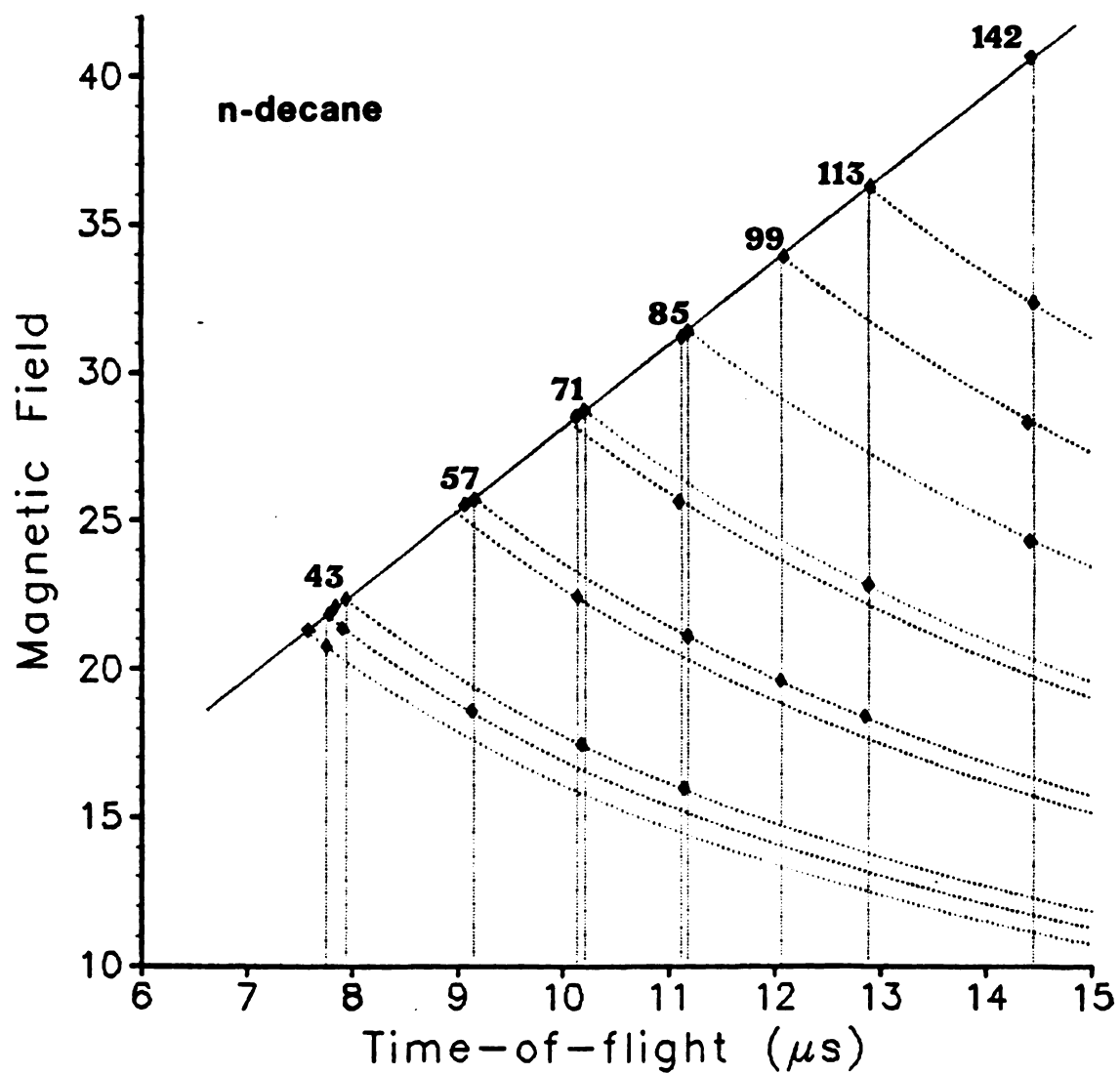
Figure 4.1. Observed peaks for n-decane (indicated by diamonds) in the B-t data field. The dotted lines are calculated from the calibration (see Table 4.1).

MS/MS Scans Obtained with the Data Acquisition/Control System

The calibration accuracy and linked scanning capabilities of the data system are demonstrated in this section, again with n-decane. Calibration was achieved by the procedure outlined in Chapter 3. Either n-decane or perfluorokerosene (PFK) was used for calibration.

A conventional mass spectrum of n-decane utilizing no pulsing of the ion source and no time resolution of the signal is shown in Figure 4.2a. A stable ion scan, obtained with a pulsed ion source, is shown in Figure 4.2b. The latter scan requires that the flight time be linked to the magnetic field strength. The close agreement of the two spectra demonstrates the accuracy of the linked scanning procedure. Differences between the two spectra may be due to the lower sensitivity of the stable scan, and slight imperfections in the calibration used to generate the linked scan. The stable scan eliminates the contributions of any metastable peaks to the mass spectrum. There is little evidence for metastable peak discrimination in Figure 4.2, however. There are two reasons that usually preclude the appearance of metastable peaks in conventional mass spectra which are acquired by a computer: (a) metastable peaks are often superimposed on stable ion peaks, (b) most peak finding algorithms do not identify the broad, low level metastable peaks.

Figure 4.3 shows the daughter ion scans of several n-decane parent ions. Although daughter ion scans do not require changing the sampled flight time during data acquisition, measurement of the flight time as
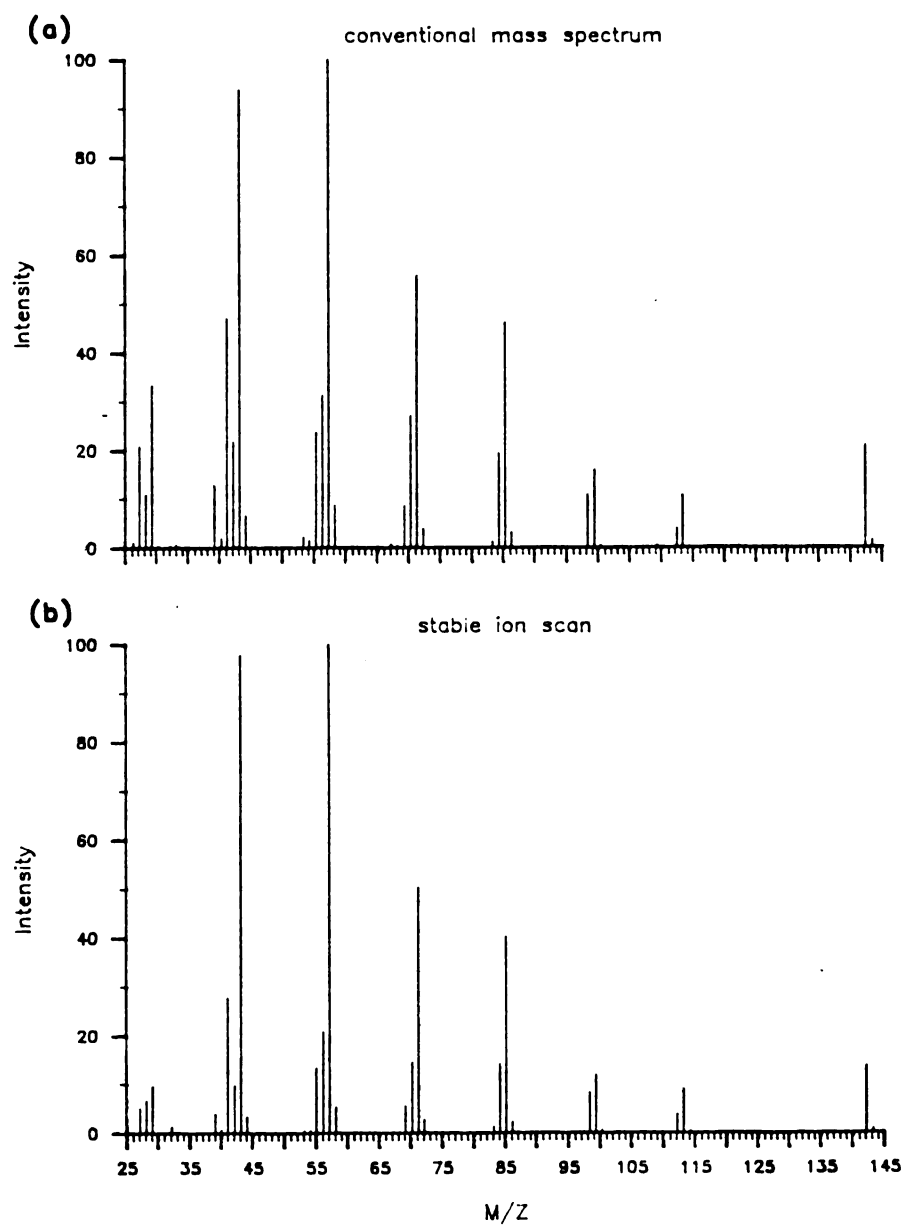
Figure 4.2. Conventional mass spectrum (a) and TRIMS stable ion scan (b) of n-decane.

Daughter Spectra of n—decane

(a)

parent mass 85

(÷200)

Intensity

(b)

parent mass 113

(÷50)

Intensity

(c)

parent mass 142

(÷50)

Intensity

M/Z
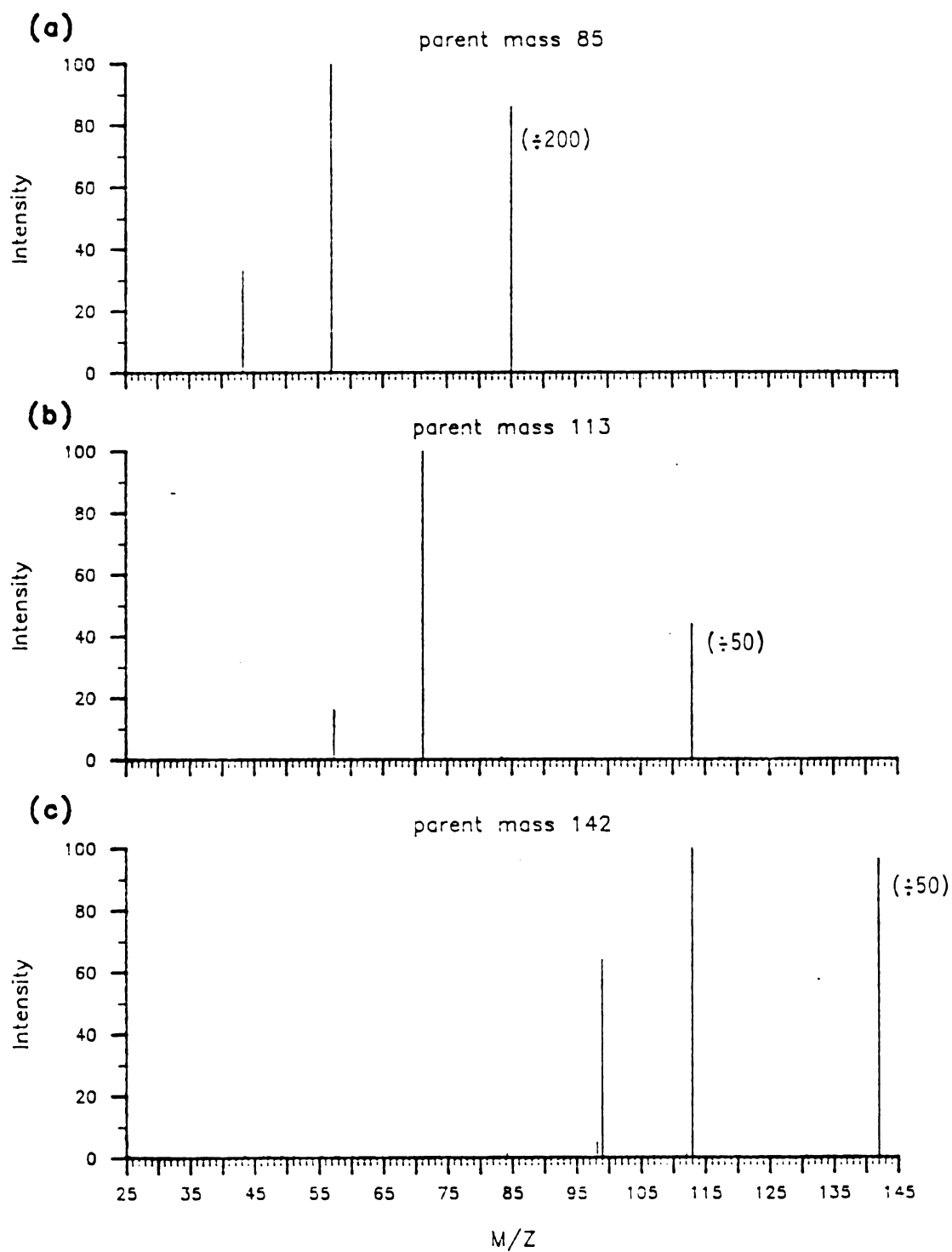
Figure 4.3. Selected daughter spectra of n-decane for ions formed by metastable decomposition.

well as the magnetic field strength are needed to assign the daughter
ion masses accurately. The mass assignments in Figure 4.3 match those
expected (see Tables 4.1 and 4.2). The pulsed extraction technique
used for these spectra provides better sensitivity than the original
beam deflection technique used to produce the data in Figure 4.1. The
increased sensitivity is evidenced by the appearance of additional
peaks at m/z 98 and 112 in the daughter spectrum of parent mass 142.
The technique, however, still lacks the sensitivity to observe the very
low intensity daughter ions of n-decane that been found with other
techniques (1,2).

Figure 4.4 is a parent ion scan of n-decane daughter mass 57. The
parent ion scan requires that the magnetic field strength and flight
time be scanned in a linked manner so that the product B·t remains
constant; as the magnetic field strength is increased, the time at
which the measurement is made is decreased. Again, the linked scan was
accurate enough to obtain the expected peaks (see Table 4.2) and the
calibration accurately assigned the parent masses, based on the ion
flight time.

The final type of MS/MS scan and generally the most difficult to
obtain is the neutral loss scan. Figures 4.5a and 4.5b show neutral
loss scans of n-decane for losses of 28 and 42 daltons, respectively.
More accurately, this scan should be called a parent scan at constant
neutral loss. For example, Figure 4.5a shows that parent masses 85,
99, and 113 all produce daughter ions by loss of 42 daltons. The
neutral loss scan is a linked scan in which the difference between the

Parent Spectrum of n-decane

daughter mass 57
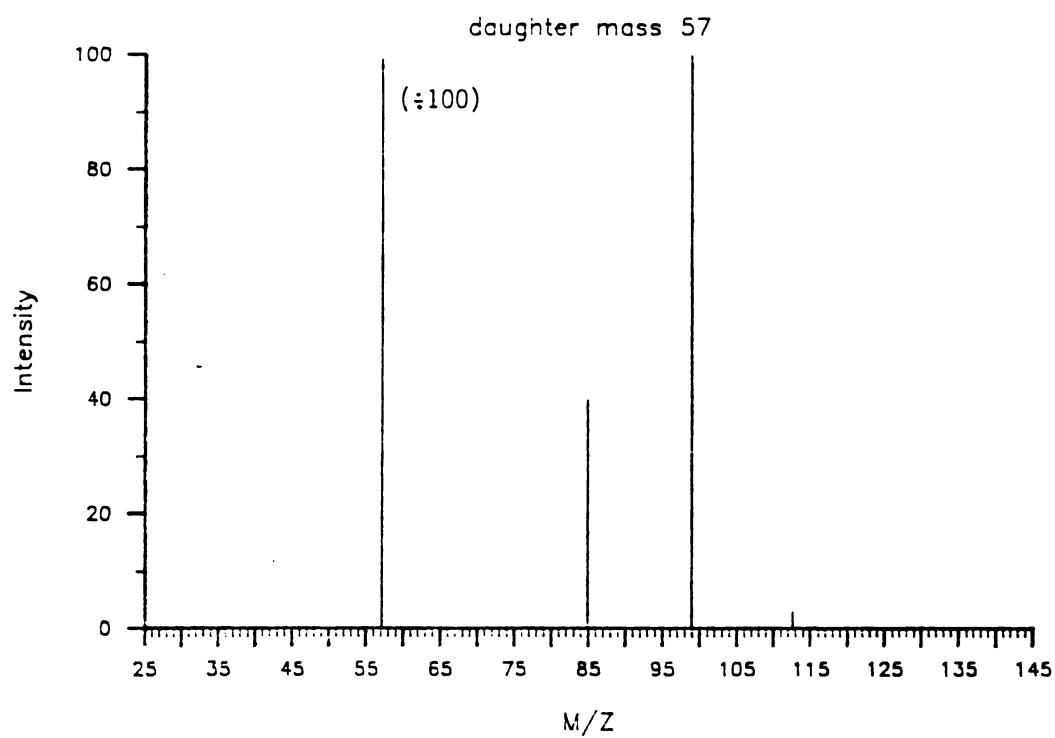
Figure 4.4. A typical parent spectrum of n-decane
(ions formed by metastable decomposition).

Neutral Loss Scans of n–decane

(a)

neutral loss = 28

(b)

neutral loss = 42

M/Z
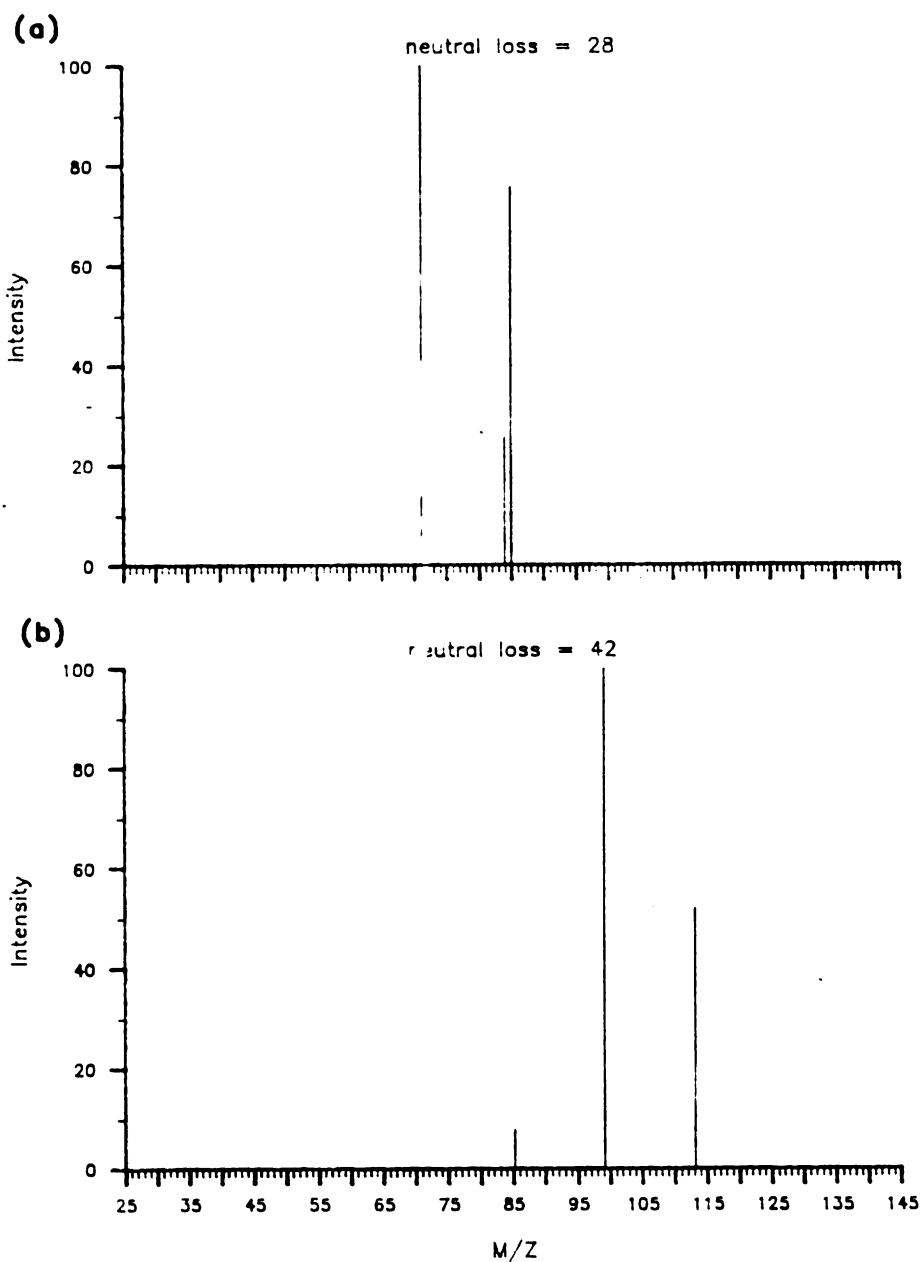
Figure 4.5. Selected neutral loss scans of n-decane
(ions formed by metastable decomposition).

parent and daughter ion masses must be kept constant while scanning both B and t. Although the scan function is complex, the data system can easily follow it, as these scans demonstrate. The observed peaks match those found in Table 4.2.

As mentioned briefly in Chapter 2, MS/MS scans can also be obtained by first collecting the full MS/MS data field and then extracting points for the desired scans from that matrix of data. The present data system would require an inordinate amount of time and disk space to acquire the full data field for even a moderate size compound. However, a small portion of the data field for benzene has been obtained to show the utility of this data acquisition method. Figure 4.6 shows the molecular ion region of benzene. No ion abundance information is displayed in this plot, only the locations of the ions in the B-t data field. Three-dimensional, contour, or color plots, which also display ion abundance data, would be more informative. From a complete data field, one would have information not only on ion masses and abundances, but also peak shapes and kinetic energy release for metastable decompositions. Poorly resolved peaks would be apparent as would any artifact peaks that might be present in an individual mass scan. Individual scans could be obtained by "scanning" the data file, using the same scan functions and calibration as for a normal scan.
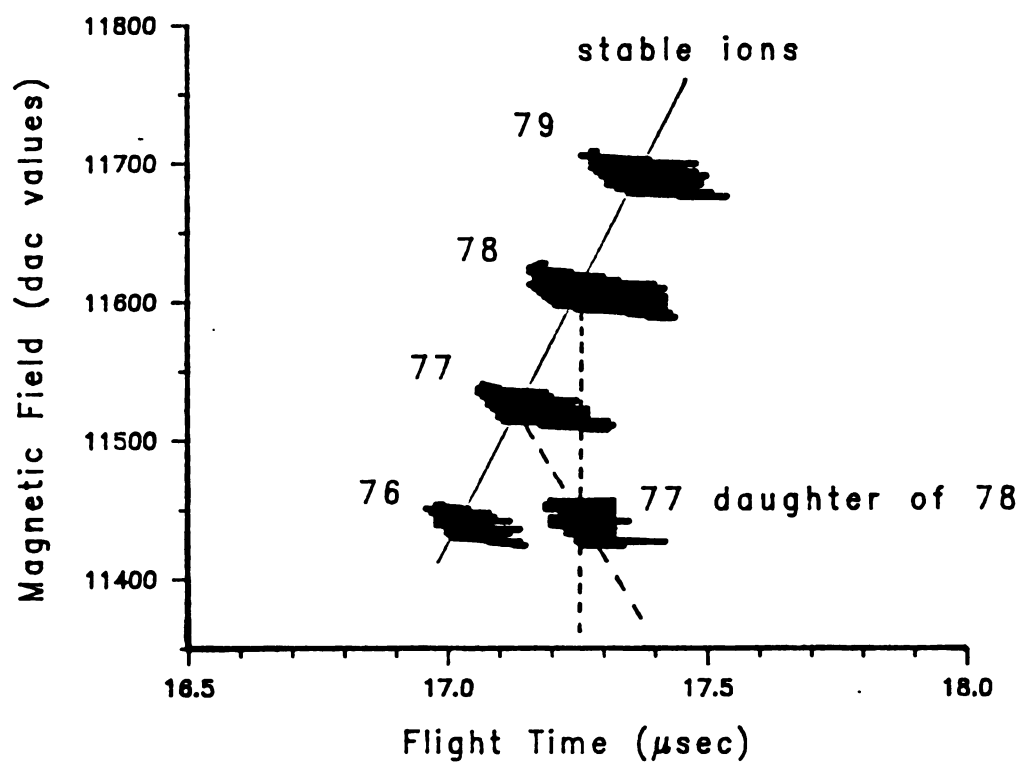
Figure 4.6.   Locations of ion intensity in the B-t data field
for the molecular ion region of benzene.

Collisional Activation

Metastable decompositions can reveal much about the fragmentation pathways of ions and can be useful for identifying ion structures. However, they are usually observed for a limited number of ions and when present, are generally found in very small abundance. Collisionally activated dissociation (CAD) can produce daughter ions which are not formed by metastable decomposition, and can produce them often in much greater numbers, leading to an increase in both the qualitative and quantitative information available from MS/MS scans. More of the details of CAD are given in Chapter 1.

Initial trials in which a "collision needle" (5) was used to introduce the collision gas were unsuccessful because the single 4-inch diffusion pump on the ion source region of the instrument was unable to accomodate the increased gas load. The needle was converted to a collision cell that showed much better efficiency and reduced the gas load on the pumping system. This cell was used for the CAD experiments. The cell has been improved by reducing the ion beam apertures to decrease the gas load further (6). Deuterium was used as the collision gas which was added until the parent ion beam intensity was attenuated by 75% (6,7).

Daughter ion scans were obtained for parent ion mass 105 of mesitylene (1,3,5-trimethylbenzene, MW=120). Figure 4.7a shows the daughter ions produced by metastable decomposition. Figure 4.7b shows the daughter ions produced by CAD. Although masses 53 and 79 have

Daughter Scans of Mesitylene mass 105
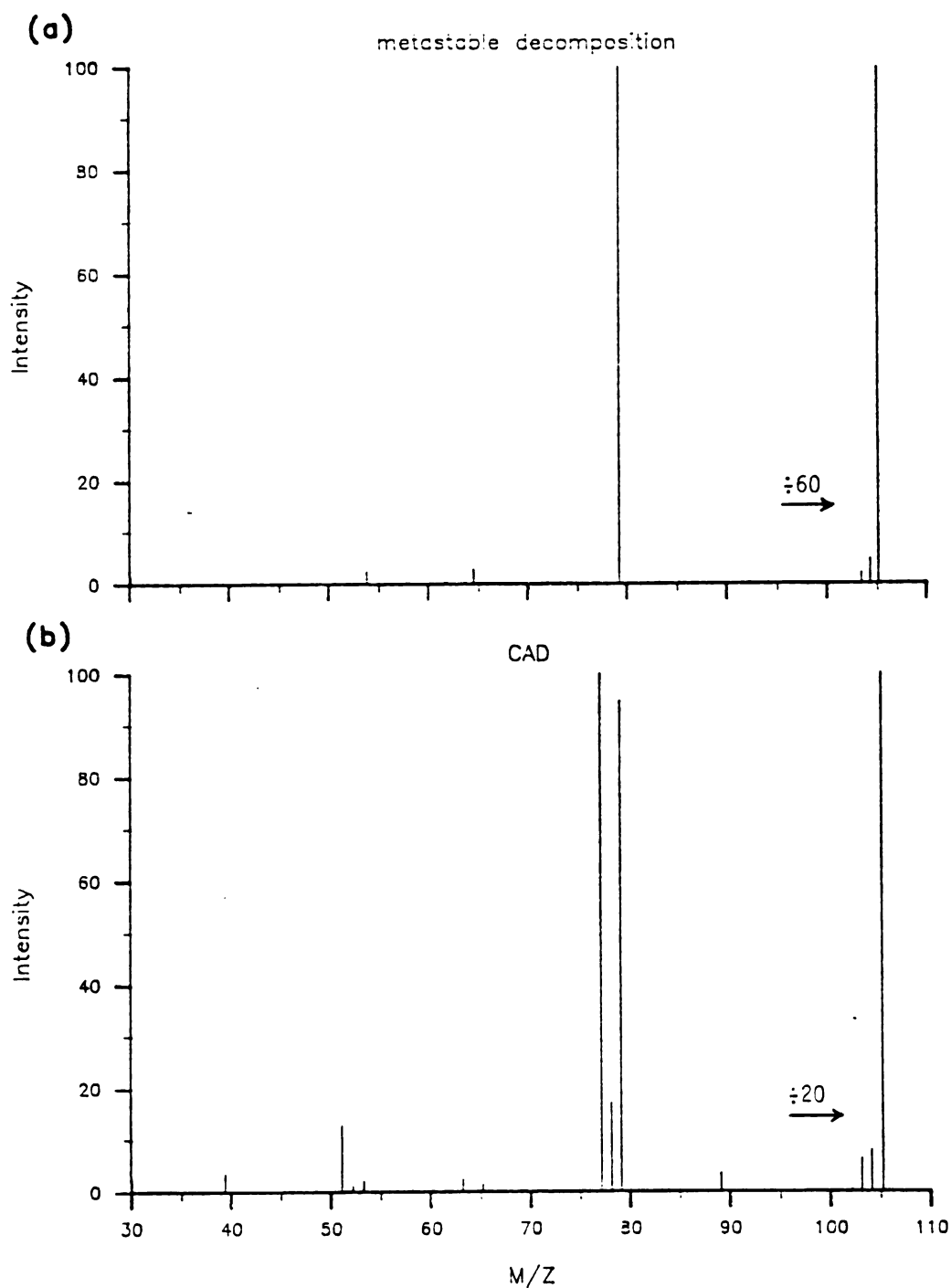
Figure 4.7. Daughter spectra of mesitylene (1,3,5-trimethylbenzene) parent mass 105: (a) metastable decomposition, (b) collisionally activated dissociation.

metastable components, they also show an increase in intensity in the presence of collision gas. These spectra represent several scans, summed to increase the signal-to-noise level. Peaks appear at non-integral masses because of their mass defect and/or because of calibration inaccuracy. The peak-finding algorithm does not currently round off to nominal masses.

The pumping system still is not adequate for making good CAD measurements. To obtain the results in Figure 4.7b, the pressure in the ion source/collision region reached 4×10^{-5} torr as indicated by the Penning gauge.. Taking into account the increased sensitivity of the ion gauge to deuterium over air, this represents a pressure of 1×10^{-4} torr in this region. This value indicates that collisions are probably occurring along the entire flight path between the ion source and the magnetic sector. The lack of a single collision "point" reduces the sensitivity and resolution because the focusing properties of the magnet are not fully utilized. Fortunately, the pressure on the detector side of the magnet remains at about 2×10^{-6} torr during the CAD experiments, so losses due to collisional scattering in this region are minimal. Increased pumping capacity and/or a more efficient collision cell are needed to improve the CAD measurements.

Resolution

Resolution for Stable Ions and Daughter Ions

A discussion of resolution can be divided into two parts, one concerning the performance of the instrument and the precision of the measurement (the instrument resolving power), the other regarding the observed peak widths (the mass resolution). Both types of factors contribute to the overall resolution and mass assignment precision, as will be seen. The factors contributing to the imprecision in the mass assignments of both parent and daughter ions are principally the imprecision in the measurements of flight time and magnetic field strength. The precision in the magnetic field measurement is determined by the field inhomogeneity, field stability, the effect of fringing fields, as well as the precision of the signal from the magnetic field sensor, and the accuracy of any calibration procedure. The uncertainty in path length is determined partly by slit widths and partly by the focusing action of the magnetic sector. The resulting mass uncertainty due to the magnetic sector should be the same as that obtained with the magnetic spectrometer operated in the normal (non-time-resolved) mode with monoenergetic ions formed at a single point in the ion source. Timing precision is limited by the uncertainty in the start time, the accuracy in measuring the delay time, and the aperture window of the sampling electronics. Precision in the flight length is determined by the depth of the ion volume sampled and by the different paths through the magnetic sector due to first-order focusing in the sector. Flight time precisions comparable

to those obtained with conventional time-of-flight mass spectrometers when measuring monoenergetic ions with no metastable decompositions should be achievable (0.5-1.0 parts per thousand).

The diagram in Figure 4.8 is an expanded portion of a hypothetical B-t plane for two stable ions differing by one mass unit. The solid curves represent the locations in the B-t data field where ion abundance is expected due to energetic variations when the uncertainty in the radius and path length is zero. The shaded regions containing the solid curves represent the "width" of each curve caused by uncertainties in the radius and path length. The density of the shading represents the expected ion abundance. The uncertainties in B and t are also shown. Energy differences in ions of the same mass will cause them to spread out along the lines of constant $B \cdot t$ as shown by the length of each curve but will cause no increase in the width of the line. For a single mass, higher energy ions appear at shorter arrival times and higher field strengths than ions of lower energy. This energy spread in ions of the same mass affects the separate resolutions of B and of t but not of $B \cdot t$. Thus, resolution in two dimensions and the use of the $B \cdot t$ product for mass assignment remove the effect of energy spread as a factor in mass determinations. Hence, the time-resolved ion momentum spectrometer should provide unit mass resolution to 1000 mass units for both stable and daughter ion masses. Additionally, measurement of the distribution of ion current along the line of constant $B \cdot t$ will provide an energy spread profile useful for studying the energetics of ion fragmentation.
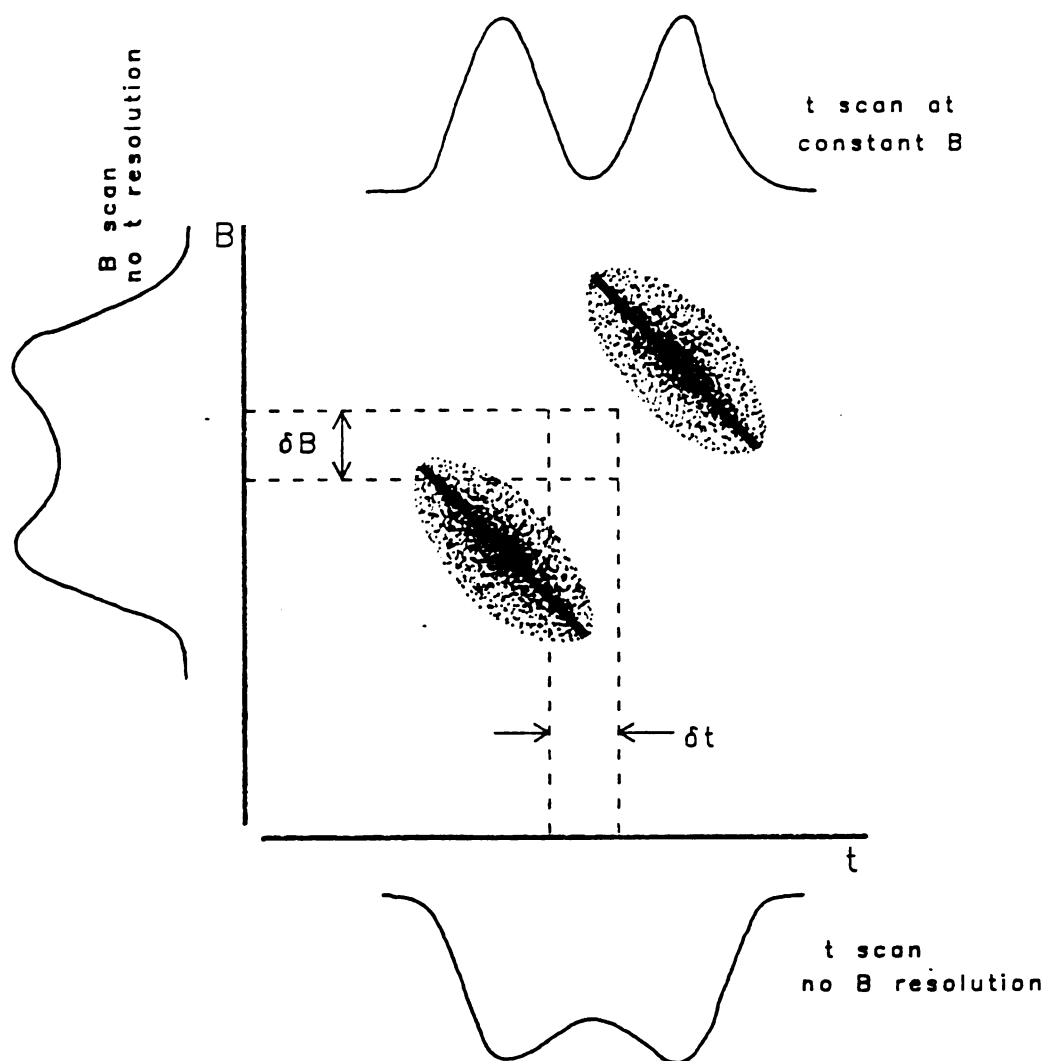
Figure 4.8. Demonstration of TRIMS resolving power for two stable
ions of adjacent mass in a hypothetical B-t data field. Bottom
axis shows expected peak overlap for no magnetic field
resolution. Left axis shows expected peak overlap for no time
resolution. Top shows expected peak overlap for a time scan
at constant B.

The diagram in Figure 4.8 can also be used to compare the resolutions expected for simple magnetic, simple time-of-flight, and TRIMS instruments. For the magnetic instrument with no time resolution, the ion intensity would be projected onto the B-axis only. In effect, δt is very large. The low-field edge of the higher mass ion distribution will overlap with the high-field edge of the lower mass ion distribution to give less than fully resolved peaks. The extent of this overlap depends on the ion energy distribution, the relative ion abundances, and the resolving power of the instrument. Likewise, in a TOF instrument with no momentum dispersion, the two ion distributions will overlap on the t-axis giving less than complete resolution. On the other hand, the TRIMS instrument determines a two-dimensional section of the plot and as such is potentially capable of higher resolving power than with either B or t separately. The masses represented by the two curves will be completely resolved if the region delineated by δB and δt contains relatively little ion intensity in the space between the adjacent B·t curves even if the masses are not resolved by B or t alone. As the mass increases, the ability to resolve adjacent masses will decrease because of the decreasing separation of the B·t curves of adjacent mass values.

The above discussion is valid only for ions that are pulsed after ion formation and acceleration processes. Only in this case is the time between pulsing and arrival at the detector an accurate measure of the ion velocity. In reality, the measured flight time with the pulsed extraction method is the sum of the ion acceleration time in the ion source and the transit time through the instrument at its final

velocity.   The   acceleration time can contribute >1 μs to the overall flight time.   As a result, over a short region, the ion current for any one mass can actually be observed to move to <u>longer</u> times as the magnetic field strength is increased.   This observation is examined in greater detail in Chapter V.   Furthermore, ions can acquire a considerable distribution of energies due to the large extraction voltages used, a larger distribution than found in a conventional magnetic sector instrument.   The large extraction voltages are required for adequate resolution in the time-of-flight dimension.   The magnetic field resolution is generally degraded to $m/\Delta m$ <100 by the large extraction voltage.   As an example, at a single magnetic field strength, stable ions separated by one mass unit may appear at the same magnetic field strength, the lighter ions appearing at longer flight times than the heavier ions.   The decreased resolution significantly degrades the resolution for stable and daughter scans.

The magnetic field resolution for daughter scans is demonstrated in Figure 4.9, showing the 92^+ and 93^+ daughter ions of mass 120 of nitrotoluene.   These ions cannot be resolved by a MIKES instrument (8). The values on the x-axis are the DAC values used to control the magnet current.   Although not a direct measure of the field strength, the DAC values are proportional to the field strength.   These ions were pulsed by ion extraction which degrades the magnetic sector resolution.   Use of ion beam deflection should allow complete resolution of these peaks.

92,93 daughter ions of parent 120 of o—nitrotoluene
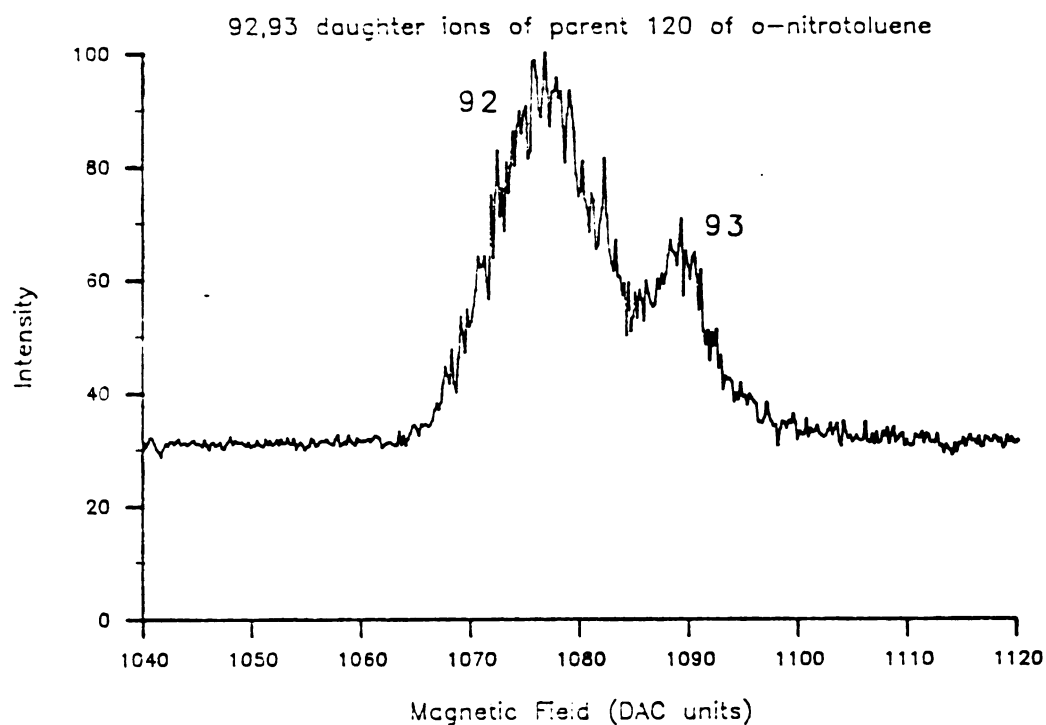
Figure 4.9. Daughter ion peaks at m/z 92 and 93 formed by
   metastable decomposition from parent mass 120 of o-nitrotoluene
   showing daughter mass resolving power.

Resolution for Parent Ion Determinations

Due to the release of kinetic energy during the dissociation process (typically less than 1 eV) the energy spread of the daughter ions will be greater than that for stable ions. In the previous section it was shown that this energy spread has no effect on the accuracy of daughter mass assignment because the value of B·t is not affected. The selection of the parent ion which gives rise to a given daughter is, however, based on the flight time of the daughter ion. Therefore, peak broadening along the time axis, especially for higher masses and large kinetic energy releases, could make it difficult to assign a parent mass for a daughter ion if there are several possible parents within that same velocity range. Correct assignment of the parent ion mass in this case could be aided by peak intensity centroiding along the B·t curve for both parent and daughter ions. For more serious cases involving daughter ion arrival time overlap, deconvolution, factor analysis, or other chemometric techniques could be invoked.

The magnetic field resolution is typically adjusted to $m/\Delta m = 200$ (10% valley definition) for non-pulsed operation by closing the slit widths from fully open in order to attenuate the ion beam intensity by 50%. The maximum resolution of the LKB-9000 is quoted as $m/\Delta m = 800$ at mass 1000. A lower resolution is used because most compounds studied to date have a molecular weight below 200 daltons, the lower resolution provides greater sensitivity, and for pulsed extraction, the initial positions of ions in the ion source is the limiting factor in the

magnetic field resolution.

The flight time resolution depends on the extraction voltage during pulsed extraction. The extraction voltage can be adjusted to provide space focusing and peak widths of 50 ns (at base) have been observed. During normal operation, however, peak widths of approximately 120 ns are observed which corresponds to a resolution of $m/\Delta m$ = 100. Figure 4.10 shows the resolution obtained for peaks in the molecular ion region of toluene. Three different magnetic field strengths, a, b, and c, are shown which correspond to stable ion masses 92, 91, and 90, respectively. The time-of-flight resolution is sufficient to resolve the stable ion peaks and to resolve the 91 daughter ion of parent mass 92 from the stable ion at m/z 90.

The resolution for a parent ion scan is shown in Figure 4.11 for the daughter ions that result from loss of Cl from the molecular ions of chlorobenzene. As will be discussed in Chapter VI, this scan also shows the full kinetic energy release of the metastable transition. For comparison, a computer program was written to determine the flight time difference between adjacent masses. Figure 4.12 shows the calculated flight times for different masses in the TRIMS instrument, assuming a flight path of 1.5 m and energy of 3.5 kV. The time difference between each mass from Figure 4.12 is plotted in Figure 4.13 to show the maximum peak width allowable for a given absolute resolution at any mass.
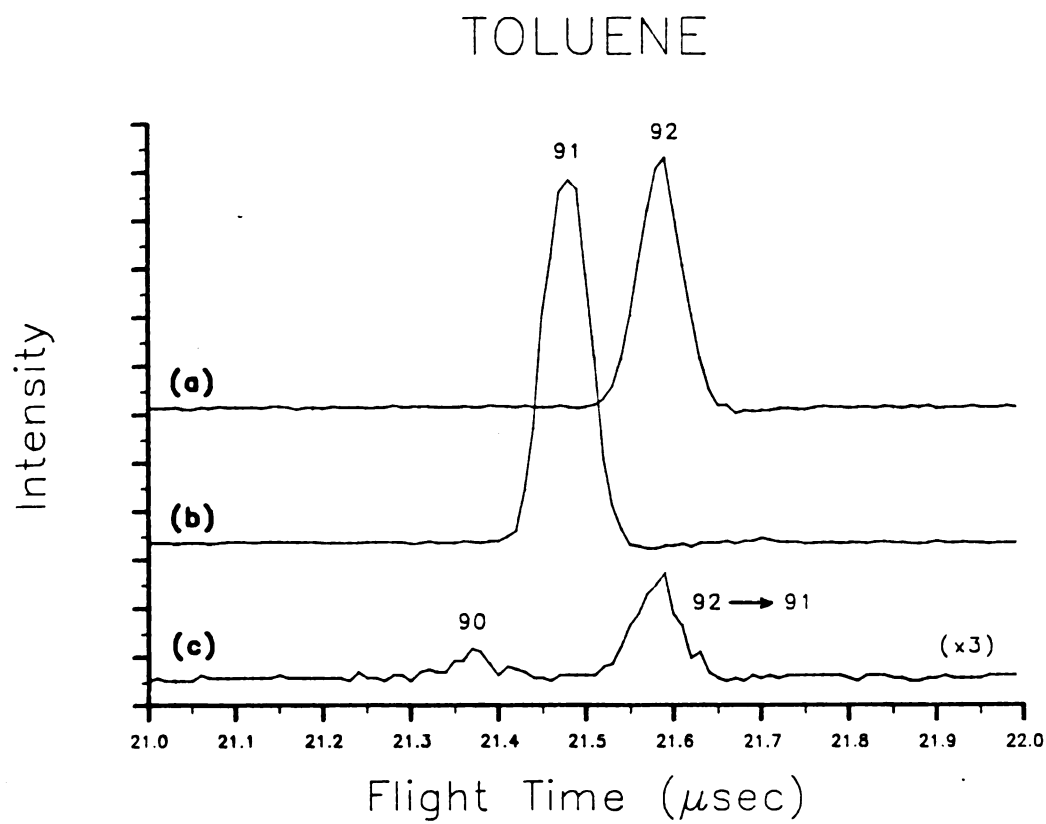
Figure 4.10. Time sweeps at three magnetic field settings (a,b,c) showing the resolution in the molecular ion region of toluene.

Chlorobenzene
Parent scan of daughter mass 77
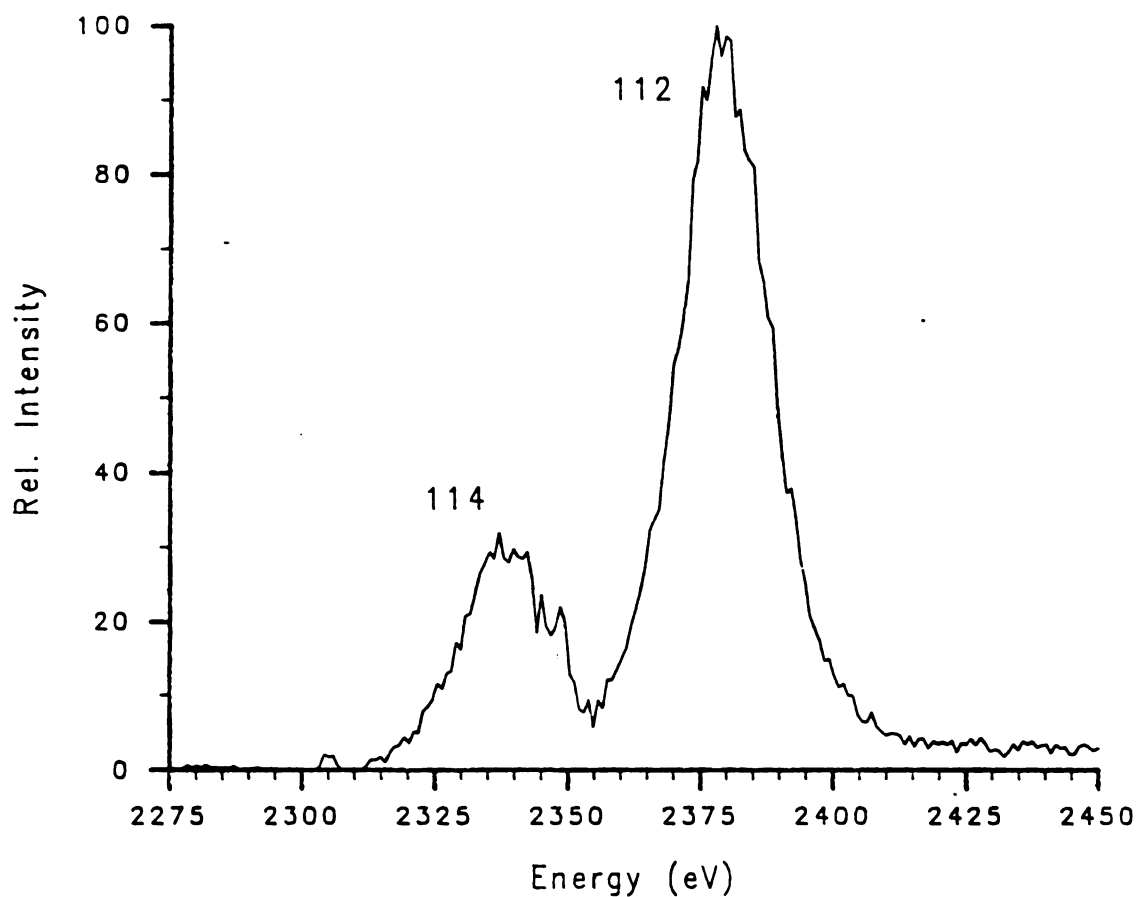
Figure 4.11. Daughter ion peaks along a line of constant B·t (mass=77) formed by metastable decomposition from parents of mass 112 and 114 of chlorobenzene. Release of kinetic energy in the dissociation process reduces the ability to distinguish daughters formed from different parents.
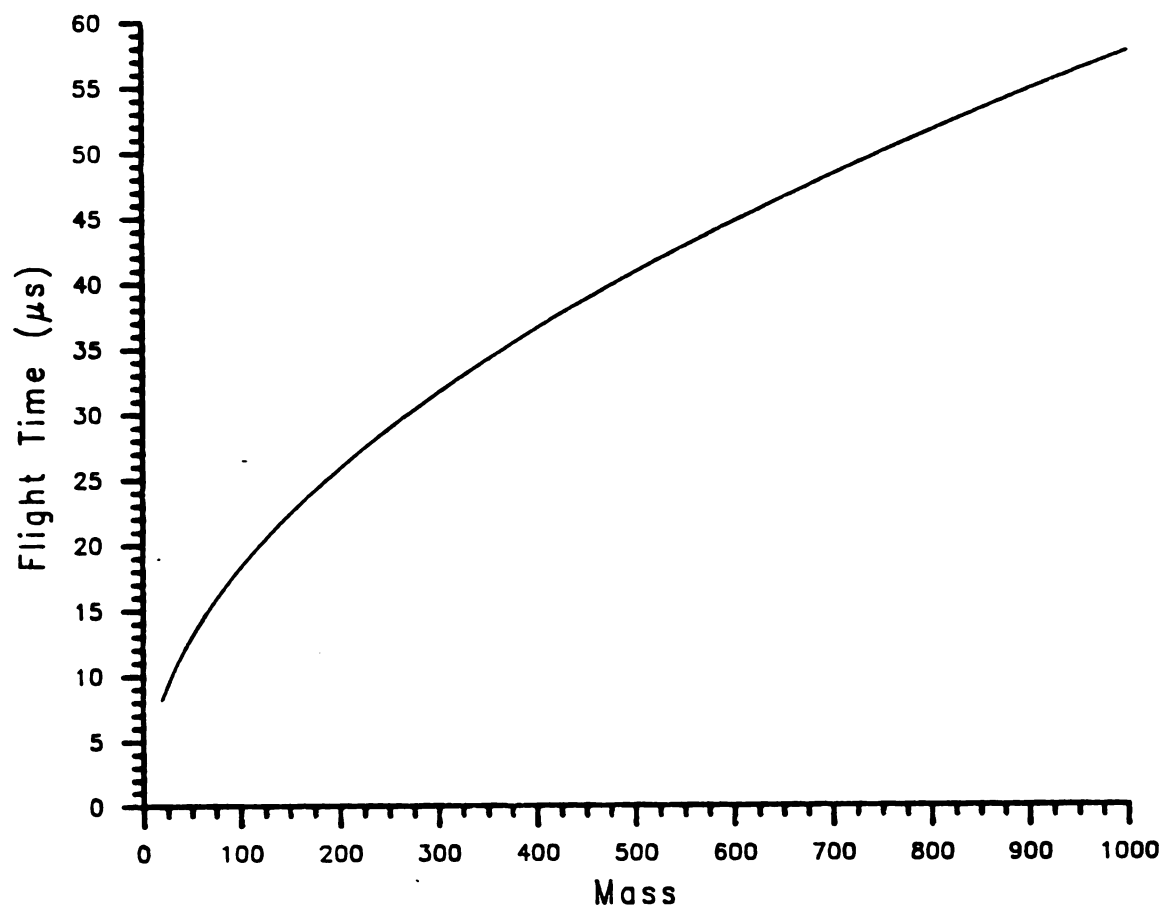
Figure 4.12. Calculated ion flight times in the TRIMS instrument for d=1.5 m, V=3.5 kV.
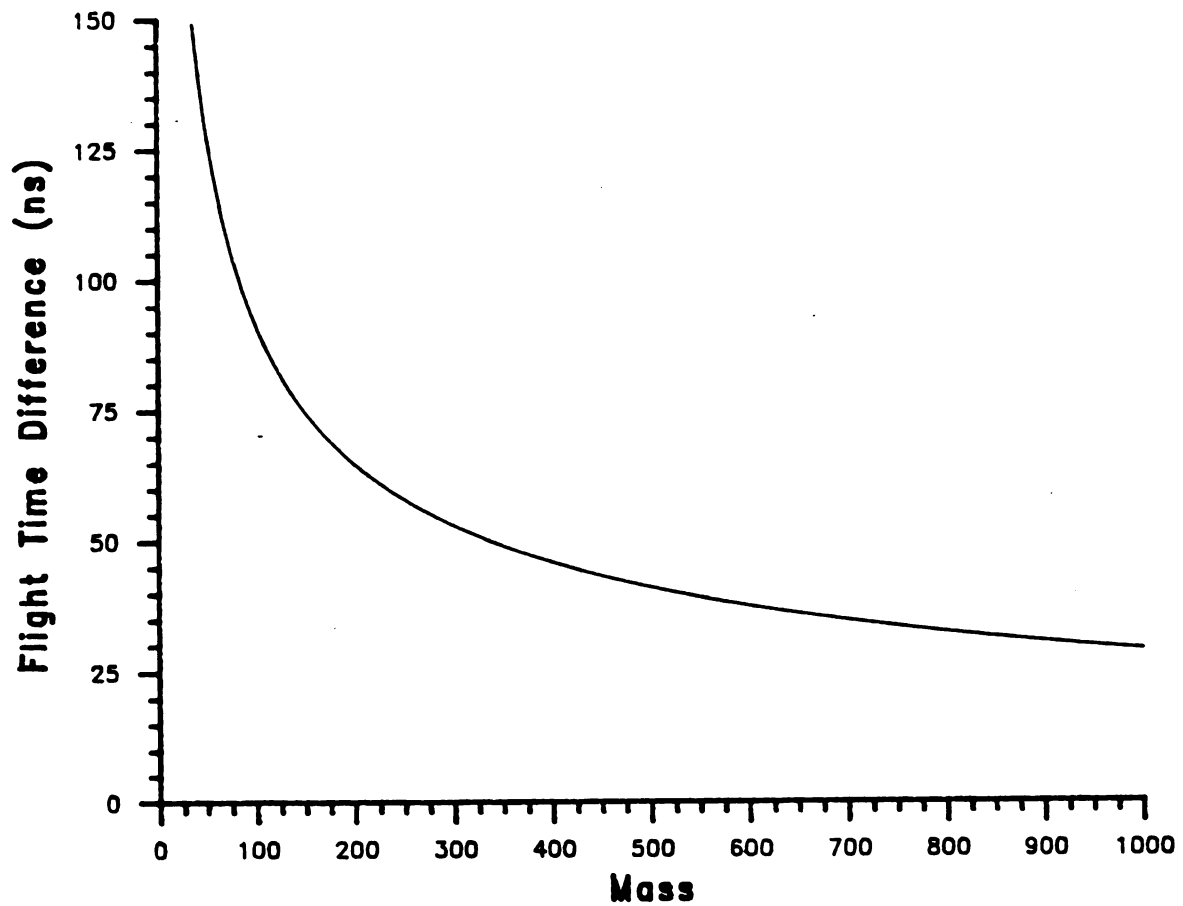
Figure 4.13. Calculated flight time difference between adjacent
   masses in the TRIMS instrument as a function of mass for
   d=1.5 m, V=3.5 kV.

Dissociations within Non-Field-Free Regions

An additional factor that will affect the appearance of the spectrum and the mass resolution is the dissociation of ions during acceleration or within the magnetic sector (9). Dissociations within the accelerating field do not affect the daughter ion mass assignment because this mass assignment is solely defined by the value of B·t. The arrival time will decrease, though, resulting in a low-level continuum along the curve of constant B·t between the arrival time for a stable ion and the arrival time for the same transition occurring in the field-free region. This continuum is observed in Figure 11 as the elevated baseline at the high-energy side of the peak. Likewise, dissociations within the magnetic sector result in a continuum that extends from the stable ion B·t position along a line of constant arrival time. The intensity along the continuum should be very small compared to the intensity at the B·t value of the daughter ion because all dissociations occurring in the field-free region are concentrated there while all occurring in the magnet are distributed along the continuum. The use of a collision cell to enhance dissociations in the field-free region should further suppress the continuum intensity.

Artifact Peaks

Artifact peaks in single mass scans could occur for a number of reasons. First, there might be inadequate resolution of the parent ion masses. For example, a daughter ion scan of parent mass 100 of any given compound might contain peaks that really represent daughters of

parent ions with mass 99 or 101. Second, some kinetic energy release in the daughter ion formation process is always observed. This effect would manifest itself in the same way as for inadequate parent ion resolution. Third, the ion continuum from dissociations in non-field-free regions could appear in parent and daughter ion scans. Fourth, for certain settings of the ion source voltages, the ion beam may "leak" out of the source continuously, resulting in a continuum at all flight times for those magnetic field strengths that correspond to intense stable ion masses. Scans that cut across this time-of-flight continuum, e.g., a daughter scan, would record a false peak. The only way to be absolutely certain that artifact peaks are not present is by viewing the entire data field, or at least a portion of the data field in question, to see what peaks are present and to assess their peak shape.

Sensitivity

As with other mass spectrometric techniques, sensitivity and resolution are inversely related in the TRIMS instrument, so one must consider both parameters when setting up an experiment. Increasing the resolution may improve the selectivity of a measurement, but only at the expense of sensitivity. The sensitivity of the TRIMS instrument is dependent on three factors: the setting of the instrumental resolution, the ion pulsing mechanism, and the signal detection scheme.

Pulsing Techniques

There are two basic methods for creating a pulse or packet of ions: ion beam deflection and pulsed ion extraction. In ion beam deflection, the ions are continuously formed and extracted out of the ion source. The continuous beam is then chopped, usually by rapid electrical deflection, to create a pulse of ions (10,11). The chopping in TRIMS can occur either before or after the magnet. Pulsing does not change the momentum of the ions so its position with respect to the magnet is immaterial; it only encodes time information on the signal. The sensitivity is limited by the duty cycle, the ratio of the time the beam is "on" to the total period of the pulsing cycle. Referring again to Figure 4.13, to measure a peak at mass 100 with unit resolution requires a peak width of approximately 100 ns and, if mass 100 is the largest ion, a period of approximately 20 μs. This yields a duty cycle of 100ns/20μs = 0.005. The present detection circuitry has a minimum period of 100 μs, reducing the duty cycle to 0.001. Stated another way, only 0.1% of the ions which leave the ion source in a conventional magnetic sector mass spectrometer are used in the TRIMS instrument. One would thus expect a reduction in sensitivity of 99.9% with respect to a conventional magnetic sector instrument. Higher resolution required by larger molecules would further reduce the duty cycle.

One way to improve the duty cycle limitation is by using correlation techniques. Although the measurement period in the present system is limited by the detection electronics, the theoretical limit

is imposed by the time required for the heaviest ion to reach the detector. This limit is necessary so that ions from consecutive ion source pulses do not overlap. However, intentional overlap could be applied. If the source is pulsed in a known but random sequence (pseudorandom sequence) the detected signal can be cross-correlated with the pseudorandom sequence to obtain the mass spectrum (12-15). Alternately, the ion source could be pulsed at a given frequency and a Fourier Transform applied to the detected signal to obtain the mass spectrum (16,17). These correlation techniques allow the ion source to be pulsed quite often, increasing the duty cycle (up to 50%) and hence sensitivity.

An alternative to ion beam deflection is pulsed ion extraction. In pulsed ion extraction, the ions are formed in the ion source and then extracted by a pulse applied to one or more of the ion source lenses. The extraction pulse must be at least 2μs long to allow all ions to leave the ion source and acquire the same kinetic energy. The pulsing period limitation is the same as for the beam deflection technique but there is the potential for storing ions in the ion source between pulses to increase the signal. The duty cycle is effectively increased because ions are utilized which are formed over a greater period of time. As will be demonstrated in the next chapter, however, pulsed ion extraction in TRIMS results in degraded resolution along the magnetic field axis.

Ion Storage Mechanisms

There are several methods for storing or trapping ions in the ion source. The most widely used is the trapping of positive ions in the negative space charge (negative potential well) of the electron beam which is used for electron impact ionization. Positive ions can be trapped in this well until the number of positive charges equals the number of negative charges, a condition known as space charge neutralization or the space charge limit. Space charge trapping was studied during the 1950's as a means of obtaining larger electron current densities in electron tubes and the theory was developed in that context (18,19).

Space charge trapping in an electron beam of a mass spectrometer was first used by Studier (20) to increase sensitivity in a time-of-flight instrument. In this approach, which Studier called continuous ionization, the electron beam remained on from the end of one extraction pulse to the beginning of the next. More recently, others have used space charge trapping for studying consecutive ionizations (21-23), ion-molecule reactions (24,25), and for producing a time delay between ion formation and ion extraction in order to derive information on the kinetics and energetics of metastable decompositions (26). Although space charge trapping can significantly increase the concentration of ions in the ion source, long storage times at high electron energies can lead to multiply charged ions (21), ion-molecule reactions (24), and excessive fragmentation (27).

Other methods for trapping ions have been developed but have not yet been utilized in time-of-flight applications. The ion cyclotron resonance cell (28,29), the quadrupole ion storage trap (30-32), the Penning trap (33), the Brink trap (34), and the cylindrical ion trap (35) have been shown to trap ions efficiently for relatively long periods of time. However, they have the problem of not creating ions in a plane (poor space resolution). For TRIMS, an additional constraint is the need to focus ions into a narrow slit image. Various focusing devices could be used to do this but they could create further space resolution problems because of the necessarily non-homogeneous fields.

Ion Storage Evaluation

If all the ions formed between ion extraction pulses could be stored and then extracted, the effective duty cycle would approach 100%. Of course, storage efficiency, particularly with space charge trapping, is considerably less. There is a limit to the number of ions that can be held in the ion source and there is also a limit to the number of ions that can travel through the instrument at one time without distortion of the ion optics (36). Even so, pulsed ion extraction should provide greater sensitivity than the ion beam deflection technique.

The ion storage characteristics of the TRIMS instrument were evaluated by examining the ion intensity as a function of storage time,

sample pressure, and electron trap current. It was found that the time required to fill the trap was constant at 2 μs, regardless of the sample pressure or trap current. Higher trap current or sample pressure simply altered the maximum intensity that could be achieved by ion trapping. These data indicate that the ion trapping is fairly inefficient, i.e., ions are lost from the source quite rapidly and only by increasing the number of electrons or the number of sample molecules available for ionization, can the intensity be increased. The intensity was also dependent on the extraction lens voltage during the ion storage time. The maximum intensity occurs when the extraction lens voltage is exactly equal to the ionization chamber voltage. Slight increases or decreases (greater than 2 V) in that voltage reduce the signal intensity by 75%. Unfortunately, operation at the optimal trapping voltage allows ions to leak out of the source, creating a dc continuum. An extra lens needs to be added to the ion source to repel these ions during the storage time while allowing the extraction voltage to be equal to the ionization chamber voltage.

One concern with trapping the ions for long periods of time is the potential for ion-electron, ion-neutral, and ion-ion interactions. None of these were observed in any of the systems studied in this work.

To evaluate the duty cycle factor of the TRIMS instrument, the detection limit for the molecular ion of n-decane was measured, both with and without ion source pulsing, by selected ion monitoring. All instrument conditions and measurement parameters were the same for both experiments. The sample was introduced in hexane solvent via the gas

chromatograph, using a 2mm x 3ft glass column packed with 3% SP-2100 on 80/100 Supelcoport. The column temperature was held at 80°C, the injector heater at 130 C, and the separator at 130°C. The trap current was 60 μA, the electron multiplier voltage controller set to 7, and the magnet was set manually to mass 142, using n-decane to set and periodically to check the magnetic field setting. A 65 V, 4 μs long extraction pulse was used. The gated integrator settings were: sensitivity = 50 mV, time constant = 100 μs, SUM, DC, 50 ohm. The aperture duration (time slice) was set at 5 μs and the delay from the source pulse was 25 μs. A point was recorded every 0.1 s with 500 time-slices summed per point. The ion source was pulsed once every 120 μs. In non-pulsed mode, the trigger to the pulse generator was disconnected, but all other conditions were the same. The gated integrator measured a 5 μs segment of the continuous ion beam every 120 μs. A signal-to-noise ratio (S/N) of 5 was chosen to define the detection limit. In the non-pulsed mode, the detection limit was reached at 200ng. In the pulsed mode, the detection limit was reached at 2μg.

These values can be used to compare the number of ions which reach the detector. It is assumed that the detection limit for both pulsed and non-pulsed modes corresponds to the same number of ions reaching the detector per 5 μs time slice. Although the full time-of-flight peak was detected during this 5 μs time slice in the pulsed mode, only those ions reaching the detector in one 5 μs interval out of the full 120 μs were measured in the non-pulsed mode. Therefore, only 5μs/120μs = 1/24 of the non-pulsed signal available was measured. If it were

possible, the equivalent amount of compound to produce the same ion intensity during only the measured 5 μs time slice would be 1/24th as large, 200ng/24 = 8 ng. Therefore, the same number of ions are measured for 200 ng of sample in the pulsed mode and for 8 ng of sample in the continuous mode. This calculation yields a ratio for the number of ions produced by pulsed and continuous extraction of 2μg/8ng = 250. Had the pulsing been achieved by beam deflection instead, one would expect the detected ion ratio to be 1000 (120 ns wide pulse, 120 μs period). Therefore, the pulsed extraction gives a factor of 4 improvement in ion signal, presumably due to ion storage.

A separate experiment was performed to determine the detection limit for the non-pulsed mode, using a conventional low bandwidth, high gain amplifier. The sample introduction and mass spectrometer conditions were identical to those in the previous experiment. The data system recorded the ion abundance once every 0.1 s. The detection limit for the n-decane molecular ion was found to be 0.4 ng. This value demonstrates the rather poor sensitivity of the time-resolved detection electronics, which for the same experiment gave a detection limit of 200 ng. This disparity could be decreased by increased signal averaging and by working to reduce some of the grounding problems in the gated integrator.

The sensitivity in TRIMS is ultimately limited by the efficiency of the ion source. In electron impact, less than one in 10^5 of the sample molecules are actually ionized. The duty cycle of pulse

formation further reduces the number of ions that leave the ion source, even when ion storage is employed. Furthermore, there is a space charge limit to the number of ions that can accumulate in the ion source and that can pass through the instrument. Ionization techniques that utilize a condensed sample matrix and are in themselves pulsed, e.g., laser desorption (37) and pulsed secondary ion mass spectrometry (38,39), would lend themselves quite readily to TRIMS. With these types of desorption ionization techniques, no sample is lost between ionization pulses, which could produce a considerable enhancement of sensitivity.

References

1. Wachs, T.; Bente, P.F.; McLafferty, F.W. Int. J. Mass Spectrom. Ion Phys. 1972, 9, 333-341.

2. Coutant, J.E.; McLafferty, F.W. Int. J. Mass Spectrom. Ion Phys. 1972, 8, 323-339.

3. Stults, J.T.; Enke, C.G.; Holland, J.F. Anal. Chem. 1983, 55, 1323-30.

4. Martin, F.E.; Holland, J.F.; Sweeley, C.C. In "Biomedical Applications of Mass Spectrometry, First Supplementary Volume"; Waller, G.R.; Dermer, O.C., Eds.; Wiley-Interscience:New York, 1980. p. 51.

5. Glish, G.L.; Todd, P.J. Anal. Chem. 1982, 54, 842-3.

6. Eckenrode, B., Michigan State University, Chemistry Dept., unpublished work.

7. Kim, M.S.; McLafferty, F.W. J. Am. Chem. Soc. 1978, 100, 3279-82.

8. Herbert, C.G.; Larka, E.A.; Beynon, J.H. Org. Mass Spectrom. 1984, 19, 306-310.

9. Fraefel, A.; Seibl, J. Mass Spectrom. Rev. 1985, 4, 151-221.

10. Bakker, J.M.B. J. Phys. E 1973, 6, 785-9.

11. Bakker, J.M.B. J. Phys. E 1974, 7, 354-8.

12. Bailey, C.A.; Kilvington, J.; Robinson, N.W. Vacuum, 1971, 21, 461-4.

13. Nowikow, C.V.; Grice, R. J. Phys. E 1979, 12, 515-21.

14. Ducorps, A.M.; Yashinovitz, Rev. Sci. Instrum. 1983, 54, 444-53.

15. Duren, R.; Groger, W.; Liedtke, Rev. Sci. Instrum. 1985, 56, 377-81.

16. Knorr, F.J.; Eatherton, R.L.; Siems, W.F.; Hill, H.H., Jr. Anal. Chem. 1985, 57, 402-6.

17. Knorr, F.J.; Chatfield, D. presented at the 33rd Annual Conference on Mass Spectrometry and Allied Topics, San Diego, May 26-31, 1985.

18. Linder, E.G.; Hernqvist, K.G. J. Appl. Phys. 1950, 21, 1088-97.

19. Hines, M.E.; Hoffman, G.W.; Saloom, J.A. J. Appl. Phys. 1955, 26, 1157-62.

20. Studier, M.H. Rev. Sci. Instrum. 1963, 34, 1367-1370.

21. Baker, F.A.; Hasted, J.B. Phil. Trans. Roy. Soc. London, A 1966, 261, 33-65.

22. Cuthbert, J.; Farren, J.; Prahallada Rao, B.S.; Preece, E.R. Proc. Phys. Soc. (London) 1966, 88, 91-100.

23. Redhead. P.A. Can. J. Phys. 1967, 45, 1791-1812.

24. Herod, A.A.; Harrison, A.G. Int. J. Mass Spectrom. Ion Phys. 1970, 4, 415-31.

25. Bourne, A.J.; Danby, C.J. J. Phys. E 1968, 1, 155.

26. Lifshitz, C.; Gefen, S.; Arakawa, R. J. Phys. Chem, 1984, 88, 4242-46.

27. Plumblee, R.H. Rev. Sci. Instrum. 1957, 28, 830-2.

28. McIver, R.T. Rev. Sci. Instrum. 1970, 41, 555-8.

29. McMahon, T.B.; Beauchamp, J.L. Rev. Sci. Instrum., 1972, 43, 509-12.

30. Fulford, J.E.; March, R.E. Int. J. Mass Spectrom. Ion Phys. 1979, 30, 39-55.

31. Dawson, P.H.; Todd, J.F.J.; Bonner, R.F. Dyn. Mass Spectrom. 1976, 4, 39-81.

32. Dawson, P.H. Adv. Electron. Electron Phys., Suppl. 13B 1970, 173-256.

33. Heppner, R.A.; Walls, F.L.; Armstrong, W.T.; Dunn, G.H. Phys. Rev. A 1976, 13, 1000-11.

34. Brink, G.O. Rev. Sci. Instrum. 1975, 46, 739-42.

35. Fulford, J.E.; March, R.E.; Mather, R.E.; Todd, J.F.J.; Waldren, R.M. Can. J. Spectrosc. 1980, 25, 85-97.

36. Robinson, C.F. Rev. Sci. Instrum. 1949, 20, 745.

37. Cotter, R.J.; Tabet, J.C. Int. J. Mass Spectrom. Ion Phys. 1983, 53, 151-166.

38. Chait, B.T.; Standing, K.G. Int. J. Mass Spectrom. Ion Phys. 1981, 40, 185-193.

39. Benninghoven, A. Int. J. Mass Spectrom. Ion Phys. 1983, 53, 85-99.

CHAPTER V

EFFECTS OF INITIAL ION ENERGY AND SPATIAL DISTRIBUTIONS

Observed Deviations from Theory

It was demonstrated in Chapter 4 that the theory derived for TRIMS accurately describes the operation of the TRIMS instrument, i.e., ion mass is determined by the B·t product and parent-daughter ion relationships are determined by the ion flight time. Ions with the same mass but different energies appear at different values of B and t, but the product B·t is the same.

Any spread in ion energy for stable ions of the same mass should, in principle, cause the ion abundance profile to be broadened along the B·t curve in the B-t data field. Figure 5.1a shows the expected locus of those points. For ions of the same mass, ions of higher energy appear at larger magnetic field strengths but at shorter flight times than ions of lower energy. However, initially the locus of points was found experimentally to have a slope of opposite polarity when pulsed extraction was employed, as shown in Figure 5.1b. Those ions appearing at larger magnetic field strengths had longer flight times. Furthermore, the voltages applied to the extraction pulse also affect the ion current profile in the B-t data field.

The extraction pulse is the voltage pulse applied to the first lens (extraction lens) in the ion source (see Figure 5.2). The voltage

144
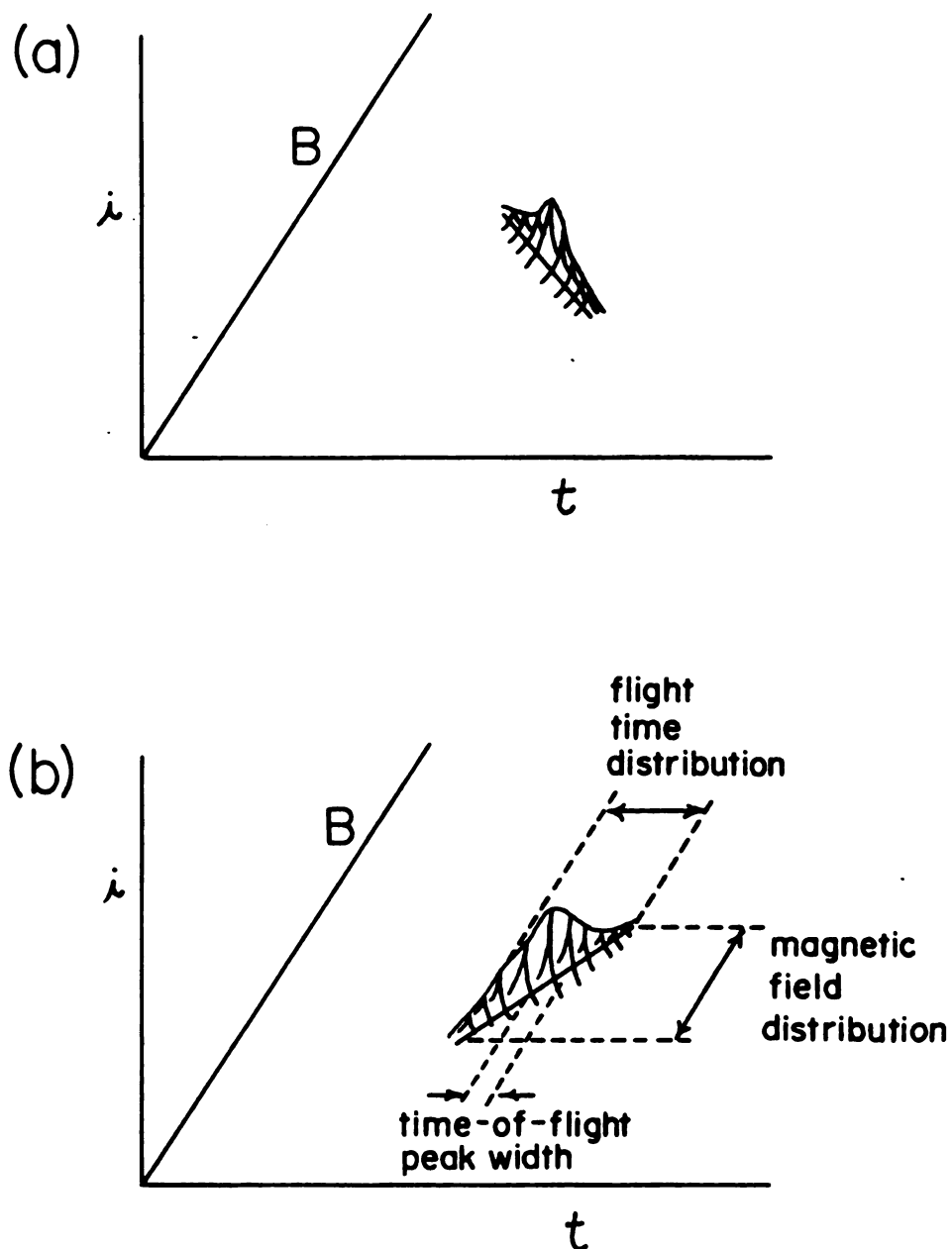
Figure 5.1. Shapes of typical ion abundance profiles in the B-t data field of the TRIMS instrument, (a) expected, (b) observed.
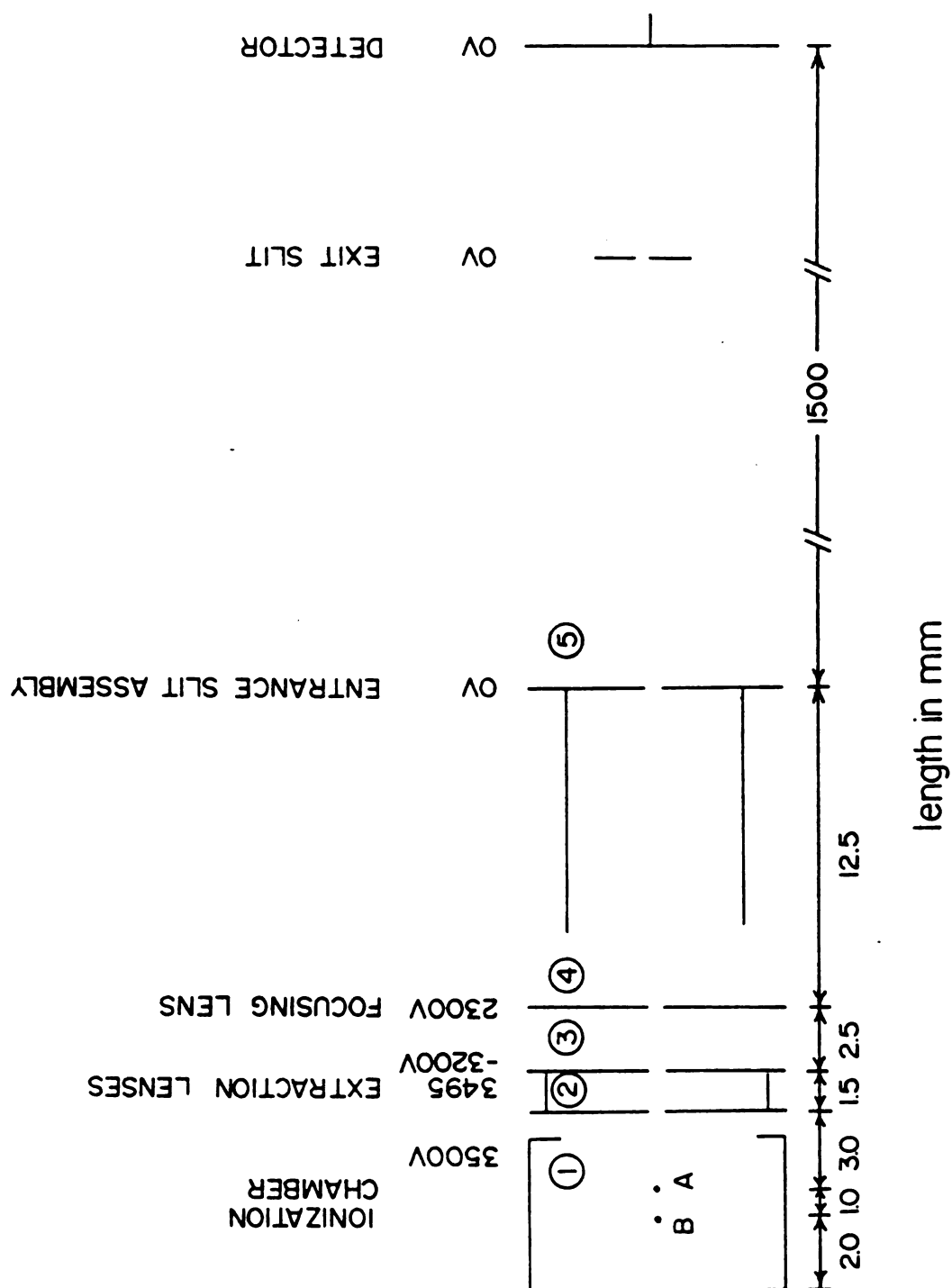
Figure 5.2. LKB-9000 ion source and drift tube dimensions and lens potentials.

on the ionization chamber and on all other lenses remains fixed, as does the overall accelerating voltage. The value of the extraction voltage is the magnitude of that voltage <u>below</u> the accelerating voltage, 3500 V. For example, when the extraction voltage is 100 V, the voltage on the extraction lens is 3400 V. Figure 5.1b shows the locus of points for only a single extraction voltage.

For stable ions of the same mass, as the extraction voltage was increased, the following trends were observed:

1. ion flight times decreased

2. ions appeared at lower magnetic field strengths

3. resolution along the B-axis decreased

4. resolution along the t-axis increased

5. flight time peak width decreased

6. ion intensity increased.

Observation 1 could be explained by an increase in ion energy, but observation 2 suggests a decrease in ion energy. Why would increased extraction voltage cause a change in the ion energy? What might be the cause of the other observations?

The theory developed in Chapter 2 did not include any secondary effects caused by the initial spatial and energy distributions in the ion source. Nor did the theory consider that ions start nominally from rest and must be accelerated to their final velocity. It should. The measured flight time is really the time for an ion to travel from the instrument entrance slit to the detector <u>plus</u> the time required for acceleration of the ion in the ion source. This acceleration time can

be appreciable, particularly at lower extraction voltages. A simple
model based on the ion source dimensions and potentials is developed in
this chapter. It is then used to explain all the observations listed
above.

Space and Energy Focusing in Conventional TOF Instruments

As mentioned briefly in Chapter 1, resolution in conventional
time-of-flight mass spectrometry suffers for two reasons: ions are
formed and accelerated from different positions in the ion source, and
ions have an initial kinetic energy. Corrections for the former are
classed as space-focusing and corrections for the latter are classed as
energy-focusing (1-3).

Wiley and McLaren (1) developed the classic solution to this
problem. Space-focusing was accomplished by a two-region acceleration
source, as shown in Figure 5.2. Ions formed at different positions in
the ion source experience different potential drops in the first
acceleration region. Ions at point B acquire a greater energy than
those at position A. By proper choice of the ion source lens voltages
and the instrument dimensions, ions formed at position B have a higher
velocity that allows them to catch up to the ions formed at position A
just as they reach the detector.

Energy-focusing was accomplished first by making the total
accelerating voltage as large as possible so that the initial energy
(<2 eV) is negligible when compared to the total ion energy. This

value, however, is constrained by the space-focusing condition. A
larger problem, however, is related to the fact that the ions have
initial velocity vectors in all directions. Those ions moving away
from the detector must be stopped and pulled in the other direction,
resulting in a "turnaround time." Wiley and McLaren (1) corrected for
the turnaround by time-lag focusing -- ions are allowed to drift at
their initial velocities for a short period of time after their
formation but before they are accelerated out of the source. Those
ions that are initially moving away from the exit slit continue to move
farther away during the time lag. Once the accelerating voltage is
turned on, they fall through a larger potential drop so that their
higher velocity compensates for the turnaround time. Any one time lag
setting, unfortunately, is correct over only a small mass range.

Other approaches to energy- or time-focusing (4) have been
developed, usually combining a field-free drift region with an "active"
focusing device, most often an electric sector (5-11) or an
electrostatic reflection device (12,13). These configurations,
however, do not allow for simultaneous space-focusing.

The most successful approaches for eliminating all the focusing
problems involve pulse generation by ion beam deflection (14,15)
followed by an energy focusing device (16,17). A similar approach
utilizes a continuous source and an electric sector to produce a
monoenergetic ion beam, followed by the beam deflection technique for
pulsing (18). Energy focusing or filtering eliminates the energy

differences caused by initial spatial or energy distributions. The beam deflection technique eliminates the turnaround time and space-focusing problems. Beam deflection, however, is the worst type of pulsing mechanism from a sensitivity standpoint. Only those ions transmitted during the short slice of the ion beam are utilized. At least with the pulsed extraction technique there is the potential for ion storage between pulses (19,20). In all cases of pulsed extraction, the flight time is the sum of the turnaround time, the ion acceleration time, and the drift time through the instrument. Therefore, the total flight time is not an accurate measure of the ion velocity. This fact must be taken into consideration in TRIMS. Furthermore, in focused time-of-flight measurements, different ion energies are used to achieve constant flight times. In TRIMS, those added energy differences appear as momentum differences, reducing the resolution along the magnetic field axis below that obtained with the same instrument when the source is not pulsed.

Unlike the time-of-flight instrument, in which the goal of focusing is to achieve the same flight time for all ions of the same mass, the goal of focusing in a magnetic sector instrument is to achieve the same velocity for all ions of the same mass. In a magnetic sector instrument, this is accomplished by using a large accelerating voltage to make the initial ion energy negligible and by making the initial extraction voltage as small as possible (usually <10 V) to minimize energy differences of ions formed in different regions of the ion source (21,22). The latter requirement contradicts the TOF

requirements — that larger extraction voltages are needed to reduce the turnaround time and that the optimum extraction voltage is determined by the space-focusing condition .

The TRIMS instrument shows the effects of pulsed extraction in both the time-of-flight and magnetic sector domains. An understanding of the effects of initial spatial and energy distributions in TRIMS aids in explaining the ion distributions in the B-t data field and provides a basis for adjusting the instrumental parameters for optimum performance.

The spatial and energy distributions are treated separately below. As will be shown, the effects of each are experimentally distinct. The difference in initial position of isobaric ions determines the extent of ion spread orthogonal to the constant B·t line while the initial energy distribution influences the spread in flight times at any one magnetic field strength (see Figure 5.1).

Ion Distribution in the B-t Data Field — Spatial Effects

Computer Simulation of the Ion Source Conditions

Based on the voltages and dimensions of the LKB-9000 ion source and TRIMS-modified flight path, a computer program was written to calculate ion flight times, velocities, and energies for different extraction voltages. It was assumed that all the lenses acted like

perfect, infinitely wide grids, so that all electric fields were linear. Although this is not the case, it is a good first approximation, as the results will demonstrate. Moreover, the electron beam collimating magnet in the source is assumed to have negligible effect on the ion motion, the ions are assumed to have taken identical paths through the instrument, and the focusing field of the deflection plates, positioned after the entrance slit for z-axis focusing, is assumed to be negligible.

The instrument voltages and dimensions are shown in Figure 5.2. The program calculates the flight time for each region, then sums these times to obtain the total flight time. The flight time in the ionization chamber is calculated for the acceleration of an ion from rest. The ion velocity at the extraction plate depends on the distance the ion travels in the electric field in this region. The spatial distribution is taken as the breadth of the electron beam. The ion energies and velocities at the entrance and exit of each subsequent region are then calculated. Since the acceleration force is constant in each region, the flight time for each can be calculated from the average velocity. The flight time from the end of the acceleration region to the detector is the simple quotient of the flight distance and the final velocity, assuming all detected ions take identical paths through the magnetic sector.

The total energy an ion receives from acceleration is a function of the extraction voltage for a fixed accelerating voltage. The total gain in ion kinetic energy decreases as the extraction voltage

increases because an ion only falls through a fraction of the potential drop in the ionization chamber. For example, if an ion starts in the middle of the ionization chamber and the extraction voltage is 10 V, the ion picks up 5 eV of energy in this region, but it is denied 5 eV of the total acceleration energy since the total potential drop in the whole ion source remains constant. (The back of the ionization chamber remains fixed at 3500 V.) If the extraction voltage is 100 V for the same ion, 50 eV of the total acceleration energy will not be availabl to it. For the same reason, the energy distribution caused by a spatial distribution in the ion source also becomes larger as the extraction voltage increases.

Comparison of Simulated and Observed Results

Figure 5.3, from the simulation program, shows the ion kinetic energy as a function of extraction voltage. A direct experimental measure of the ion energy was not available for comparison. The decrease in the final ion energy also means that there is a decrease in the final ion velocity.

The dotted lines in Figure 5.4 show the computer-calculated values for the final ion velocity as a function of the extraction voltage for ions starting at two different positions, A and B, in the ion source. The prediction of this model is compared with the result of the following experiment. The ion current distribution of mass 71 of n-decane in the B-t data field was measured at four different values of the extraction voltage, 33 V, 65 V, 100 V, and 140 V. For each of

Ion Energy —— m/z 71

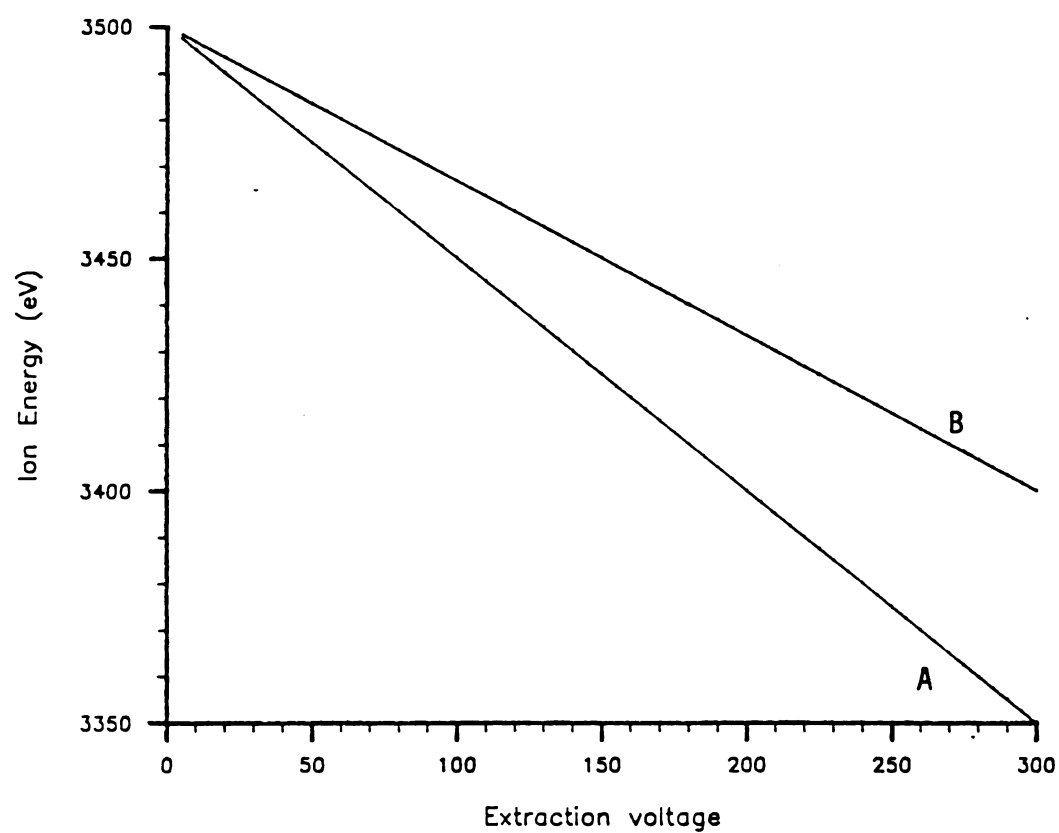Figure 5.3. Calculated final ion energy vs. extraction voltage
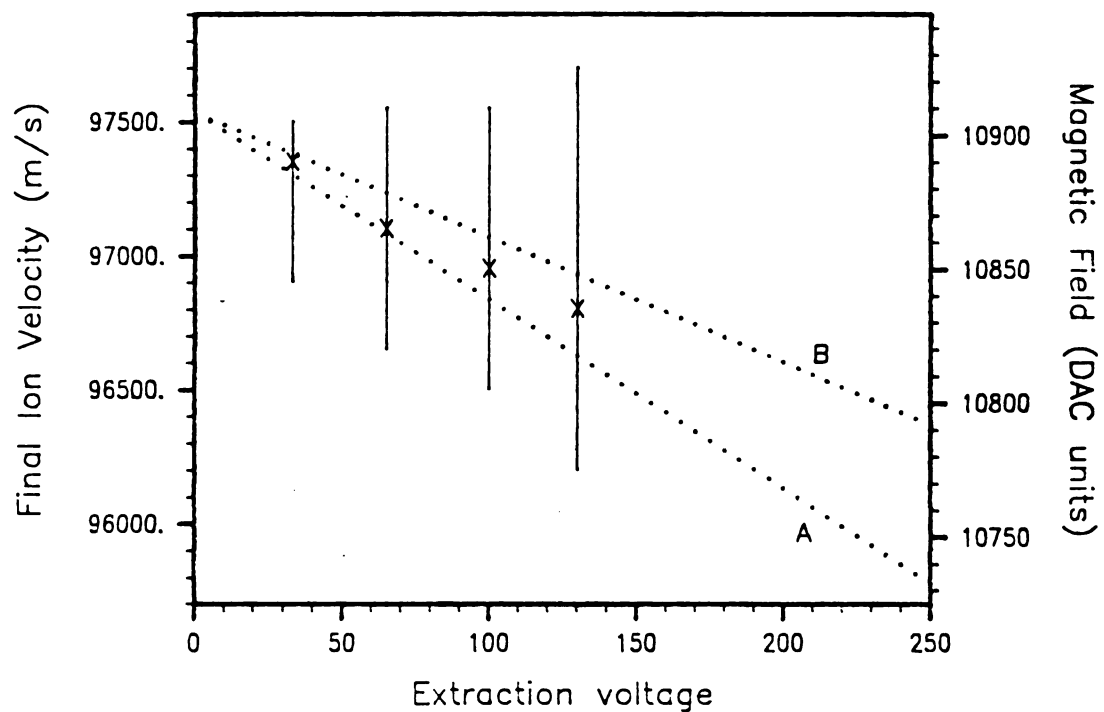for mass 71 (ions formed at points A and B in the ion source).

Figure 5.4. Final ion velocity vs. extraction voltage for mass 71.
The dotted lines are the calculated velocity values for ions
formed at points A and B in the ion source. The vertical lines
show the values of magnetic field strength at which ion abundance
was observed.

these voltages, time sweeps were taken as the magnetic field was incremented over the peak. The flight time of maximum intensity was recorded for each magnetic field value. The distribution in magnetic field strength at which ion intensity is actually observed is shown by the vertical lines in Figure 5.4. Since the magnetic field is a measure of momentum, it is also a measure of ion velocity for a constant mass. The point of maximum ion intensity at each extraction voltage is identified by an "x". There is good agreement for the downward trend of the final ion velocity and of the increase in the velocity distribution as the extraction voltage is increased. This explains why the magnetic field resolution decreases when the extraction voltage is increased.

The curved lines in Figure 5.5 show the computer simulation of the ion flight times for two ions, A and B, that start at different places in the ion source. Note that at extraction voltage = 135 V, the flight times of the two ions are the same. This voltage corresponds to the space-focusing condition for this particular instrument. Further calculations show that this space-focusing point (flight time difference = 0) is identical for ions of all masses, as expected (1). The vertical lines in Figure 5.5 show the experimental data, again with the ion intensity maximum at each extraction voltage indicated by an "x". These are the flight times observed at different magnetic field settings across the entire peak, i.e., the spread is not the arrival time peak width at a single magnetic field setting. The same trends are observed experimentally as were predicted by the calculated values: with an increase in extraction voltage there is a decrease in average
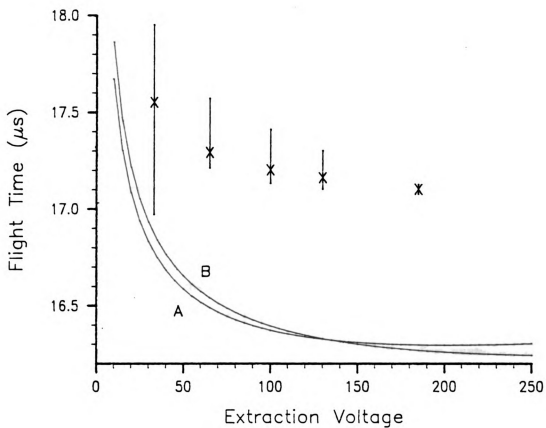
Figure 5.5. Total ion flight time vs. extraction voltage for mass 71. The curved lines show the calculated values for ions formed at points A and B in the ion source. The vertical lines show the observed values.

flight time and a decrease in the flight time distribution. The differences between the calculated and observed flight times reflects delay times in the measured values, and also, most likely, reflects the effects of secondary factors in the ion source model that were assumed to negligible (e.g., ideal grids, no source magnet, no deflection lens deceleration).

Temporary modification of the pulse amplifier allowed operation at higher extraction voltages. The space focusing point on the TRIMS instrument was observed to be 185 V.

The majority of the flight time distribution, especially at low extraction voltages, is due to the difference in acceleration time in the ionization chamber. Table 5.1 lists the calculated flight times in different regions of the instrument. At 10 V, for example, the simulation program gives an acceleration time from rest (no initial kinetic energy) to the extraction lens as 1.628 μs for mass 71 ions starting at position A, and 1.879 μs for the same ions starting at position B.

The calculated final ion velocity and flight time data are combined in one graph, Figure 5.6a, which is equivalent to the ion current distribution in the B-t data field. Figure 5.6b shows the experimental results. As mentioned earlier, modification of the pulse amplifier allowed larger extraction voltages to be used. It was found that the space focusing condition was met at an extraction voltage of 185 V. At higher voltages, the slope of the line in the B-t data field

Table5.1.Calculated flight times for mass 71 ions
in different regions of the TRIMS instrument as numbered in Fig. 5.2.

Extraction Lens Potential	Initial Position	Initial Energy	------- Flight Time in Region -------					Total Flight Time	Final Velocity
			1	2	3	4	5		
10V	A(3mm)	0eV	1.628µs	0.407µs	0.082µs	0.162µs	15.390µs	17.669µs	97,465 m/s
		0.5	1.192	0.388	0.082	0.162	15.389	17.213	97,472
		-0.5	2.222	0.388	0.082	0.162	15.389	18.243	97,472
	B(4mm)	0	1.879	0.352	0.082	0.162	15.386	17.862	97,489
		0.5	1.434	0.340	0.081	0.162	15.385	17.402	97,496
		-0.5	2.463	0.340	0.081	0.162	15.385	18.432	97,496
100V	A	0	0.515	0.129	0.074	0.164	15.490	16.371	96,836
		0.5	0.466	0.128	0.074	0.164	15.489	16.320	96,843
		-0.5	0.569	0.128	0.074	0.164	15.489	16.423	96,843
	B	0	0.594	0.111	0.072	0.163	15.453	16.393	97,070
		0.5	0.545	0.111	0.072	0.163	15.452	16.342	97,076
		-0.5	0.648	0.111	0.072	0.163	15.452	16.445	97,076
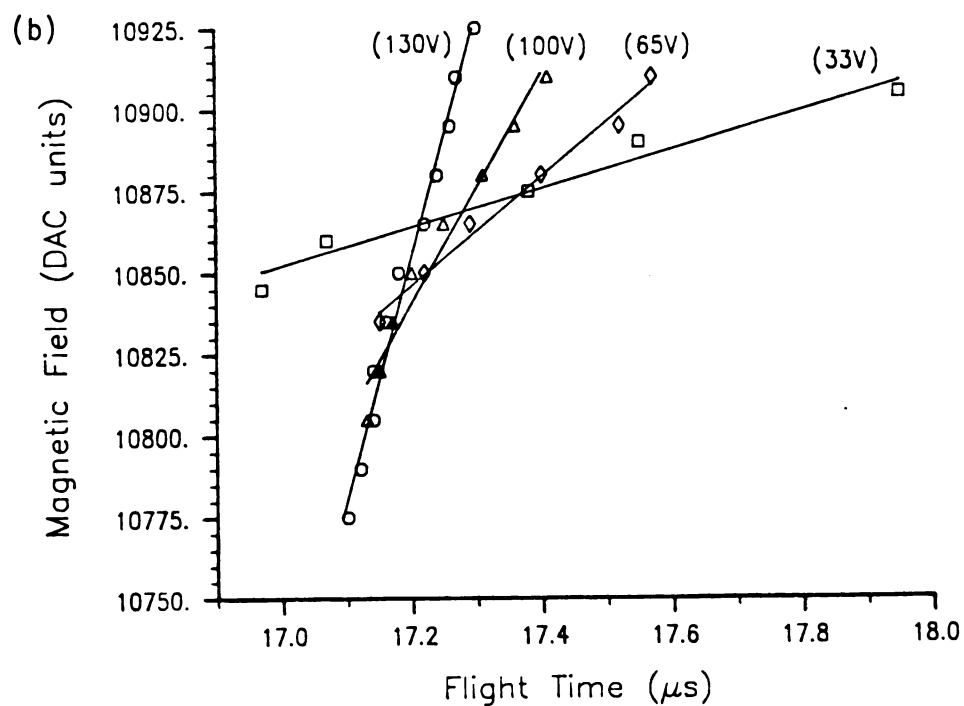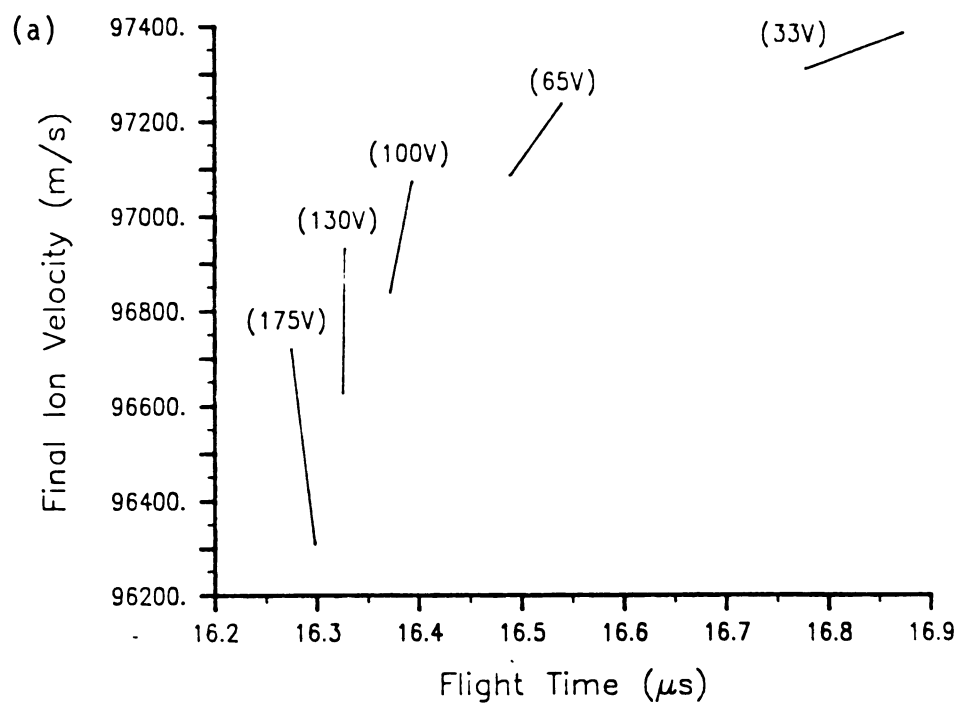
Figure 5.6. Final ion velocity vs. total flight time for mass 71 at several extraction voltages: (a) calculated, (b) observed.

was found to go negative, as calculated values predicted.

An increase in the extraction voltage results in a decrease in flight time, a lowering of final velocity and energy, a loss of resolution along the B-axis, and a increase in resolution along the t-axis. These results adequately explain the first four observations listed at the beginning of this section. The remaining observations, a decrease in TOF peak width and an increase in signal intensity, require consideration of a second effect, initial ion energy.

Ion Distribution in the B-t Data Field — Energy Effects

Computer Simulation of Ion Source Conditions

So far, only the initial spatial distribution of ions in the source has been considered. The initial energy distribution also affects the final velocity and total flight time. The initial energy distribution is partly due to the thermal energy of the ions; however, at 250°C, a typical ion source temperature, the average energy is only 0.07 eV. A much larger energy spread is due to the kinetic energy release during ion fragmentations in the ion source, which can be 0.5 eV or more (23).

The computer program used to simulate initial kinetic energy distributions was identical to the one used for the spatial distribution simulation except the ions were assumed to start from one position but with different kinetic energies. Clearly, the worst case

would be for ion energies with opposite trajectories, forward and backward. The simulation was performed for ions of 0.5 eV initial kinetic energy, initially moving in opposite directions in the ionization chamber.

Comparison of Simulated and Observed Results

Again, the ion current distributions for mass 71 of n-decane were used, measured at four different extraction voltages. The width of the time-of-flight peak at ±2 standard deviations (assuming Gaussian distribution), taken at the magnetic field strength of maximum ion abundance, was used to measure the flight time distribution due to ion energies. As will be shown, ions with initial energy differences of 0.5 eV have very different flight times but virtually identical velocities so they will appear at nearly the same magnetic field strength.

The curve in Figure 5.7 shows the calculated differences in flight times for two ions with the same absolute kinetic energy (0.5 eV) but opposite initial direction. The experimentally measured peak widths are indicated as diamonds, showing a close correspondence. As discussed earlier, differences between the calculated and observed values reflect the simplifying assumptions that were made in the ion source model. Table 5.1 lists the calculated flight times in different regions of the ion source. The turnaround time is the difference in flight time in region 1 between ions with initial kinetic energies of 0.5 and -0.5 eV (the sign indicates initial direction). For an ion of
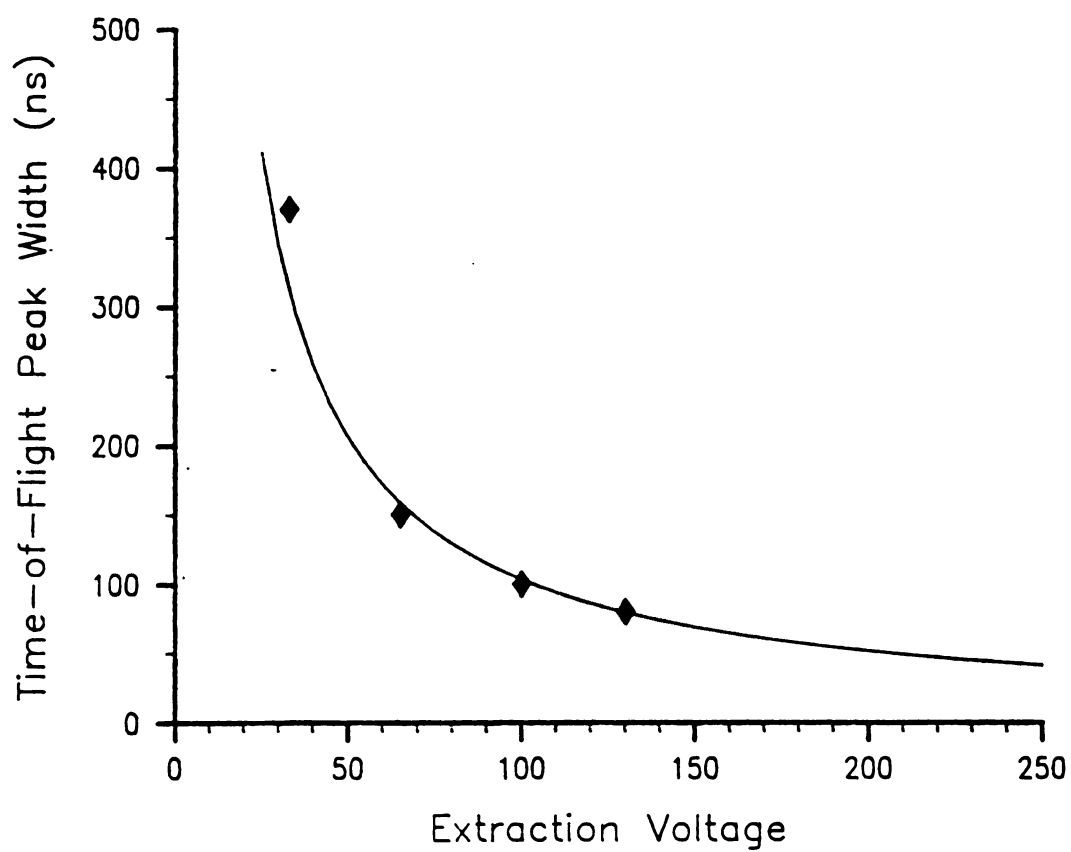
Figure 5.7. Time-of-flight peak width vs. extraction voltage for mass 71 ions with 0.5 eV initial energy. The curved line shows the calculated values. The diamonds are the measured values.

mass 71 with 0.5 eV initial energy, the calculated turnaround time is 1.032 μs for 10 V extraction voltage, the ion starting at point A. Clearly, the turnaround time is the most significant contribution to the flight time difference. The difference in final velocity between ions of 0 and 0.5 eV initial kinetic energy was calculated from the source model to be 7 m/s for all extraction voltages. This value is negligibly small compared to the velocity spread due to the initial spatial distribution (see Figure 5.4). Thus, at any one magnetic field strength, the peak width in time is due mainly to initial ion kinetic energies. (Other factors, such as slightly different paths through the magnet, were discussed in the previous chapter under the heading of resolution.)

The initial ion energy distribution, then, explains observations 5 and 6 at the beginning of this chapter. As the extraction voltage is increased, the time-of-flight peak widths decrease. Because the peak widths decrease, the total ion charge, assumed to be constant, is observed in a shorter period of time, producing more intense peaks. In addition, the larger voltage should extract ions more efficiently, providing a further enhancement in peak intensity.

Implications for Instrument Operation

The initial distributions of ion kinetic energies and ion positions in the ion source of the TRIMS instrument are the causes for the observed signal distribution in the B-t data field when using pulsed extraction. Computer calculations, based on a simple model of

the LKB-9000 ion source, give remarkably good agreement with the experimental results. All the observed changes in siganl distributions with respect to the extraction voltage are explained by this model. The initial spatial distribution of ions in the ion source produces ion intensity profiles in the B-t data field that are opposite of those expected by classical mass spectrometry theory. Increasing extraction voltages produce lower ion energies and velocities, an increased spread of ion intensity along the B-axis, and a decreased spread of ion intensity along the t-axis. The initial energy distribution causes a spread of ion intensity along the t-axis at any one magnetic field strength. An increase in extraction voltage causes the peak width along the t-axis to decrease with a concomitant increase in peak height. In summary, the initial position in the ion source determines the values of B and t at which a signal will appear and the initial energy spread determines the TOF width of the peak at that B,t coordinate.

These data are useful for determining the operating parameters of the instrument. For maximum B-resolution, a low extraction voltage must be used, but for optimal flight time resolution, minimum peak width, and maximum intensity, a large extraction voltage is required. As an example, to resolve two daughter ions of similar mass that are derived from the same parent mass, one would probably use a low extraction voltage to obtain good B-resolution. On the other hand, to resolve two daughters of the same mass but derived from parent ions of slightly different mass, one would opt for a high extraction voltage.

In practice, two more features warrant consideration. At extraction voltages below approximately 50 V, the electron beam is not completely deflected during the extraction pulse so that a background signal will be observed unless the electron beam is turned off. Second, the instrument must be calibrated at the extraction voltage to be used, since the arrival time and field strength at which a particular mass is observed change with the extraction voltage.

One way to circumvent this whole problem is to use ion beam deflection or chopping rather than pulsed extraction. For ion beam deflection, the flight time $\underline{is}$ a direct measure of the ion velocity and not a sum of acceleration and drift times. Unfortunately, the ion beam deflection method gives up some of the signal gained by ion storage in the pulsed extraction method. The trade-off between resolution and sensitivity reigns supreme. In any case, the particular experiment will dictate the pulsing method which will give optimum results.

References

1. Wiley, W.C.; McLauren, I.H. Rev. Sci. Instrum. 1955, 26, 1150.

2. Sanzone, G. Rev. Sci. Instrum. 1970, 41, 741-742.

3. Stein, R. Int. J. Mass Spectrom. Ion Phys. 1974, 14, 205-18.

4. Bakker, J.M.B. Dyn. Mass Spectrom. 1976, 4, 25-37.

5. Poschenrieder, W.P. Int. J. Mass Spectrom. Ion Phys. 1971, 6, 413-426.

6. Poschenrieder, W.P. Int. J. Mass Spectrom. Ion Phys. 1972, 9, 357-73.

7. Poschenrieder, W.P.; Oetjen, G.-H. J. Vac. Sci. and Technol. 1972, 9, 212-15.

8. Poschenrieder, W.P. U.S. Patent 3 863 068, 1975.

9. Moorman, C.J.; Parmater, J.Q. U.S. Patent 3 576 992, 1971.

10. Kilius, L.R.; Hallin, E.L.; Chang, K.H.; Litherland, A.E. Nucl. Instrum. Meth. 1981, 191, 27-33.

11. Oetjen, G.-H.; Poschenrieder, W.P. Int. J. Mass Spectrom. Ion Phys. 1975, 16, 353-367.

12. Karataev, V.I.; Mamyrin, B.A.; Shmikk, D.V. Sov. Phys.-Tech. Phys. (Engl. Transl.) 1972, 16, 1177-79; Zh. Tekh. Fiz. 1971, 41, 1498-1501.

13. Mamyrin, B.A.; Karataev, V.I.; Shmikk, D.V.; Zagulin, V.A. Sov. Phys. JETP (Engl. Transl.) 1973, 37, 45-48; Zh. Eksp. Teor. Fiz. 1973, 64, 82-89.

14. Bakker, J.M.B. J. Phys. E 1973, 6, 785-789.

15. Bakker, J.M.B. J. Phys. E 1974, 7, 364-368.

16. Bakker, J.M.B. Int. J. Mass Spectrom. Ion Phys. 1971, 6, 291-5.

17. Bakker, J.M.B. Adv. Mass Spectrom. 1971, 5, 278-282.

18. Pinkston, J.D. presented at the 33rd Annual Conference on Mass Spectrometry and Allied Topics, San Diego, May 26-31, 1985.

19. Studier, M.H. Rev. Sci. Instrum. 1963, 34, 1367-70.

20. Baker, F.A.; Hasted, J.B. Phil. Trans. Roy. Soc. London, A, 1966, 261, 33-65.

21. Elliot, R.M. In "Mass Spectrometry"; McDowell, C.A., Ed.;
    McGraw-Hill:New York, 1963. p. 74.

22. Chait, E.M., Anal. Chem. 1972, 44(3), 77A-91A.

23. Jones, E.G.; Beynon, J.H.; Cooks, R.G. J. Chem. Phys. 1972, 57,
    2652-58.

CHAPTER VI

KINETIC ENERGY RELEASE MEASUREMENTS

Introduction

Whenever an ion undergoes fragmentation after leaving the ion source (metastable decomposition or collisionally activated dissociation), there is an accompanying release of kinetic energy (1). This energy release results when a portion of the internal energy (vibrational) of the precursor ion is converted into translational energy of the products. Because of this additional translational energy imparted in all directions to the daughter ions, metastable peaks are broader than other peaks in the mass spectrometer.

The magnitude of the the kinetic energy release can be related to the potential energy surface for the metastable dissociation and to the internal energy of the metastable ion activated complex (2). Since the potential energy surface is characteristic of a particular reaction, the kinetic energy release is often also characteristic of a particular reaction. This fact has been exploited to investigate ion structure and to differentiate isomeric species by mass spectrometry (3-6). For example, kinetic energy release has been used to differentiate epimeric steroids (7) and to identify a wide variety of isomeric halogenated compounds (8,9).

169

A number of different techniques have evolved that can measure kinetic energy release. The most common are ion kinetic energy spectrometry (IKES) (10-12) and mass-analyzed ion kinetic energy spectrometry (MIKES) (13). These techniques are performed, respectively, with an electric sector or with a magnetic sector/electric sector combination in reverse geometry (BE). A recently developed technique with considerable promise utilizes an electric sector/quadrupole combination (EQ) (14).

The instruments mentioned so far measure energy directly with an electric sector. Kinetic energy release has also been measured by magnetic sector instruments (15,16) and time-of-flight instruments (17). With the exception of the EQ instrument, these techniques cannot resolve the kinetic energy release for daughter ions of similar mass which are all derived from the same parent mass. The electric sector or other devices mentioned also function as the daughter ion mass analyzer, i.e, the mass analysis and kinetic energy release measurement occur along the same measurement axis. In many cases, peak overlap requires sophisticated deconvolution techniques to separate the energy contributions from each daughter mass.

Kinetic Energy Release Measurements by TRIMS

The TRIMS instrument is also a useful technique for measuring the kinetic energy release that occurs during daughter ion formation (18). In TRIMS, ions of the same mass appear at constant $B \cdot t$. A spread in ion energies is manifest as a spread in ion abundance along the $B \cdot t$

curve. As shown in Chapter 2, Equation 12, the quotient B/t is
proportional to ion energy. The values of B and t serve not only to
identify the parent and daughter masses, but they also indicate the
energy of the ion.

If the ion current profile for a selected daughter mass in the B-t
data field is plotted as ion abundance vs. B/t, direct measure of the
ion energy distribution is obtained, analogous to the output of an IKES
instrument.   Moreover, the daughter ion is mass-selected. Regardless
of the magnitude of the kinetic energy release, the ion intensity for
daughter ions of similar mass should be completely resolved.

To clarify how the kinetic energy distribution is obtained by
TRIMS, consider Figure 6.1a, a portion of the B-t data field for
p-chlorotoluene.   The molecular ion (mass 126) and its M+2 isotope
(mass 128) dissociate by metastable decomposition to give (M-Cl)$^+$
daughter ions at mass 91. A time scan was recorded at each increment
of the magnet current in the region of the B-t data field where
daughter ions were expected. Each data point in the figure represents
the coordinate at which the maximum ion intensity was observed for each
time scan.   The 91$^+$ daughters of the 126$^+$ and 128$^+$ parents fall on a
line of constant B·t. The energy spread in the daughter ions causes
the intensity of the peak to be distributed along this curve, with a
reduction in parent resolution.   By calculating the energy at each
point and replotting the data as ion abundance vs. energy, an energy
distribution profile is obtained, as shown in Figure 6.1b.

172

P-CHLOROTOLUENE

(a)

Parent Mass

(b)

ENERGY DISTRIBUTION PROFILE FOR P-CHLOROTOLUENE
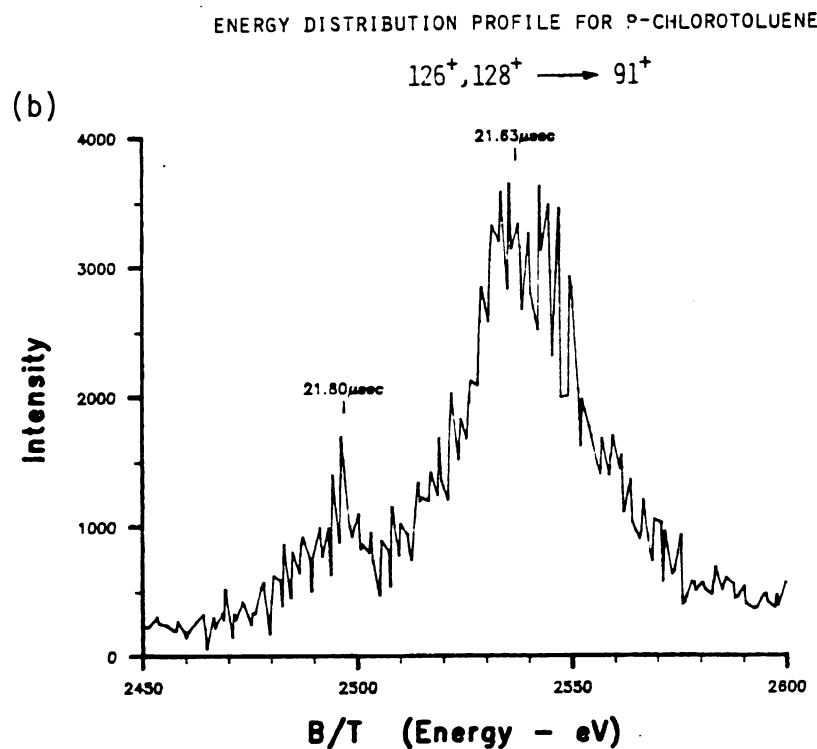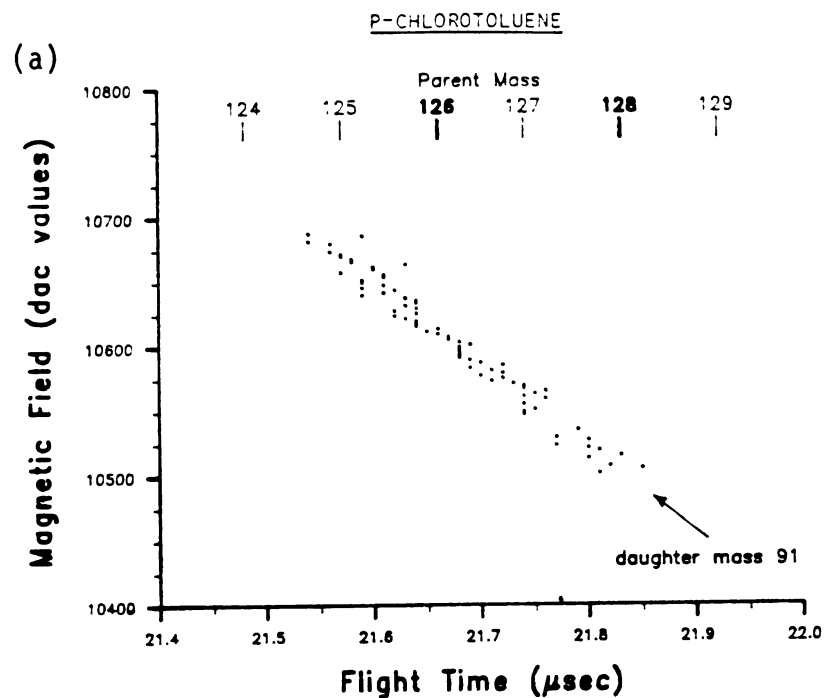
$$126^+, 128^+ \longrightarrow 91^+$$

Figure 6.1. Kinetic energy distribution profile for daughter ions of mass 91 formed by metastable decomposition from parent ions of mass 126 and 128 of p-chlorotoluene. (a) Location of ions in the B-t data field. (b) Energy profile along a line of constant B·t.

The kinetic energy release, T, is a function of the observed energy distribution, as given by Equation 1 (19), where m_1, m_2, and m_3

$$T = \frac{m_1 \, \Delta E^2}{16 m_2 m_3 E} \qquad (1)$$

are the parent, daughter, and neutral masses, respectively, E is the energy of the stable ions, and ΔE is the corrected energy distribution of the daughter ions. Some of the daughter ion kinetic energy distribution is due to the energy distribution of the parent ions, which is caused by the energy spread in the ion source. Furthermore, the daughter ion distribution with no kinetic energy release should display the same percentage energy distribution as the stable ions. Therefore, a correction for this inherent energy distribution is needed. This correction is related to the energy spread of the stable ions by Equation 2 (1), where ΔE_{obs} is the observed energy distribution

$$\Delta E = \Delta E_{obs} - \left(\frac{m_2}{m_1}\right) \Delta E_{stable} \qquad (2)$$

and ΔE_{stable} is the stable ion energy distribution. The energy distributions are generally measured at a constant peak height, most often at 50% of the maximum intensity (5,20).

Measurement of Kinetic Energy Release

Going throught the process described above, base on the data set exemplified by Figure 6.1, is tedious in acquisition and interpretation. A more efficient method is to scan along the line of constant $B \cdot t$ that corresponds to the daughter under study. A special

data system command, ESWEEP, achieves this measurement, recording the ion intensity and ion energy for each point as the magnet current and sampled flight time are slowly incremented along the B·t curve. The proper flight time is calculated from the calibration at each point and set to maintain a constant B·t. The data are then plotted as ion intensity vs energy, as demonstrated in Figure 6.1b. The width at half height is measured, and using Equations 1 and 2, the kinetic energy release is calculated.

Figure 6.2 shows the kinetic energy distribution for $(M-Cl)^+$ daughter ions (mass 77) of chlorobenzene (MW=112). The two peaks correspond to the two parent ion isotopes of mass 112 and 114. The peak width at 50% of the peak height is 20 eV. The peak width for the stable ions of mass 112 is 6 eV. Using Equations 1 and 2, the energy release calculated for this reaction is 21.6±0.3 eV. This value compares favorably with the literature value of 21.0±0.2 eV (9). The differences in these values could be due to the use of different instruments or to different ion source conditions.

The daughter ion peaks corresponding to the two parent masses are not completely resolved, a consequence of broadening by the kinetic energy release. The ions should be resolved from daughter ions of other masses, if present, e.g., daughter ions of masses 76 or 78 would not interfere with this measurement. For this reason, TRIMS is a complementary technique to MIKES. In MIKES, kinetic energy release information is obtained with good parent ion resolution but poor daughter ion resolution. In TRIMS, kinetic energy release information
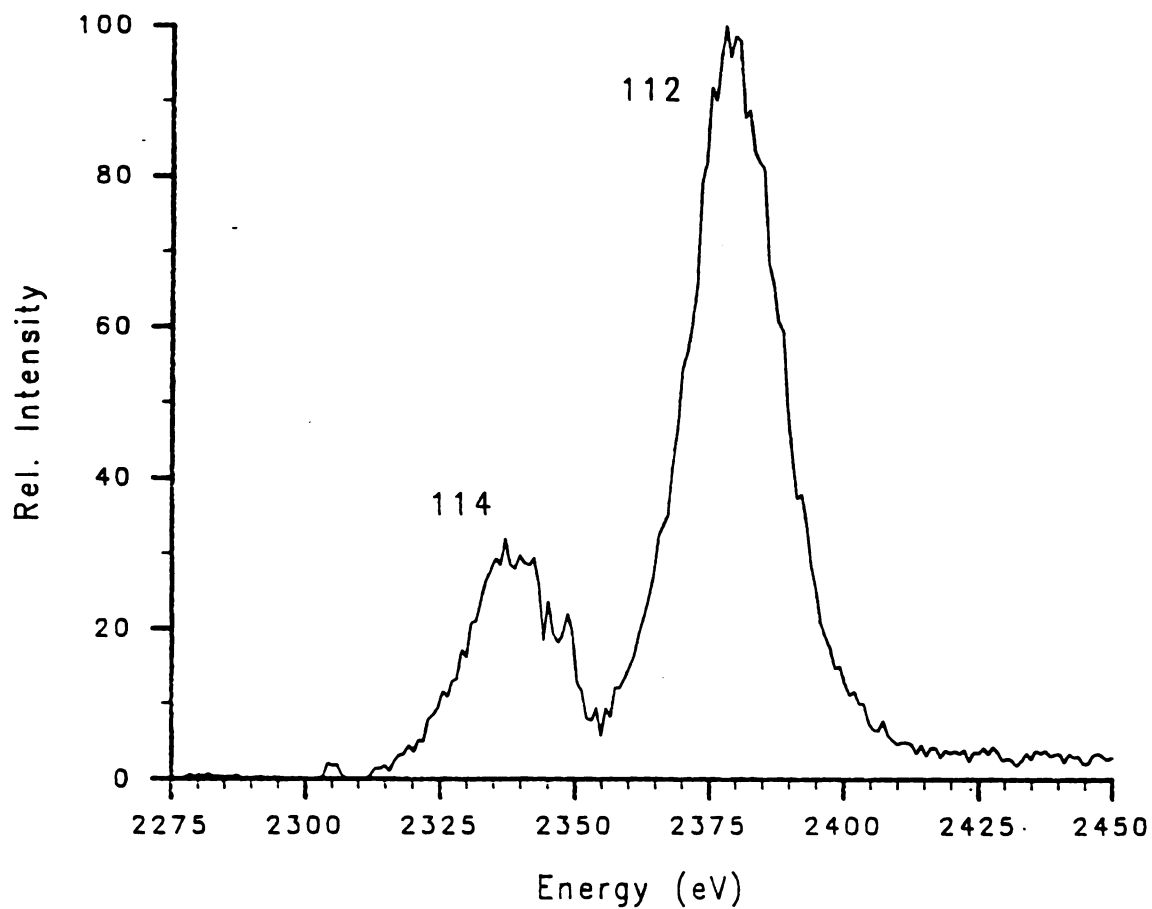
Figure 6.2. Kinetic energy distribution profile for daughter ion peaks along a line of constant B·t (mass=77) formed by metastable decomposition from parents of mass 112 and 114 of chlorobenzene.

is obtained with poor parent ion resolution but good daughter ion resolution.

Summary

Kinetic energy release for ion dissociations, either by metastable decomposition or CAD, can be measured by TRIMS. Good resolution of the daughter ion masses is obtained by TRIMS; however, parent ion resolution is limited by the kinetic energy release. Expected improvements in resolution and sensitivity should make TRIMS a valuable technique for acquiring this type of data. Already, TRIMS has been applied by Lifshitz et al to measure kinetic energy release as a function of ion lifetime (21). Other applications are likely to follow.

References

1. Cooks, R.G.; Beynon, J.H.; Caprioli, R.M.; Lester, G.R. "Metastable Ions"; Elsevier:New York, 1973. pp. 57-70, 104-121.

2. Jones, E.G.; Beynon, J.H.; Cooks, R.G. J. Chem. Phys. 1972, 57, 2652-58.

3. Shannon, T.W.; McLafferty, F.W. J. Am. Chem. Soc. 1966, 88, 5021-22.

4. Jones, E.G.; Bauman, L.E.; Beynon, J.H.; Cooks, R.G. Org. Mass Spectrom. 1973, 7, 185-192.

5. Holmes, J.L.; Terlouw, J.K. Org. Mass Spectrom. 1980, 15, 383-396.

6. Levsen, K. "Fundamental Aspects of Organic Mass Spectrometry"; Verlag Chemie:New York, 1978. pp. 237-242.

7. Zaretskii, Z.V.I.; Dan, P.; Kustanovich, Z.; Larka, E.A.; Herbert, C.G.; Beynon, J.H.; Djerassi, C. Org. Mass Spectrom. 1984, 19, 321-325.

8. Hass, J.R.; Tondeur, Y.; Voyksner, R.D. Anal. Chem. 1983, 55, 295-297.

9. Voyksner, R.D; Hass, J.R.; Bursey, M.M. Anal. Chem. 1983, 55, 914-920.

10. Beynon, J.H.; Caprioli, R.M.; Baitinger, W.E.; Amy, J.W. Int. J. Mass Spectrom. Ion Phys. 1969, 3, 313-321.

11. Beynon, J.H.; Cooks, R.G. J. Phys. E 1974, 7, 10-18.

12. Beynon, J.H.; Cooks, R.G. Int. J. Mass Spectrom. Ion Phys. 1976, 19, 107-137.

13. Beynon, J.H.; Cooks, R.G.; Amy, J.W.; Baitinger, W.E.; Riley, T.Y. Anal. Chem. 1973, 45, 1023A-1031A.

14. Harris, F.M.; Keenan, G.A.; Bolton, P.D.; Davies, S.B.; Singh, S.; Beynon, J.H. Int. J. Mass Spectrom. Ion Phys. 1984, 58, 273-292.

15. Beynon, J.H.; Saunders, R.A.; Williams, A.E. Z. Naturforsch 1965, 20A, 180.

16. SenSharma, D.K.; Franklin, J.L. Int. J. Mass Spectrom. Ion Phys. 1974, 13, 139-150.

17. Franklin, J.L.; Hierl, P.M.; Whan, D.A. J. Chem. Phys. 1967, 47, 3148-53.

18. Stults, J.T.; Enke, C.G.; Holland, J.F. presented at the 32nd Annual Conference on Mass Spectrometry and Allied Topics, San Antonio, TX, May 27 - June 1, 1984, bound volume pp. 519-520.

19. Beynon, J.H.; Caprioli, R.M.; Baitinger, W.E.; Amy, J.W. Org. Mass Spectrom. 1970, 3, 661-668.

20. Terwilliger, D.T.; Beynon, J.H.; Cooks, R.G. Proc. R. Soc. London, Ser. A 1974, 341, 135.

21. Lifshitz, C.; Gefen, S.; Arakawa, R. J. Phys. Chem. 1984, 88, 4242-46.

CHAPTER VII

FUTURE PROSPECTS

Significant progress has been made in the development and improvement of TRIMS. There are, however, several areas in which improvements are still necessary in order to make TRIMS less of a research subject and more of an analytical tool.

Improvements in Resolution

In the context of pulsed ion extraction, several improvements could be made. The electron beam should be considerably more collimated. Since the initial spatial distribution of ions leads to a large velocity spread at the space-focusing condition, a marked improvement in resolution along the magnetic field axis should be observed. In addition, an extra grid or lens should be added directly after the extraction plates with a potential that is at most times higher than the ionization chamber (or repeller plate, if present). The potential on this lens would be pulsed low in conjunction with the extraction lens. This extra lens would prevent ions from escaping during ionization time and allow the extraction plate to be operated at the same voltage as the ionization chamber in order to maximize ion trapping efficiency (1).

From Chapter 5, it is clear that pulsed ion extraction is not the ideal pulsing technique for TRIMS. Ion beam deflection (2,3) would

circumvent many of the problems presented by pulsed ion extraction. The flight time would be a direct measure of the velocity and no space focusing would be required. The ion source could be operated with a low extraction voltage to minimize the energy distribution due to the spatial distribution in the ion source. The energy spread of the ions would show up as a distribution of ion abundance along the B·t curve so that it would not interfere with stable or daughter ion resolution at all. Resolution along the magnetic field axis would be the same as that obtained with the instrument in the non-pulsed mode. The time-of-flight resolution would depend on the duration of the intersection of the deflected beam with the limiting aperture, which can be made quite short.

Placement of the beam deflection plates is important. Deflection immediately following the entrance slit requires that the beam be deflected exactly at right angles to the magnetic dispersion plane to prevent interference with the momentum analysis. This position also requires deflection along the long dimension of the slit image, which precludes optimum time-of-flight resolution. The deflection may also cause ion movement in the nonhomogeneous fringing field of the magnet which would degrade the magnetic sector resolution.

A better location for the beam deflection plates would be immediately following the exit slit at the detector end of the instrument (4). The magnetic sector instrument could be adjusted for optimal resolution and sensitivity, and absolutely no modification of the ion source would be required. Deflection would be along the narrow

dimension of the slit image for maximum time-of-flight resolution. A flight tube extension would be necessary but that is essentially a piece of pipe with flanges at either end. Although this location of the pulsing apparatus would remove the simultaneous nature of the momentum-flight time measurement, the physics of the mass separation and mass assignment remain completely unchanged. Ion dissociations must still occur between the ion source and the magnetic sector.

Improvements in Sensitivity

There are no simple solutions for improving the sensitivity in TRIMS. More efficient ionization and better trapping of ions in the ion source would, of course, be helpful but not easily achieved. One area in which TRIMS would be quite useful is pulsed desorption from a condensed matrix. The immobilized sample would not be lost between ionization/extraction pulses so the "sample duty cycle" would be improved considerably. The surface would also establish a common plane of origin to minimize the initial ion spatial distribution. Techniques such as laser desorption (LD) (5-8) and pulsed secondary ion mass spectrometry (SIMS) (9-11) could lend themselves quite readily to TRIMS.

Improvements in collision efficiency would also yield improved daughter ion sensitivity. In the present instrument, improvements in pumping in the field-free region following the ion source need to be made in order to reduce the pressure and ion scattering in this region.

As an alternative to CAD, photodissociation (8,12,13) would be one way to produce daughter ions, often with great selectivity, without introducing any gas load.

Improvements in sensitivity could also be made through enhancement of the detection electronics. The present amplifier/gated integrator has noise that has been difficult to isolate and remove. Attenuation of this noise would yield improvement in the signal-to-noise ratio. In some instances where very small ion signals are present, ion counting would improve the signal-to-noise level (14,15). One of the limitations of the present instrument is the low amplification of the signal, forcing the gated integrator to be operated at its limit of sensitivity. Better amplification would relieve the strain on the gated integrator, but large gains are difficult to achieve at the large bandwidths necessary for amplifying the narrow time-of-flight peaks.

Time array detection (TAD) (16) should provide a significant improvement in sensitivity for certain experiments as mentioned in Chapter 3. When a single MS/MS scan is desired (e.g. one daughter scan), only one timed amplitude measurement is made per magnetic field setting. However, when more than one scan is desired, then TAD, by sampling ion abundance at all arrival times, would provide improved sensitivity for identical measurement time or the same sensitivity for shorter analysis times.

Future Applications of TRIMS

As a pulsed technique, TRIMS would lend itself quite readily to experiments which are already pulsed in nature. For example, laser desorption (5-8), as already mentioned, produces a pulsed signal, and the ions formed usually show a considerable energy spread. TRIMS could match the repetition frequency of the desorption event, resolve the energy contributions (because they would fall along the B·t curve and not interfere with stable or daughter ion resolution), and provide the capability for performing MS/MS experiments. The time-resolved nature of the mass analysis could also prove useful in studying the desorption mechanism (17,18).

The decrease in analysis time by the use of TAD could make TRIMS useful for obtaining a significant amount of MS/MS data in a relatively short period of time. If sufficient sensitivity is achieved, TRIMS with TAD has the capability of obtaining the full MS/MS data field (all daughter ions of all parents) on the timescale of chromatographic peak elution. This would provide much more rapid MS/MS data acquisition than any other technique presently available. The capabilities for performing GC/MS/MS or LC/MS/MS (to obtain all available MS/MS data on each chromatographic peak) could provide significant improvements in the speed and selectivity of analysis.

Other laboratories have already begun to use TRIMS. Workers at the National Bureau of Standards (19) have employed time resolution on a magnetic sector instrument to discriminate against ions with momentum

variations caused by collisional scattering. Using resonance ionization, they hope to achieve better isotope ratio measurements. Lifshitz et al (20) have used TRIMS to measure the time-resolved kinetic energy release of metastable ions which have been stored for various periods of time in the ion source. TRIMS is ideal for this case because an MS/MS technique is required for an experiment with a pulsed ion source.

Time-resolved ion momentum spectrometry has made an impressive showing out of the starting blocks. There remain yet a few hurdles to be overcome, but with further effort, coupled to continuing improvements in technology, the future for TRIMS is promising, very promising.

References

1. Damoth, D.C. In "Mass Spectrometry"; Reed, R.I., Ed.; Academic Press:New York, 1965; pp. 61-71.

2. Bakker, J.M.B. J. Phys. E. 1973, 6, 785-789.

3. Bakker, J.M.B. J. Phys. E. 1974, 7, 364-368.

4. Pinkston, J.D., presented at the 33rd Annual Conference on Mass Spectrometry and Allied Topics, San Diego, May 26-31, 1985.

5. Zakett, D.; Schoen, A.E.; Cooks, R.G. J. Am. Chem. Soc. 1981, 103, 1295-1297.

6. Denoyer, E.; Van Grieken, R.; Adams, F.; Natusch, D.F.S. Anal. Chem. 1982, 54, 26A-41A.

7. Cotter, R.J.; Tabet, J.C. Int. J. Mass Spectrom. Ion Phys. 1983, 53, 151-166.

8. Cotter, R.J. Anal. Chem. 1984, 56, 485A-504A.

9. Chait, B.T.; Standing, K.B. Int. J. Mass Spectrom. Ion Phys. 1981, 40, 185-193.

10. Benninghoven, A. Int. J. Mass Spectrom. Ion Phys. 1983, 53, 85-99.

11. Steffens, P.; Niehuis, E.; Friese, T.; Greifendorf, D.; Benninghoven, A.; In "Secondary Ion Mass Spectrometry: SIMS IV"; Benninghoven, A.; Okamo, J.; Shimizu, R.; Werner, H.W., Eds.; Springer-Verlag:New York, 1984; pp. 404-408.

12. McGilvery, D.C.; Morrison, J.O. Int. J. Mass Spectrom. Ion Phys. 1978, 28, 81.

13. Mukhtar, E.S.; Griffiths, I.W.; Harris, F.M.; Beynon, J.H. Int. J. Mass Spectrom. Ion Phys. 1981, 37, 150.

14. Frendenthal, J.; Gramberg, L.G. Anal. Chem. 1977, 49, 2205-2208.

15. Darland, E.J.; Leroi, G.E.; Enke, C.G. Anal. Chem. 1980, 52, 714-723.

16. Holland, J.F.; Enke, C.G.; Allison, J.; Stults, J.T.; Pinkston, J.D.; Newcome, B.; Watson, J.T. Anal. Chem. 1983, 55, 997A.

17. VanBreemen, R.B.; Snow, M.; Cotter, R.J. Int. J. Mass Spectrom. Ion Phys. 1983, 49, 35-50.

18. Tabet, J.C.; Cotter, R.J. Int. J. Mass Spectrom. Ion Phys. 1983, 54, 151-158.

19. Zeininger, H.; Fassett, J.D.; Moore, L.J. presented at the 33rd Annual Conference on Mass Spectrometry and Allied Topics, San Diego, May 26-31, 1985.

20. Lifshitz, C.; Gefen, S.; Arakawa, R. J. Phys. Chem. 1984, 88, 4242-4246.